Acknowledgements

I wish to express my sincere appreciation and thanks to Professor Michalis Zerbakis for his guidance and his support during the implementation of this thesis and his assistance in the preparation of this manuscript.

I am also grateful to Dr. Noni Maravelaki – Kalaitzaki for her invaluable help, guidance and support throughout the duration of this thesis. As well as for her suggestions for the improvement of the current thesis.

Last but no least, I wish to thank my family for their support and encouragement as well as my friends for sharing my thoughts, worries and expectations during these years.

"Imagination is more important than knowledge"

"Albert Einstein"

This work is dedicated to human imagination and inspiration, which led to the conquest of knowledge.

Overview of the work

During the past decades there has been a growing concern about the changes in air quality. Much of this concern was focused on public health issues. A complementary is the effect on building materials particularly their deterioration and maintenance arising from pollution. The degradation effects on stone surfaces are studied by the chemists in order to detect the exact locations on the stonework, where decay areas prevail. The efficient detection of the corroded areas is a key step for the efficient removal of the degradation effects and the restoration of the stonework. The methods used so far for the detection of the decay follow the procedure of obtaining specimens from the stone surface and subsequently studying these specimens with the aid of several chemical methods. The process of taking these specimens, which is accompanied by ablation of stone surface, cracks etc, is considered to be destructive. Thus it is necessary the development of methods which are non-destructive and can be applied in situ. The diagnosis methods implemented in this work satisfy the above criteria. More specifically, images are obtained from the surfaces under consideration via a Monitoring system, and at a further step by applying the Image Processing algorithms on the studied images we extract the specific locations on the image where deteriorated regions prevail. Eight Image Processing Algorithms were developed and all the algorithms managed to detect the degradation effects with a very good accuracy, but each one approaches better a specific feature of the deterioration patterns. Further to the detection of the co-ordinates of polluted particles our methods managed also to classify these particles according to their chemical composition and to extract some characteristics concerning their shape, surface size and thickness. Images depicting the deterioration effects on stone surfaces after the application of various chemical cleaning methods as well as images presenting the decay phenomena on surfaces where different conditions of exposure prevail are processed with the algorithms implemented in this work.

Table of Contents

1   INTRODUCTION

A. A problem Description

During the past decades there has been a growing concern about the changes in air quality. Much of this concern was focused on public health issues. A complementary is the effect on building materials particularly their deterioration and maintenance arising from pollution .It could be said that the accelerated deterioration phenomena observed at the majority of the monuments should be considered as another effect of the modern civilization. During the last decades an important number of investigations were carried out in order to isolate all these factors, which result in the corrosion of stone monuments, and to detect the mechanism in which each of these agents act. The fact that the corrosion phenomena are mainly observed in the last decades indicates that the action of the climate conditions are surely of lower importance than the action of the derivatives of human's activity (ex industry). The comprehension of the way in which each of these factors is associated with the stone erosion will help us in our effort to manage the restoration (if this is possible) of the stonework. In the following paragraphs an overview of all these causes leading to the deterioration of the stone monuments is given while the phenomenology of the problems arose of each of these causes are briefly described.

1.1   Effects of ozone and   NOx on the deterioration of Stone

Airborne pollutants affect buildings in two ways, decay and soiling. Soiling is the discoloration of a building whilst decay results in the destruction of the building fabric. Nitrogen oxides are gaseous components, which react directly with the stone surface by forming acids in the presence of water and oxidizing agents. These acids react with the stone to form salts, which either crystallizes out within the stonework resulting in physical damage, or they are washed away resulting in a loss of material. Nitrate salts are more soluble and expand less than other salts leading to little if any damage by this mechanism. A further factor relevant to nitrogen oxide levels relates to their importance as catalysts, which increase the rate of oxidation of the sulphate compounds in the conversion of the gaseous, and particle forms to acids. Thus the levels of nitrogen oxides generated by traffic could contribute to this effect. From the literature it is

known that the oxidation of SO_2 aqueous phase is the key step in the formation of gypsum on the surface of the stone. Atmospheric concentrations of NOx are strongly linked to the amount of O3, another major oxidant within the system. O_3 and its oxidizing activity is of high importance as it reacts rapidly with the surface sulphite to form sulphate both at dry and humid conditions. Apparently the salts formed by the mechanism analyzed above greatly affect the surface of the stonework from an aesthetic point of view while it amplifies the decay phenomena. Furthermore, the formation of a gypsum layer on the surface of the stone leads to an increase of the porosity of the stone which in turns absorbs a greater amount of gaseous pollutants, carbonaceous particles, dust, black smoke and in general the deterioration of the stone is accelerated. [1]

1.2   SO2   - Calcite Reaction

Sulphur dioxide (SO_2) attacks calcite ($CaCO_3$) in calcareous stone producing gypsum ($CaSO_4$. .$2H_2O$), which forms crusts at rain-sheltered surfaces and accelerates erosion at areas exposed to rain. [2]. Black crusts presence is a factor, which greatly affects the aesthetic view of historical monuments. Their thickness ranges from 200μm to several mm and the investigations carried out concerning this topic evidenced that these layers can be distinguished in 3 or more successive sub layers on the basis of the chemical composition of the compounds present on the crusts. The more frequently encountered chemical constituents in black crusts are calcite, silicates, potassium nitrate, iron oxides, quartz and numerous organic constituents in lower concentrations. [3] Further analysis on the structure of gypsum crusts, revealed that the sub layers mentioned above vary in thickness and physical properties as it was formed by different chemical processes. It could be mentioned at this point that the inner layer whose width was measured to be greater than 100μm was generated by the sulphation mechanism. In this sub layer somebody could observe the presence of empty cavities and residual particles of calcite. The high porosity, which was experimentally measured on this part of the gypsum crusts, is reflected on the absorption of metal oxides and the other materials. [3] Moreover we should not underestimate the important role of this layer in other mechanisms of stone erosion. More Specifically at this point it should be taken under consideration the combination of gypsum existence along with the humidity's presence. As it is well known the crusts on the stone's

surfaces absorb a great amount of humidity, thus its friability increases and this leads in a lamellar texture and flaking of the stone. It is apparent that humidity's action in combination with the absorption of various oxides can lead in the abruption of the crust and extensively in loss of the stone material, discoloration, and aesthetic damage.
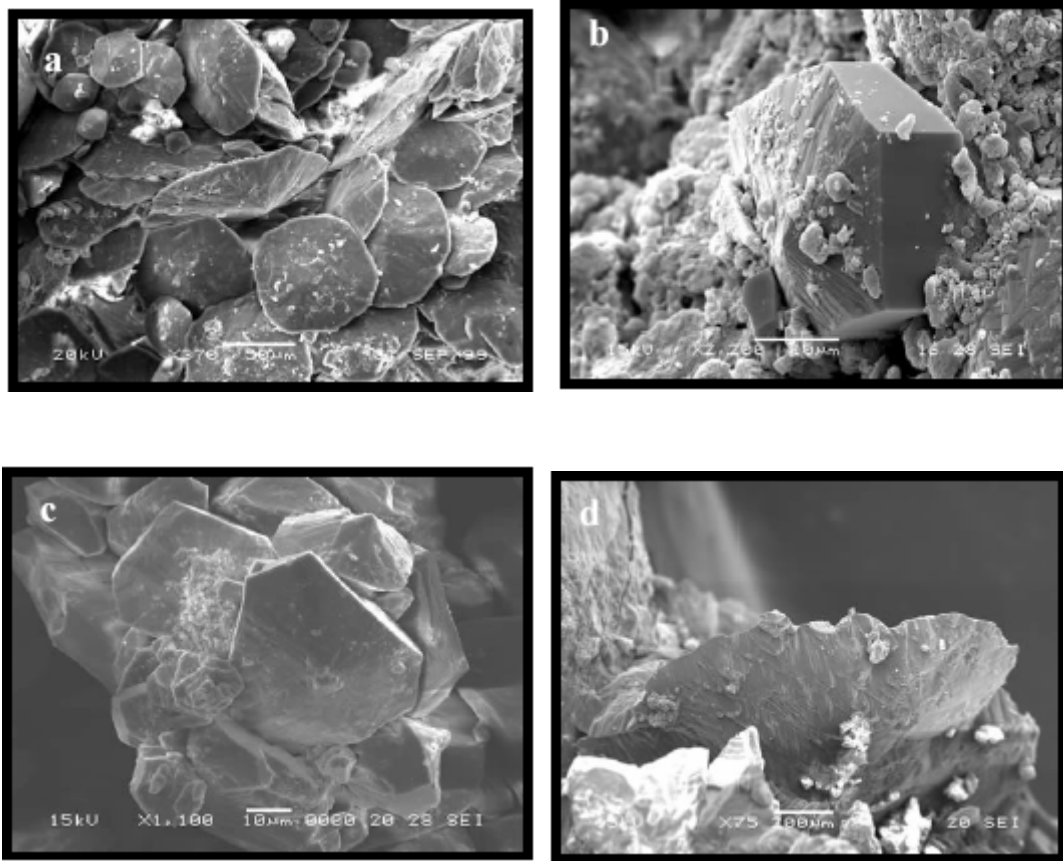
Image 1: (a) Cluster of lenticullar gypsum crystals (b) tabular gypsum crystal (c) lenticular and tabular gypsum crystals (d) lenticular gypsum crystals exhibiting dissolution features

1.3 Carbonaceous Particles and in general particles carrying strong primary acidity

Fly ash emitted by the incomplete combustion of solid and liquid fuels, containing both metal oxides and unburnt carbon, has been considered the most interesting particulate in the respect of deterioration of stone monuments. The role of fly ash particles is of great concern as they are very

commonly encountered in black crusts adhering to degraded stones. As it was stated above, investigations found that fly ash particles formed black crusts in gypsum crystals under the presence of humidity. Therefore, although the slow sulphation of, for instance, calcareous stone at high degrees of humidity and in the presence of SO_2 is fully demonstrated nevertheless the effect of particulate, as a sulphation catalyst is uncertain. This does not exclude the possibility that fly ash particulate may act in synergy with sulphation according to some other mechanisms. According to the results, revealed by investigations, ashes commonly constituted of unburnt carbon, vanadium, iron, nickel, magnesium and sulphur. The presence of ash particles with the chemical combustion described above and in synergy with medium humidity levels lead to the recrystallization of the superficial calcite layer in gypsum. [4] Optical microscope photographs were taken and revealed that the appearance of coloration is ranging from green to reddish brown and yellow which intensifies the longer the stone is submitted to the conditions described above. Many researchers claim that when a particle of ash is stuck on the stone surface it creates a hole around itself with the acidity that releases and, as it was observed, gypsum was crystallized at the margins of the crater. As we can conclude from the mechanism analyzed, gypsum formation increases the porosity of the stone, which further to the aesthetic alteration of the stone as it changes the view of the stone due to the cavities formed (texture) and the color alteration, it also enforces the dry deposition phenomena by the absorption of black particles. At this point it should be stated that this type of deterioration is commonly observed near industrial regions, as well as in monuments located in urban areas. Another key factor, which greatly affects the progress of this type of erosion, is the winds velocities and weathering phenomena in general .At first we are examining the way that wind velocities affect the problem. Apparently in areas where winds of high velocities prevail, dust, smoke and particles originating of oil burning are transferred in larger distances and with a brunt which enables the adherence of black particles on the stone's surface.

Humidity levels in the atmosphere as well as the location of the examined surface (whether the surface is sheltered or unsheltered) not only affect the process of the phenomenon, but the visual aspect of the deterioration as well. More specifically, a weathering form, which is very frequently encountered and affects all the stone types, is the dissolution of carbonate particles on exposed surfaces. Rain's action leads to the dissolution of the carbonaceous salts and as a result to discoloration of the stone as we can observe a green to reddish-brown and yellow layer perfectly

adhering to the skin of the marble. An important factor in the enhancement of the phenomenon described here is the grain size, and the distribution of carbonaceous particles.

The images presented below depict the deterioration patterns (black\white particles), which are encountered on stone surfaces. The aim of the presentation is to estimate the extent of the deterioration patterns as well as the structure of the crusts. It should be mentioned that the images were obtained by using different monitoring systems.

Image 1:

In this FOM image we can observe the co-existence of gypsum crystals and black particles on a crust.
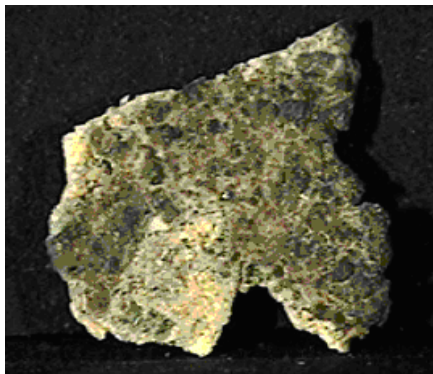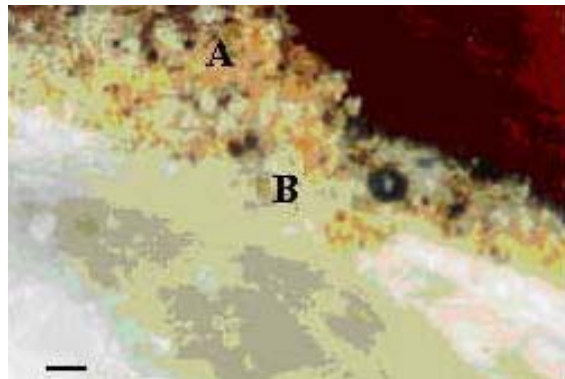
Image 2   **Image 3**

Image 2: *In the image above we can see a crust as it is frequently encountered on stones surfaces and the black particles which where formed by the mechanisms analyzed.* **Image 3:** *Polished cross section of a dendritic crust with an average thickness of 300 μm, with two alteration layers: an external of*

macrocrystalline gypsum (A: 200 μm thick), and an internal one (B: 100 μm thick) of microcrystalline gypsum Pentelic marble, under the polarizing microscope with reflected light (pol. //, 100 X, bar = 100 μm).
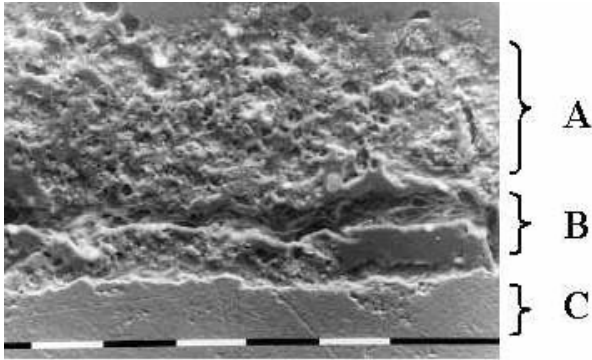
Image 4

Image 4: Polished transverse section of a dendritic crust with an average thickness of 300 μm, with two alteration layers: an external of microcrystalline gypsum (A: 200 μm thick), and an internal one (B: 100 μm thick) of microcrystalline gypsum and calcite on un-weathered Pentelic marble (C), under the SEM (150 X, bar = 100 μm).

1.4   Biodeterioration of Stone Monuments

Besides the chemical deterioration, the microbiological deterioration, caused by microorganisms on the material surfaces is of great importance. Many researchers, until recently demonstrated that numerous heterotrophic microorganisms present on the stonework can utilize, for their growth, the airborne organic compounds settled on the stone surface.[5] Such an observation makes clear that atmospheric pollutants enforces the biodeterioration of stone monuments. Biodeterioration of stone monuments is a well-recognized problem in regions where the environmental factors such as high temperatures, high relative humidity levels, and heavy rainfall favor the growth and sustenance of a wide variety of living microorganisms on stone surfaces. Direct observation of the alterations allowed pointing out the different distribution and the extension of the stains over the litho types. SEM applications evidenced traces of chemical corrosion, which appears differently because of the different granulometry of the litho types. The different decay of the litho types is more evident on the unsheltered regions. In this case we have quantified material loss due to the combined action of pollution and rain, which produced,

12

decohesion of crystal and their removal. Biodeterioration of stone monuments can be briefly classified into 3 broad categories: biophysical, biochemical, and aesthetic deterioration.

Biophysical deterioration of stone may occur due to pressure exerted on the surrounding surface material during the growth or movement of an organism or its parts. Attachment devices, such as hyphae and extensive root systems, penetrate deeply into the stone through preexisting cracks or crevices, causing stresses that lead to physical damage of surrounding stone material. Fragmentation may also occur due to periodic loosening of attachment devices during repeated wet and dry cycles.

The biochemical deterioration of stone due to corrosive metabolites occurs when inorganic and organic acids form. These acids decompose stone minerals by producing salts and chelates, some of which may be subsequently dissolved and washed away. An increased volume of soluble salts or chelates may also cause stresses in the pores, resulting in the formation of cracks. Carbon dioxide, produced by aerobic organisms through respiration, changes into carbonic acid in an aqueous environment. Carbonic acid can dissolve carbonates such as limestone and marble

The aesthetic or visual effects of biodeterioration of stone are conceptually subjective but nonetheless important. The growth of biological populations on stone surfaces alters their appearance due to chromatic alterations and development of biological crusts.[6]

In the following table there is given the phenomenology of biological alterations on stone monuments

Organism	Alteration
Autotrophic bacteria	Black crust, black-brown layers, exfoliation, powdering
Heterotrophic bacteria	*Black crust, black layers, exfoliation, color change*
Actinomycetes	*Whitish gray powder, layers, white efflorescence*
Cyanobacteria	*Patinas and sheets of various colors and consistency*
Fungi	*Colored stains and patches, exfoliation, pitting*
Algae	*Patinas and sheets of various colors and consistency*
Lichens	*Crusts, patches, and pitting*
Mosses and liverworts	*Discoloration, green-gray patches*
Higher plants	*Cracks, collapse, detachment of materials*

1.5   Influence of climate conditions on the deterioration of Stone   Monuments

Some climate factors such as the high temperatures or a wide range in the changes of temperature, humidity and frost are considered to be responsible for the onset or the reinforcement of the erosion. Especially the presence of a temperature not extremely high but of medium values is capable of generating cracks on the stone's surface. This is mainly observed on marbles with a high content of dolomite and Al. As a result the surface of this type of stone is spongy in texture. The atmosphere's humidity reinforces the gradual evolution of the desquamation of the stone. Furthermore, high temperatures are considered to be responsible for the color alternation (weakness) occurring on stone monuments as well as for the formation of alveolate texture. Variations on the degree of corrosion are observed amongst sheltered and unsheltered areas, more specifically it should be noted that in sheltered areas where dry decay phenomena prevail black crusts exhibit anomalous relief and high friability .In the surface of stonework exposed to rain, greater decay phenomena exist .In the vast majority of the cases water leaks and rain wash cause discoloration of the stone and the formation of orange to brown stains which owe their origin to the dissolution of carbonate minerals   as well as the development of the pore skin of the stone which in turn amplifies the moisture's and Aeolian erosion .Rain wash also affects monuments as it leads to a loss of stone mass whilst removing salts formed on the wall .Frost may also play a great role at these areas .

In the following figures we can observe the occurrence of the decay phenomenon whose existence and reinforcement is amplified by the climate conditions.

Image 4. Decay observed accompanied   image 5. Decay observed
By ablation of parts of the stone
Consequent upon mechanical reasons
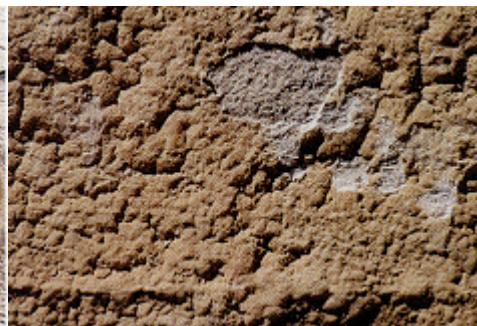
1.6 Deterioration on stone monuments constructed by seldom used litho types

In this section we shall attempt to describe the phenomenology of stone decay as this is observed in monuments constructed by some seldom used lithotypes such as sandstone, soapstone and volcanic stratums as NYT (Neapolitan Yellow Tuff).

Soapstone has been quarried, used and appreciated throughout the world since the dawn of the civilization. This rock is soft enough to be worked so it was used as a material for constructing vessels, moulds and sculpture in general. The most commonly encountered weathering decay observed in soapstone is dissolution of carbonating minerals on exposed surfaces. Stones with large carbonate veins show this type of erosion in a large extent. The quantities and distribution of the carbonate minerals in the stone greatly affect the extent, color and thickness of the crusts observed. As a result the crusts observed range in color from green and green – yellow to brown- black. Another typical weathering form usually encountered is slight to heavy crumbling of the upper surface often combined with growth of lichens. Gypsum is present on soapstone's surfaces and we should mention that gypsum is formed in the more sheltered regions. Gypsum may stem from air pollution or from oxidation of sulphites in the stones. It could be possible that gypsum forms within the micro cracks of the foliated stones, hence contributing to the loss of carved details along foliation planes.

NYT is the stone type constituting many buildings in the ancient city of Naples. There were some key factors, which promoted the use of NYT for building construction. It is the high porosity along with the abundant presence of zeolites in the bonding matrix that makes this rock a good heat and sound insulator. The deterioration is easily recognizable on many important monuments, which are built of NYT and especially in unprotected and unsheltered surfaces. The most common weathering typologies of NYT are:

- *Scaling and exfoliation both due to the action of damp waters through the stone and later crystallization of soluble salts.*

- *Disaggregation: also due to infiltration of water and the consequent dissolution of the constituent phases of the stone.*

- *Crusts, stains, efflorescence extensively present on surfaces subjected to intense dissolution and evaporation of damp waters.*

The sandstone used in monuments can be classified into three types based on the color, texture, chemical composition and constituent mineral. Constituent minerals, porosity and bioactivity can be listed up as the factors controlling the decay of the stone materials used in monuments. The water action is the main cause of the deterioration .In the deteriorated rocks, kaolinite is formed by the hydrolysis of feldspars. The sandstone shows exfoliation, and most relief on the surface is detached. Gypsum is found in varying amounts in almost all deteriorated sandstones. Gypsum often shows a needle-like shape and grows perpendicular to the exfoliation surface. As it is well known, crystallization of gypsum in the interior of stone materials brings cracking to crystallization pressure. Biological alteration of the sandstones leads to discoloration of the exposed surfaces. The yellowish -brown surface of the sandstones is frequently changed to black. This is due to the growth of algae. Many white spots due to lichens are also observed on the sandstone's surfaces.

1.7   Needs for Non-Destructive Evaluation

The presence of deteriorated regions on stone surfaces affects not only the aesthetic view of stonework but also leads to further decay. Gypsum layers and black crusts that prevail on stone surfaces absorb a great deal of humidity and this fact increases its friability and leads to the development of lamellar texture and flaking of the stone. Moreover we should state that humidity's action in combination with the absorption of various metal oxides could lead to the abruption of the crust and extensively in loss of the stone material, discoloration, and aesthetic damage. At this point we should not underestimate the catalyzing function of black particles in the formation of crusts. It is well known by the literature that the presence of black crusts on stone surfaces intensifies the gypsum formation as the metal oxides, which are the main constituents of black crusts, function as catalyzing agents in the oxidation process. Thus gypsum layers and black crusts accelerate the deterioration effects and finally results in the total destruction of the stonework. As it is obvious, the development of methods of chemical cleaning is essential not only for the restoration of the deteriorated regions but also for preventing further erosion phenomena. The cleaning methods applied on stone surfaces should aim at removing pollutants without losing stone material. Thus, in order to develop efficient conservation methods we should have previously determined the type and the extent of erosion. In other words

the diagnosis methods used, should estimate efficiently the thickness of the crusts that prevail as well as the specific locations on the surfaces where corroded regions are encountered. The diagnosis processes used so far are based on assessments of the deterioration state by using chemical methods. More specifically, specimens are obtained from the surfaces under consideration and then these specimens are studied in a chemical laboratory. The process of taking these specimens, which is accompanied by ablation of stone surface, cracks etc, is considered as a destructive process because further to the aesthetic alteration that it causes it also enforces decay phenomena as the internal layers of the stone are more exposed to weathering. Thus it is necessary to develop methods that are non-destructive and can be applied in situ. The diagnosis methods implemented in this work satisfy the above criteria. More specifically images are obtained from the surfaces under consideration via a Monitoring system, and at a further step by applying the Image Processing algorithms on the images studied we extract the specific locations on the image where deteriorated regions prevail. Further to the detection of the co-ordinates of polluted particles, our methods managed also to classify these particles according to their chemical composition and to extract some characteristics concerning their shape, surface size and thickness.

1.8   Brief overview of the work and description of its objectives

The purpose of the current study is to try to detect the phenomenology of decay on stone monuments by using Image Processing techniques. More specifically   a number of different image processing algorithms are being used in order to detect the specific points on the image where brown to black crusts, calcite salts or any other type of erosion occur and study some issues referring to their extension, the mean surface of the crusts which exist in each image, the standard deviation of the surfaces extension around the mean surface as well the number of black particle detected on each images .The preservation of the shape of black particles recognized is an aspect of great importance for the current study. The different types of deterioration encountered on stonework, is the main reason which enforced the current study to   effort a classification of the damage observed, based on the chemical composition of the detected eroded areas.

Prior to our study chemists examined specimens of the stone monument in order to detect the pollutants present on the surfaces as well as to determine the degree of corrosion. The specimens

were taken from pillars of Parthenon and we have samples both of arrises and of cannelures. Further to the process of determination of corrosion type and extent, several chemical methods were applied in an effort to remove signs of deterioration and the effects of each of these methods are noted. Furthermore data have been collected on the type and amount of pollutants that each of the methods used, managed to remove. Our observations revealed that in cannelures we have greater concentrations of black particles and other airborne pollutants because these areas are not affected by the rain's action, while cannelures function as cavities that accumulate pollutants.

A Fiber Optics Microscope monitoring system was used to depict the regions of monuments, which were examined by the chemists, and the image Processing Algorithms developed were applied in an effort to estimate the state of deterioration. Finally the results of this work were compared with the conclusions, which came up during the chemical processing.

A little work has been done in the aspect of detecting texture features on images depicting the deterioration effects on stonework or on works of art in general. There are more articles concerning the quantification of color alteration observed on stonework, old paintings etc. Furthermore, the aspect of detecting texture features was an issue, which was studied in greater extent through the investigation of medical images. The process of detecting infected tissues on medical images is an aspect, which demonstrates many characteristics in common with the detection of decay areas on stone surfaces. In the following sections a brief overview of the related work is presented.

B. Related Work

The conservation of stonework and work of art in general is an aspect of great importance nowadays. The researches are concerning the isolation of the deterioration effects and the development of chemical techniques in aim to restore the degraded regions of an artwork. As it is obvious, the key step in managing an efficient restoration of stonework or an old painting is the accurate diagnosis of the degradation effects. Image Processing techniques are a useful tool for the assessment of the deterioration state, as it guarantees a non-destructing process of sampling and detecting the corrosion conditions. Despite the fact that image-processing techniques can be

used in extracting information about polluted areas in the art works, it is observed that a little work has been done so far. By reading the literature we can see that art conservation and diagnosis methods continue to be an issue of interest for the chemists and mineralogists.

A survey at quantifying the color alteration caused by weathering and observed on stone surfaces was conducted by Lebrun [1]. According to the methodology reported in this research, image-processing techniques were applied on images depicting stone surfaces prior and after accelerated ageing tests. As it came out by the results of this methodology, it managed to give a precise description of the intensity of color deviations. In the Following section some specific image analysis approaches is discussed in a greater extent.

1.9   Image Analysis for Quantitative monitoring of stone alteration

The quantitative description of the behavior of stonework submitted to natural or artificial weathering is a crucial challenge no less scientific than economic [19]. Image analysis techniques were used in order to provide information concerning the quantification of color alteration on dimension stones. The whole procedure consists of techniques that are used in grabbing images of polished granite tiles before and after the accelerated ageing tests and comparing the color alteration. Color alteration is quantified by computing the Euclidean distance in a (pseudo) L*a*b color space.

The imaging system is used for monitoring the tiles before and after the accelerated ageing tests. As any other scientific instrumentation, it induces high frequency noise and drift. In order to remove the noise effects of the images that are studied, each step of the image acquisition is controlled and calibrated. The two main calibration procedures are: Color calibration and positioning calibration. After the calibration processes on the images depicting the specimens under consideration, some image processing techniques are used in order to extract numerical statistical data concerning the color alteration. At first global color deviations are measured on entire tiles in the hue-saturation- intensity space, HSI. This is a bi-conical color space directly deduced from RGB by linear transforms. The relative "before after"differences between mean global values of each channel are computed as follow:

$$dH = \frac{2*(\overline{H}_{out} - \overline{H}_{in})}{(\overline{H}_{out} + \overline{H}_{in})} \qquad dS = \frac{2*(\overline{S}_{out} - \overline{S}_{in})}{(\overline{S}_{out} + \overline{S}_{in})} \qquad dH = \frac{2*(\overline{L}_{out} - \overline{L}_{in})}{(\overline{L}_{out} + \overline{L}_{in})} \qquad (1)$$

With $\overline{H}_{out}$: the mean of hue channel in output image.

These values are convenient for explaining with understanding words the visual observations of global color deviations but they cannot be considered as quantitative measure of these changes. In order to map the quantitative color variation undergone during the accelerated ageing operations one needs to use a perceptually linear space like CIE L*a*b*. The transformation from RGB to **L*a*b*** is a non-linear procedure.

Once the L*a*b* coordinates are computed, the difference between two measured colors is given by the following relation

$\Delta E_{lab} = ((\Delta L^*)^2 + (\Delta a^*)^2 + (\Delta b^*)^2)^{1/2}$.

Where **ΔL^*, Δa^*, Δb^*** are the pixel-to-pixel differences within each of the L*, a*, b* channels before and after accelerated ageing tests. This resulting distance function is mapped in a new image in which the intensity of each pixel is proportional to the computed **L*a*b*** color distance at the corresponding point. In order to have a more quantitative estimation of the global color deviation some statistic values are determined. More specifically, in the resulting image, which depicts the distance function they apply a threshold such that one can extract the most altered zones in the tiles and compute some useful statistics. The statistics measures, which were chosen, are:

- Number of zones
- Relative simulated areas of the zones
- Mean individual size of zones
- Mean color distance computed on the zones only.

The following figure details the flow sheet of the protocol

Image 1 | AGEING PROCEDURES: - water and heat test - Acid test | POSITIONNING CALIBRATION

$$\Delta E_{Lab} = \sqrt{(\Delta L^*)^2 + (\Delta a^*)^2 + (\Delta b^*)^2}$$
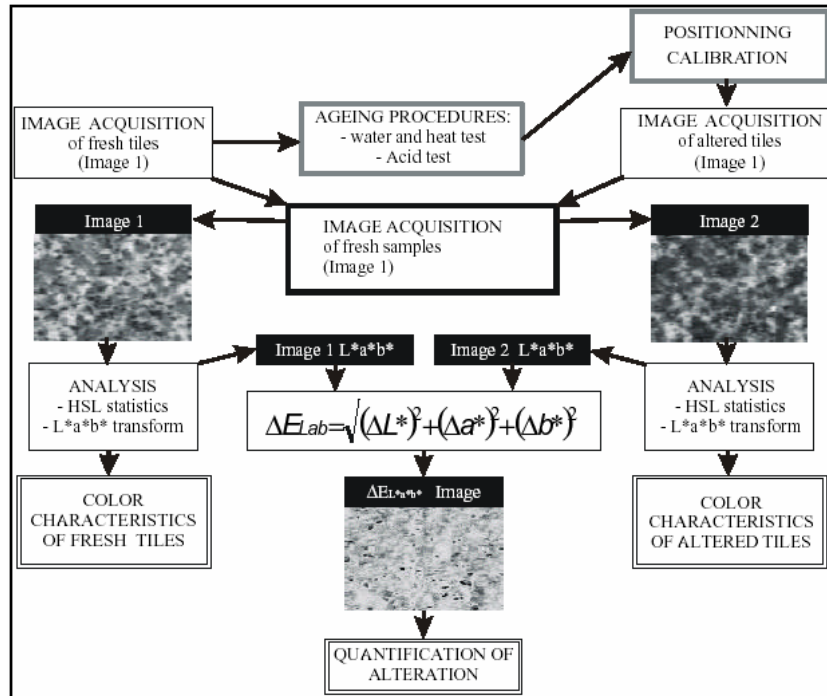
figure 1

1.10 Detection of Triple junction parameters in Microscope images depicting stone surfaces.

Further to the quantification of color alteration due to deterioration, researchers considered as an important issue the detection of cracks on stonework. Sowmya Mahadevan and David Casasent [20] carried out an investigation with the aim of determining grain boundaries on material surfaces. The steps of the algorithm implemented are briefly described below. This Research managed not only to isolate the grain boundaries but also to eliminate noise, which occur near the grain boundaries.

In this work Secondary Electron Microscope images (SEM) are analyzed in an automatic system to provide material properties for fracture analysis. The main objectives of this survey are to locate the grain boundaries and triple junctions (where three grain boundaries meet), to calculate the dihedral angles at triple junctions as well as to obtain grain orientation data.

In order to obtain the desired material science information, the location of each triple junction, the dihedral angle computation and the orientation of the backscatter points is needed. The following lines address the steps followed by the algorithm in order to extract the desired material properties.

- *Grain boundary detection – Initial image noise removal*

- *Geometric Correction*

- *Skeletonize image (produce thin grain boundaries)*

- *Locate triple junctions (TJs) and their angles. Complete all Grain Boundaries (GBs) and reduce the false TJs.*

- *Selection of Electron Back Scatter Pattern (EBSP) probe points*

The real part of a Gabor Filter (GF) function is used

$$G_n(x, y) = \exp\left[-\pi\left(\frac{\chi^2}{\alpha^2} + \frac{y^2}{a^2}\right)\right] * \exp[j * 2 * \pi(ux + vy)]$$

to locate grain boundaries. Since GBs are dark lines on lighter background the image is inverted before applying the GF. Next horizontal and vertical GFs are applied and their outputs are summed. Each 1-D GF detects GBs in a $+\text{-}45^o$ range and hence the summed GF output can locate GBs at all orientations. In order to reduce noise, blob removals are applied. In order to elongate grain boundary fragments and fill in gaps a morphological dilation operation is applied. The above procedure results in having all GB gaps filled in and also pits and precipitates, which are near the GB, are connected, thus the above process produces false grain boundaries lines. A skeletonization algorithm is applied in order to efficiently locate triple junctions [20]

At a further step TJ parameterization is used. This involves line following to locate triple junctions, measures to estimate TJ angles, methods to omit false TJs and filling in grain boundary gaps. These operations are all performed at the skeletonized image.

The skeletonized image is stored as an array of pixels that specifies if each pixel is "on" or "off" and whether the 8 neighbors are "on" or "off". The search of the image starts in the upper left and checks the pixel values. Whether a pixel is "on" and only one of its 8-neighbors is also "on" then this pixel is considered to be grain boundary pixel. On the other hand if a pixel is "on" and more than 2 of its 8-neighbors are also "on" then the pixel under consideration is a TJ pixel. Finally if no other of the 8-neighbors of the pixel is "on" the pixel is an end point. By the procedure described above an amount of false triple junctions is determined due to pits and precipitates near the grain boundaries. Thus the false triple junctions can be removed by

*eliminating all the regions in the image, which are less than **a** pixels in length (the determination of a is depended on the application).*

Several researches have been carried out with the aim of detecting specific features of stones surfaces. These surfaces are frequently related with the distribution of mineral veins observed on marble surfaces as well as with the thickness of these veins and other color characteristics. In the Following section we describe some work carried out in order to study specific features of mineral veins observed on marble surfaces.

1.11 Feature Extraction for Marble Tiles Classification

*The study of feature extraction for marble tiles classification conducted by **Deriven [21]** focuses on color content and vein distribution which are considered to be the main criteria for veins classification. A color Segmentation algorithm is used for the detection of the veins. The shape analysis of the veins is performed by utilizing the distance image. The crucial point for the classification is the distribution of the veins on a marble tile. The veins distribution on a marble tile is a random process. As it is observed, a vein is split into branches and the thickness of the vein changes through the branches. According to this study the classification of the veins is based on the thickness of the branches in a vein. Thus the definition of a vein is done with its color, area, number of branches, thickness of each branch and the contribution of each branch to the total area. The first step in image color segmentation of the tiles is to transform the color space into HSI. After this point, each color band of the resultant image is treated as gray level image. A histogram-based segmentation algorithm is applied to those bands individually. For histogram-based segmentation we have to find global minima of the histograms and locate the lobes of the histogram in order to find a similarity measure between the neighboring pixels. At a further step, a series of averaging and median filters are applied to eliminate high-frequency content of the histograms. Since there exist a few colours in the image we apply the filters iteratively until a certain number of minima are left. Thus each lobe contains pixels that belong to the same segment if they are connected. In order to locate the segments an 8-neighborhood Region Growing Algorithm is applied. After the region growing is completed for each band, we have to combine those regions down, make a post processing of merging the newly generated regions and*

find the resultant segmented image. The color and the area of each vein are calculated at the color segmentation step. In the following we describe the way in which features such as number of branches, thickness of each branch and area of each branch, are defined. As it is reported above, each vein is split into a number of branches with varying thickness and color intensities. In these cases the color and the thickness is measured separately for each branch. For this purpose a graph is used which is obtained from the distance image. The map may be called as the "perimeter percent graph". The value of the graph at distance d, is defined as

$$g(d) = \frac{Md}{\sum_{i=d}^{D} Mi} \times 100$$ *Where Md is the number of pixels at distance d and D is the maximum*

distance for the segment. The name "perimeter percent graph" comes from the fact that Md is the perimeter length for distance d. When a segment is composed of branches with varying thickness this introduces local minima in the "perimeter percent graph". The local minima occur when a certain branch is completely eroded. Therefore the distance value at the minima point also indicates a thickness measure for that branch. For the calculation of the percentage of each branch the process followed is: At first we count the pixels up to the depth of the branch and then subtracting the pixels contributing from other branches.

Genetic algorithms have been used for extracting texture information concerning medical images, or images displaying ornamental stones surfaces. In the following paragraphs it is given a report on the various investigations carried out so far with the aim of using Genetic Algorithms to achieve texture or color based segmentation.

1.12 Image Color Segmentation by Genetic Algorithms

Segmentation of color image composed of different kinds of texture regions can be a hard problem, namely to compute for an exact texture fields and a decision of the optimum number of segmentation areas in an image when it contains similar and/or unstationary texture fields. In many real world applications data clustering constitutes a fundamental issue whenever behavioral or feature domains can be mapped into topological domains. Genetic Algorithms have been used to the clustering of small regions in color feature space. More specifically, Genetic

Algorithms have been used in the color image segmentation in applications concerning Ornamental Stones and in Human Skin Mark.

Recently, researchers have investigated the application of Genetic Algorithms (GA,[4,5,6]) into the image segmentation problem. Perhaps the most extensive and detailed work on GAs within image segmentation is that of Bhanu and Lee [25]. One reason (among others) for using this kind of approach is mainly related with the GA ability to deal with large, complex search spaces in situations where only minimum knowledge is available about the objective function. Another situation wherein GAs may be a useful tool is illustrated by the work of Yoshimura and Oe [26]. In their work, the two authors formulated the segmentation problem upon textured images as an optimization problem, and adopt GAs for the clustering of small regions in a feature space, using also Kohonen's self organizing maps (SOM). They divided the original image into many small rectangular regions and extracted texture features from the data in each small region by using the two-dimensional autoregressive model (2D-AR), fractal dimension, mean and variance. In other example, Bhandakar et al.[27] defined a multi-term cost function, which is minimized using a GA-evolved configuration. The idea was to solve medical image problems, namely edge-detection. In their approach to image segmentation, edge detection is cast as the problem of minimizing an objective cost function over the space of all possible edge configurations and a population of edge images is evolved using specialized operators. Another very interesting work is this of Andrey [19]. The image to be segmented is considered as an artificial environment wherein regions with different characteristics according to the segmentation criterion are as many ecological niches. A GA is then used to evolve a population of chromosomes that are distributed all over this environment. Each chromosome belongs to one out of a number of distinct species. The GA-driven evolution leads distinct species to spread over different niches. Consequently, the distribution of the various species at the end of the run unravels the location of the homogeneous regions on the original image.

1.13 Image Processing Techniques used for the detection and restoration of degraded regions in old paintings

Further to diagnosing the degradation state that prevails on stonework researchers have investigated the deterioration effects observed on old paintings.

Kokla, Psarrou and Konstantinou [20] made an effort to relate the distribution of watercolor/ink intensity, under visible and infrared radiation, with the color alteration of old paintings. In the aspect of old paintings restoration, M.Pappas and I. Pitas [21] introduced several image processing techniques with the aim of restoring the degradation effects caused by weathering. More specifically the task, which was implemented in this work, was the production of an estimate of the painting without the existence of the degradation regions.

The restoration problem is stated as follows: Let's suppose that s is the original image and $= ( ) +$ *is the degraded one, where g(.) is the degradation function and **n** is the observation noise. If the available cleaned and degraded samples, s_i and x_i respectively, are equal to **N** (i = 1…N) then the problem is reduced to perform a blind estimation s^ that would minimize the mean square error MSE.*

$$\mathbf{MSE} \approx \frac{1}{\mathbf{N}} \times \sum_{\mathbf{n=1}}^{\mathbf{N}} \left\| \mathbf{sn} - \hat{\mathbf{s}}\mathbf{n} \right\|^2 = \frac{1}{\mathbf{N}} \times \sum_{\mathbf{n=1}}^{\mathbf{N}} \left(\mathbf{sn} - \hat{\mathbf{s}}\mathbf{n} \right)^{\mathsf{T}} \left(\mathbf{s_n} - \hat{\mathbf{s}}\mathbf{n} \right)$$

The First method, which was discussed, was the linear approximation in order to find the estimated image $\hat{s}$.

1.13.1 Linear Approximation

It is assumed that the color of a pixel is denoted by x= [x1, x2, x3] where x1, x2, x3 corresponds to the L*, a*, b* color space coordinates of the point respectively. The available samples of the oxidized and cleaned regions are denoted by xi and si respectively (i=1…N). For each degraded observation x the estimate s^ is given by the equation s^= f(x). Where f(x) is of the form: f(x) = (A+I)x

- *I is the 3x3 identity matrix*
- *A is a 3x3 coefficient matrix A=[a1 a2 a3]^T*

Another approach is based on the fact that an object may look different under different lighting conditions.

1.13.2 White point Transformation

If a clean sample and its oxidized version were viewed under the same lighting conditions different CIEXYZ (and consequently CIELAB) values would be recorded. Instead of trying to produce an estimate of the color difference for corresponding clean and oxidized samples, an assumption is made that both of the samples have similar CIEXYZ values. Thus the difference in appearance is attributed solely to the different white points used for the color estimation. If by s is denoted a vector representing the clean sample and X_{XYZ} denote the vector that contains the corresponding oxidized sample then the mapping from one color space to the other can be represented by the nonlinear operator T of the form.

$$\mathbf{x} = \mathbf{T}\{\mathbf{X}_{XYZ}; \mathbf{W}_{XYZ}\}$$

Where T{.;.} denotes the nonlinear transformation from CIEXYZ to CIELAB and W_{XYZ} is the white point tristimulus values vector. Thus, a white point vector W_{XYZ} is determined, which after the substitution into the above equation yields an estimate $\hat{s} = T\{X_{XYZ}; W_{XYZ}\}$ of the clean sample. Given the sample mean vectors $\hat{m}_{xxyz}$ of the oxidized samples, the error can be expressed as

$$e = \hat{m}_s - T\{\hat{m}_{XXYZ}; W_{XYZ}\}$$

Radial basis functions are also used in order to determine the estimate of the cleaned image s^. The estimate $\hat{s}$ is given by the equation $\hat{s} = f(x)$.

$$f(x) = \sum_{m=1}^{M} w_m \varphi(\|\mathbf{x} - \mathbf{t}_m\|)$$

Where $\{\varphi(\|\mathbf{x} - \mathbf{t}_m\|) m = 1 \cdots M\}$ is a set of M arbitrary functions, which are known as radial basis functions with corresponding centers $\mathbf{t}_m$ and weights w_m.

The results of this study evidenced that the linear approximation method and the white point transformation gave good results due to the smoothing nature of the methods.

Texture and color segmentation algorithms were also used in many medical applications. Furthermore the medical problem of detection of micro-calcifications in mammograms shows many similarities with the problem that we consider. For this reason, we also provide a short review on the approaches directed towards this problem.

1.14 Image Processing Methods used for the detection of Micro-calcifications in mammograms

The efficient detection of micro-calcifications in mammogram images is an aspect, which caused the interest of many researchers in the recent years. It was evidenced that the efficient and early detection of micro-calcification locations is vital to manage a remedy. Further to the determination of the exact locations were micro-calcifications prevail the shape and the arrangement of the micro-calcifications is also studied as it helps the radiologist to judge the likelihood of cancer being present.

Carmen Serrano [22] introduced an Image Filtering method for the accurate detection of micro-calcifications. More specifically, a high-pass filtering process was used in order to extract the micro-calcification. Considering the small size of micro-calcifications it is evident that a low-pass filter with a wide kernel could remove them from the image while conserving a background of high density. Conversely a high-pass may be used to detect micro-calcifications. Serrano used a high-pass filter of the form f(n)=1-g(n) where by g(n) it is denoted a low-pass Gaussian filter. The filter support region is depended on the image resolution. In order to improve the false positive and false negative ratios Shen et al. ([23]) used a region-growing algorithm to detect micro-calcifications in mammogram images. The region Growing Algorithm starts by selecting all the pixels above the median gray level of the mammogram as seed pixels. For each seed, the 4-connected neighbors are checked for inclusion with the following condition.

$$(1-t)*\frac{(F_{max}+F_{min})}{2} \leq p(i,j) \leq (1-t)*\frac{(F_{max}+F_{min})}{2}$$

Where p(i,j) is the pixel being checked, Fmax and Fmin are current maximum and minimum pixel values of the region being grown, and t is the region growing tolerance parameter. The tolerance is varied between 0.01 and 0.4, with a step equal to the inverse of the seed pixel value. Features are extracted for regions grown for each value of the tolerance. The value that introduces the least change in the features from one step to the following one is chosen as the optimal tolerance, and the corresponding regions and features are retained for further analysis. Finally a region grown is treated as a micro-calcification if its size in pixels meets the condition 1<T<35. This requirement is in view of the physical size of actual micro-calcifications. In order

to reduce the computational time and to improve the false positive ratio and detection accuracy a seed selection method was used ([22][23]) for subsequent region growing. The method consists of a 2-d linear prediction error filter [24] .A pixel is selected as seed for the region growing algorithm if its prediction error is greater than an experimentally determined threshold.

1.15 Computer-Aided Diagnosis of the Micro-calcifications

M.F. Salfity [25] presented methods of detecting and segmenting micro-calcifications by using a combination of Gaussians spot detector and of a top-hat transform as described by Dengler et al.[26] For both filters the resulting image is segmented with threshold based in the noise of the image. The Gaussian detector is a good detector but does not preserve the shape of the spots, while the morphological filter preserves the shape of the spots but gives a higher positive rate. The combination of the results of the two filters guarantees both preserved shape and low false positive rate. Not only individual micro-calcification shape but also cluster size and shape are important features for the classification process.

Difference of Gaussian filtering consists of several steps. First the original image f(x,y) is low-pass-filtered using a Gaussian kernel with standard deviation σ equal to 4 pixels.

$$f1(x,y) = f(x,y) - G_{\sigma=4}[f(x,y)]$$

Difference of Gaussian filtering consists in the subtraction of one smoothed version of an image from another having a different degree of smoothing. Two Gaussian kernels with different standard deviations used to smooth the images. The standard deviations were chosen to reflect the micro-calcifications dimensions and the inter-calcification distance. The weighted version of the difference of Gaussian method was used assigning a weight of 0.8 to the kernel of larger width. This procedure is applied to the background subtracted image f1.

$$F2(x,y) = 0.8 * G_{\sigma=6}[f1(x,y)] - G_{\sigma=0.25}[f1(x,y)]$$

The images resulted from the morphological and Gaussians operations were segmented by using the following process: The standard deviation of the filtered image was calculated and a first threshold equal to k1 times this standard deviation was applied. Afterwards, the standard deviation was recalculated using only the pixels that were under the initial threshold. The final threshold was set as k2 times the recalculated standard deviation. The images obtained by these operations (Gaussian and Morphological) were then combined by a conditional thickening

operation (Dengler 1993) [26]. This morphological operation extends a spot detected by the Gaussian filter until the boundaries of the spot detected by the top-hat transform are reached. Spots merged by the morphological filter are separated, and the shape of the calcifications is preserved.

1.16 Automated Detection and Enhancement of Micro-calcifications by Using Nonlinear sub-band Decomposition

In this method [27] the nonlinear image analysis structure is briefly reviewed and it is shown that the choice of the nonlinear image decomposition structure, filters and their region of support is determined according to the characteristics of micro-calcifications. At first a nonlinear image decomposition structure was used which consisted of 2 nonlinear filters H and G and they produce the low-band signal, y_a and the detail-signal, y_d from the input signal x as follows.

$$y_d[n] = x[n] - H(x[n]) \quad \textbf{(1)}$$

$$y_a[n] = x[n] + G(y_d[n]) \quad \textbf{(2)}$$

The nonlinear filter H is chosen as a median filter with a region of support equal to 21x21. Such a filter completely eliminates impulsive micro-calcification regions while retaining the approximate base level. Other nonlinear filters such as erosion and a-trimmed mean type filters can also be used for the H-filter. The nonlinear filter G, on the other hand, can be selected so that $y_a[n]$ is an enhanced version of the original image.

According to this method the detection process is carried out into two steps. First the detail image is divided into overlapping square regions. In these regions, skew-ness and kurtosis, measures of the asymmetry and impulsiveness of the distribution are estimated. If a region has high positive skew-ness and kurtosis then it is marked as a region of interest. In the second stage an outlier labeling method is used to find the locations of the micro-calcifications in theses regions. This two-step procedure decreases the computational complexity because instead of searching the whole image, only the regions with high susceptibility are processed.

Skew ness and kurtosis are higher order statistical parameters. Their mathematical definition is apposed below.

$$\gamma_3 = \frac{E\left[(x - E[x])^3\right]}{\left(E\left[(x - E[x])^2\right]\right)^{\frac{3}{2}}} \quad \textbf{(3)} \qquad \gamma_4 = \frac{E\left[(x - E[x])^4\right]}{\left(E\left[(x - E[x])^2\right]\right)^2} - 3 \quad \textbf{(4)}$$

By the term γ3 is denoted the skew-ness while by γ4 is denoted the kurtosis.

2 *IMPLEMENTATION*

2.1 Preliminary Issues

In this section we present the data acquisition method and provide the theoretical background of the tools that are used to enhance the images.

2.1.1 Data Acquisition

*The data set used in this work was obtained by a **Fiber Optics Microscope** Monitoring system. The images, which were obtained by this Monitoring system, demonstrate efficiently the texture of stone surface as well as the presence and distribution of grains. The images under consideration have been classified into some categories according to criteria relative with the study of the current issue by a physical point of view .The criteria of this classification are defined in the following chapter (chapter 3). The methods, which we implemented in order to detect and segment deterioration effects, are known in the laboratory as methods mainly, used for the detection of micro-calcifications in mammograms. The main reason, which enforced us to apply these methods in our images, was the fact that the two issues demonstrate many common characteristics. More specifically we can say that in both cases, the objects of interest are very small. They are visible as bright or dark spots respectively. These small objects are in an inhomogeneous background .The background structure may be brighter/darker in some parts of the image than the white/black particles in other parts. Another characteristic, which is observed both in mammograms and in images of stone surfaces obtained by the FOM system is the typically low contrast of the spots under consideration to the background, this contrast is sometimes close to the noise caused by the inhomogeneous background. Obviously the aim must be to be as sensitive as possible to the systematic variations caused by the presence of white or black spots while suppressing those random variations caused by noise. The images studied here are in grayscale mode.*

In the following section we will attempt to provide some theoretical background in order to make the process of understanding the detection and segmentation methods easier.

2.1.2   Image Filtering

Filtering is a technique for modifying or enhancing an image. For example we can filter an image to emphasize certain features or to remove other features.

2.1.2.1 Enhancement by Image Filtering

Enhancement in the frequency domain in principle is straightforward. We simply compute the Fourier transform of the image to be enhanced, multiply the result by a filter transfer function, and take the inverse transform to produce the enhanced image. The ideas of blurring by reduction of high frequency content or of sharpening by increasing the magnitude of high frequency components relative to low frequency components come from concepts directly related to the Fourier transform.

2.1.2.2 Low-pass Filtering

Edges and other sharp transitions (such as noise) in the gray levels of an image contribute significantly to the high frequency content of its Fourier transform. Hence blurring is achieved in the frequency domain by attenuating a specified range of high frequency components in the transform of a given image.

$$G\ (u,v) = H(u,v)F(u,v) \quad (1)$$

Where F (u,v) is the Fourier transform of an image to be smoothed . The problem is to select a filter transfer function H (u, v) that yields   G(u,v) by attenuating the high frequency components of F(u, v).The inverse transform will yield the desired smoothed image g(x,y). A 2-D ideal low-pass filter (ILPF) is one whose transfer function satisfies the relation

$$H(u,v) = \begin{cases} 1, & \text{if } D(u,v) \le D0 \\ 0, & \text{if } D(u,v) \ge D0 \end{cases} \quad (2)$$

Where Do is a specified nonnegative quantity, and D (u, v) is the distance from point (u, v) to the origin of the frequency plane, that is D(u, v) = (u² + v²)^{1/2}.   The point of transition between H (u, v)=1 and H(u, v)=0 is often called the cutoff frequency.

2.1.2.3 High-pass Filtering

In the previous section we showed that an image could be blurred by attenuating the high-frequency components of its Fourier transform. Because edges and other abrupt changes in gray levels are associated with high frequency components image sharpening can be achieved in the frequency domain by a high-pass filtering process, which attenuates the low frequency components without disturbing high frequency information in the Fourier transform. A 2-D ideal high-pass filter is one whose transfer function satisfies the relation

$$H(u,v) = \begin{cases} 0, & if \ \ D(u,v) \le D0 \\ 1, & if \ \ D(u,v) \ge D0 \end{cases} \quad \textbf{(3)}$$

Where D0 is the cutoff distance measured from the origin of the frequency plane. This filter is the opposite of the ideal low-pass filter. A high pass filtered image can be computed as the difference, between the original image and a low-pass filtered version of that image; that is ,

High-pass = Original – Low-pass **(4)**

*Gaussian filter is a low-pass filter, which is very frequently used as described by the equation (4) in order to detect edges spots and other abrupt changes in gray levels. F**igure (2.1)** shows a perspective plot of the frequency response of a Gaussian filter. And as it is clear this filter passes low frequencies and attenuates high frequencies.*
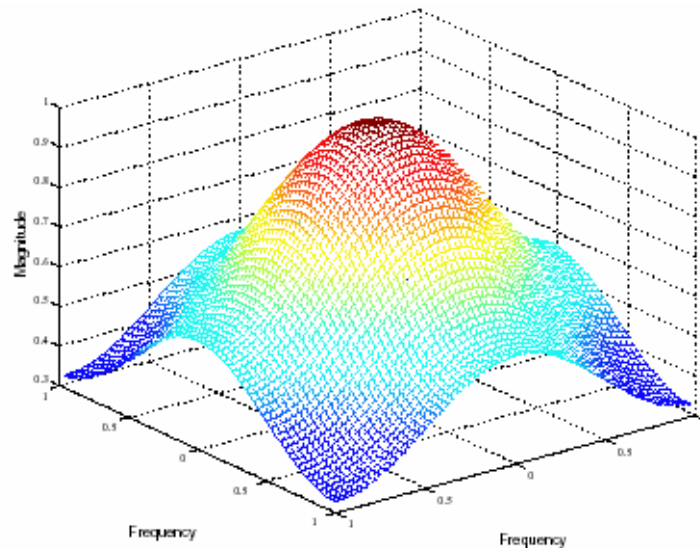
Figure 2.1
In practice, small spatial masks are used considerably more than the Fourier transform because of their simplicity of implementation and speed of operation.

*Spatial filtering is a neighborhood operation, in which the value of any given pixel in the output image is determined by applying some algorithm to the values of the pixels in the neighborhood of the corresponding input pixel. A pixel's neighborhood is some set of pixels, defined by their locations relative to that pixel. Linear filtering is filtering in which the value of an output pixel is a linear combination of the values of the pixels in the input pixel's neighborhood. Linear filters are based on concepts which state that the transfer function and the impulse or point spread function of a linear system are inverse Fourier transforms of each other. Regardless of the type of linear filter used (low-pass, band-pass, high-pass), however the basic approach is to sum products between the mask coefficients and the intensities of the pixels under the mask at a specific location in the image. Figure 2.2 shows a general 3x3 mask. Denoting the gray levels of pixels under the mask at any location by **z1, z2...z9** the response of a linear mask is*

R = w1z1 + w2z2 + . . .+w9z9 .

w1	*w2*	*w3*
w4	*w5*	*w6*
w7	*w8*	*w9*

Fig 2.2   A 3x3 mask with arbitrary coefficients

Gaussian's filter function in the spatial domain is described by the following equations:

$$\mathrm{hg(n_1, n_2)} = \frac{\exp\left[-\left(\left(n_1 - s\right)^2 + \left(n_2 - s\right)^2\right)\right]}{2 * \sigma^2}$$

$$h(n_1, n_2) = \frac{hg(n_1, n_2)}{\sum\limits_{n1}\sum\limits_{n2} hg(n_1, n_2)}$$

n_1, n_2 denotes the coefficients co-ordinates in the spatial mask, sigma denotes the standard deviation and s = (hsize+1)/2. In image detection tasks sigma and filter size are properly defined such that the edges are not eliminated by the application of the small spatial mask.

2.1.3 Morphology

Mathematical morphology is a very important tool for extracting image components that are useful in the representation and description of region shape, such as boundaries, skeletons, and convex hull. We also are interested in morphological techniques for pre or post processing, such as morphological filtering, thinning, and pruning.

Mathematical morphology offers a unified and powerful approach to numerous image-processing   problems. Sets in mathematical morphology represent the shapes of objects in an image. For example, the set of all black pixels in a binary image is a complete description of the image. In binary images, the sets in question are members of the 2-D integer space Z^2, where each element of a sample is a 2-D vector whose coordinates are the (x, y) coordinates of a black pixel in the image. Gray-scale digital images can be represented as sets whose components are in Z^3. In this case, two components of each element of the set refer to the coordinates of a pixel, and the third corresponds to its discrete intensity value. Sets in higher dimensional spaces can contain other image attributes, such as color and time varying components.

The two basic morphological operations are dilation and erosion. In the following sections we will attempt to describe the morphological operations mentioned above.

2.1.3.1 Dilation

*Gray-scale dilation of f **by b,** denoted   f⊕b, is defined as*

$$f \oplus b = \max\{f(s-x, t-y) + b(x, y) | (s-x), (t-y) \in Df; (x, y) \in Db\} \text{ (5)}$$

Where Df and Db are the domains of f and b, respectively .We denote by b the structuring element of the morphological process but note that b is now a function rather than a set. Because dilation is based on choosing the maximum of (f+b) in a neighborhood defined by the shape of the structuring element, the general effect of performing dilation on a gray-scale image is two fold: (1) if all the values of the structuring element are positive, the output image tends to be brighter than the input; and (2) dark details either are reduced or eliminated, depending on their values and shapes relate to the structuring element used for dilation. Dilation is commutative, so the alternative approach of interchanging f and b can be utilized to compute b⊕f .The result is the

same, and b now is the function translated. Dilation is a factor of extension and it tends to erode the holes and extend the acres of the item under consideration.

An essential part of the dilation and erosion operations is the structuring elements used to probe the input image. Two-dimensional or flat structuring elements consist of a matrix of 0's and 1's typically much smaller than the image being processed. The center pixel of the structuring element called the origin, identifies the pixels of interest .The pixels in the structuring element containing 1's define the neighborhood of the structuring element. These pixels are also considered in the dilation or the erosion processing.

The following figures illustrate structuring elements.

0	0	0	1	0	0	0
0						0
0	1	1	1	1	1	0
1	1	1	1	1	1	1
0						1
0	0	1	1	1	0	0
0	0	0	1	0	0	0

Figure 2.3 (a)

1	1	1	1	1
1	1	1	1	1
1	1	1	1	1
1	1	1	1	1
1	1	1	1	1
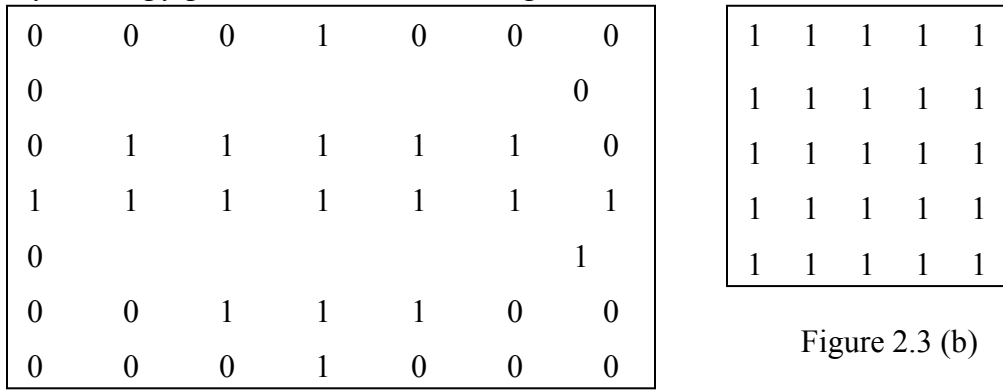
Figure 2.3 (b)

Figure 2.3(a) Diamond shapped element,(b) square shaped structuring element

2.1.3.2 Erosion

Gray-scale erosion, denoted fΘb, is defined as

$$f\Theta b = \min\{f(s+x,t+y)-b(x,y)|(s+x),(t+y)\in Df;(x,y)\in Db\} \ (6)$$

Where Df and Db are the domains of f and b, respectively. As it can be observed equation (6) is like that of 2-D correlation with the min operation replacing the sums of correlation and subtraction the products of correlation. As it is indicated in the same equation, erosion is based on choosing the minimum value of (f-b) in a neighborhood defined by the shape of the structuring element .The general effect of performing erosion on grayscale images is two-fold: (1) if all the elements of the structuring element are positive, the output image tends to be darker than the input image; and (2) the effect of bright details in the input image that are smaller in "area" than

the structuring element is reduced, with the degree of reduction being determined by the gray-level values   surrounding the bright detail and by the shape and amplitude values of the structuring element   itself .As before ,dilation   and erosion are duals with respect to function complementation and reflection. That is

$$(f\Theta b)^c(x, y) = \left(f^c \oplus \hat{b}\right)(x, y) \qquad (7)$$

Where $f^c = -f(x, y)$ and $\hat{b} = b(-x,-y)$ .Except as needed for clarity ,we simplify the notation in the following discussions by omitting the arguments of all functions.

Figure 2.4 demonstrates the results obtained after the dilation and erosion operations are applied onto an image.

| *(a)* | *(b)* | *(c)* | *(d)* |
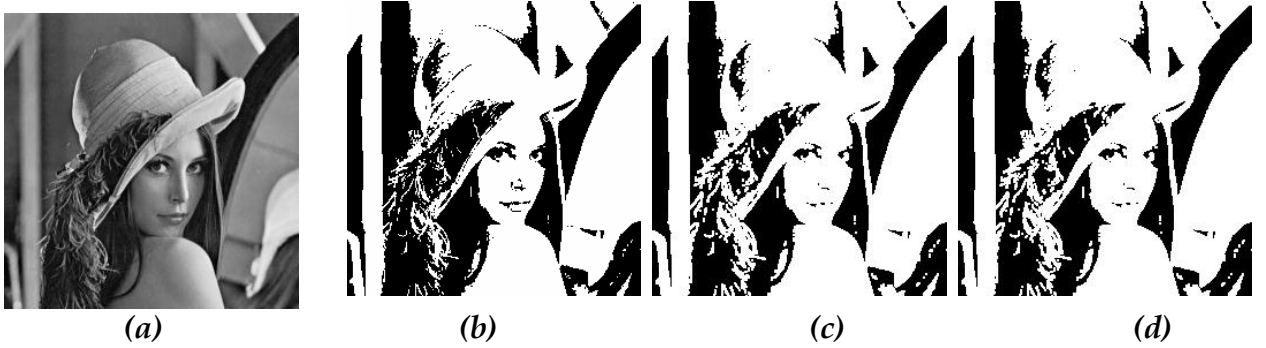
Figure 2.4

***Figure 2.4(a):** Original image, **(b):** The original after the application of a threshold, **(c):** Dilated image by using a square structuring element with dimensions a=2, **(d):** Eroded image by using a square structuring element with dimension a=2*

Dilation and erosion are frequently used in combination in order to implement image-processing operations. The most usually encountered combined morphological operations are opening and closing. The expressions for opening and closing of gray-scale images have the same form as their binary counterparts. The opening of image f by structuring element b denoted f °b, is

$$f \circ b = (f\Theta b) \oplus b \quad (8)$$

As it can be seen, opening is simply the erosion of f by b followed by a dilation of the result by b. Similarly, the closing of f by b, denoted f•b = (f $\oplus$ b)Θ b. The opening and closing of closing of images are dual with respect to complementation and reflection. That is,

$$(f \bullet b)^c = f^c \circ \hat{b} \qquad (9)$$

Because fc = - f(x,y) equation (9) can also be written in the following form $-(f \bullet b)^c = \left(- f^c \circ \hat{b}\right)$. As it is clear from the above light and dark structures are treated differently by the

*morphological operations. Their important property is idempotence. Therefore a single filter operation defines a processing state, which is not changed by the successive application of the same filter. Opening and closing of images have a simple geometric interpretation. Suppose that we view an image function f(x,y) in 3-D perspective (like a relief map), with the x and y axes being the usual spatial coordinates and the third axis being brightness (that is values of **f**). In this representation, the image appears as a discrete surface whose value at any point (x,y) is that of **f** at those coordinates .Let us now assume that we want to open **f** by a structuring element , **b**. Then the mechanics of opening f by **b** may be interpreted geometrically as the process of pushing the element against the underside of the surface while at the same time rolling it so that the underside of the surface is traversed. The opening, f° b then is the surface of the highest points reached by any part of the sphere as it slides over the entire undersurface of f .As for the closing operation, the structuring element .In other words, this means that positive peaks with surface smaller than the structuring element are removed by the opening operation. Due to the semi-continuous character of the opening operation it is very sensitive to negative noise peaks in the gray-level surface. Therefore the opening has to be preceded by suitable conditioning which can be either smoothing or a morphological closing operation with a smaller structuring element. The so-called morphological top-hat transform of an image, denoted h is defined as $h = f - (f \circ b)$ where, as before, **f** is the input image and b is the structuring element function. This transform is useful for enhancing detail in the presence of shading. Figure 2.5 shows the results of performing the morphological operations discussed above on the image 2.4(a).*

(a)   *(b)*   *(c)*

Figure 2.5

Figure 2.5 (a) *Result of performing morphological opening on the image 2.5(a) using a disk of radius 5 as a structuring element,* **(b)** *Closing,* **(c)** *tophat transform*

In the following sections the algorithms implemented in this work are described. First of all the High Pass filtering Algorithm is being described.

2.2   High-pass Filtering Algorithm

2.2.1   Introduction

The first method discussed is high-pass Filtering. Considering the small size of the black/white spots present on stones surfaces, it is evident that a low-pass filter with a wide kernel can remove them from the image while conserving a background of high density in the image. Conversely, a high-pass filter may be used to detect dark/white particles .A high-pass filtered image may be derived as the difference between the original and a low-pass filtered version of that image; this can be written as follows:

$$High\text{-}pass = Original - Low\text{-}pass$$

As a low pass filter a Gaussian filter with a wide kernel is used. The parameters of the Gaussian filter are chosen to be suitable for the detection of the decay areas. After the high-pass filtering the result images are thresholded in order to extract the black/white spots.

2.2.2   Implementation Analysis

The high pass filtering of the images under consideration is performed by evaluating the difference given by the following equation:

$$High\text{-}pass = Original - Low\text{-}pass$$

As a low-pass filter we employ a Gaussian filter. In order to ensure that the filter does not eliminate any black/white particle, a variance of 2.75 and a filter support of 21x21 pixels were chosen. The high-passed image is then thresholded for extracting the regions of the image where black/white spots occur. In order to determine the thresholds on the image we calculate the histogram of the high passed image. The form of the histogram is quite similar to the Gaussian function representation; the thresholds were determined to be located at the edges of the histogram. Figure 2.6 illustrates the original image; the highpassed image, the histogram extracted from the highpassed image and finally the spots detected on the image after the thresholds were applied.
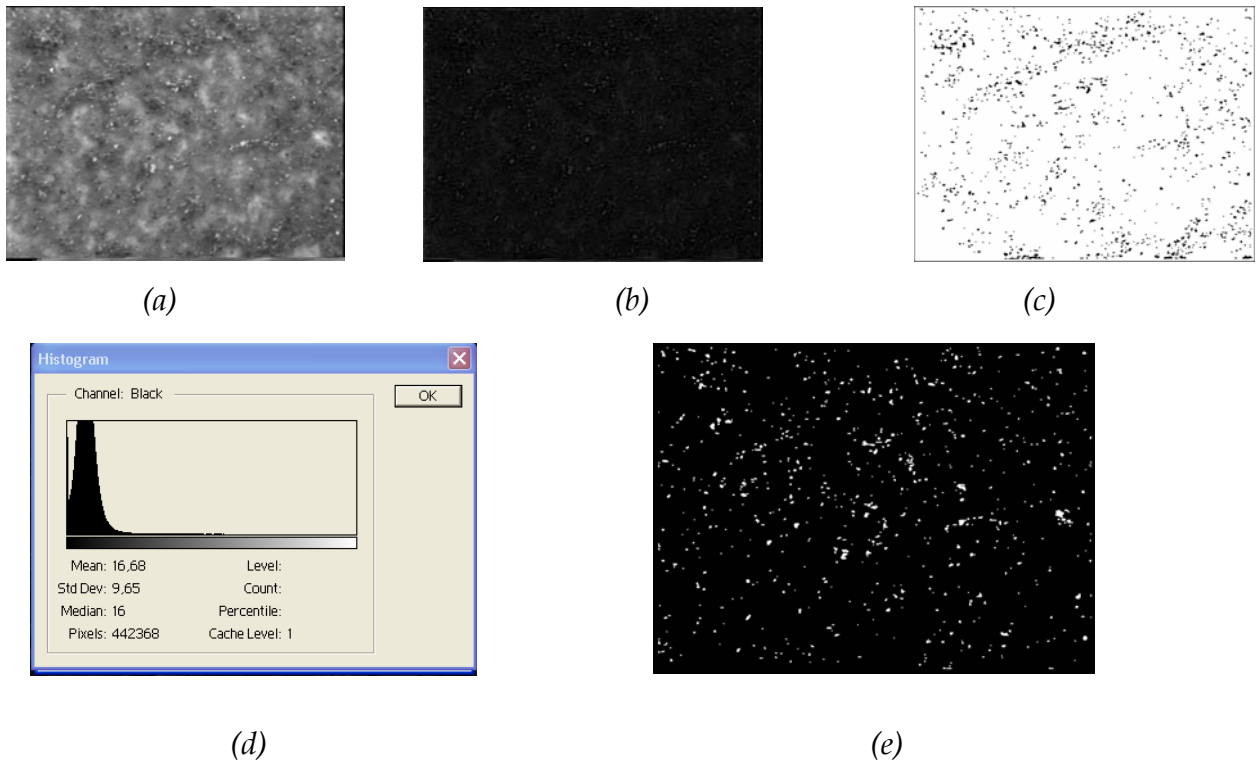
(a)   *(b)*   *(c)*

(d)   *(e)*

Figure 2.6

Fig 2.6(a) illustrates the original image, (b) High-passed image, Figure 2.6(c) depicts the regions of the image where black particles occur (d) histogram of the high-passed image, 2.6(e) black particles detected on the image.

The thresholds applied in the high passed image is th1 = 10 for the detection of dark spots and th2= 47 for detecting white particles. This means that all the pixels in the image with intensity values lower than th1 are considered to compose the black particles while pixels with values greater than th2 are defined as white spots. An attempt to modify the threshold values led to the presence of more false positives or false negative spots. By observing the images obtained after the application of thresholds we can ascertain the existence of lines, spots, and other details, which do not correspond to problematic areas, thus, it is considered essential the use of morphological filters in order to remove the noise from the images. The method described above does not take into account the local gray value variations. This reduces the accuracy of the method as the false positives and the false negatives are increased.

We should improve the capability to detect black and white particles, especially those immersed in inhomogeneous background regions. Therefore we propose an automated detection and

enhancement method by using nonlinear sub-band decomposition. We shall analyze this method in the following section.

2.3   Sub-band Decomposition Algorithm

2.3.1   Introduction

The image is first passed through a high-pass filter as it is described in the previous section. Which means that the high-pass filtered image is obtained as the difference between the original image and an image filtered by a low-pass Gaussian filter .The filter's parameters such as the variation and the region of support are determined such that the filter to eliminate impulsive "problematic" regions while to approximate the base level. In this study a variation of 2.75 and a region of support of 21x21 pixels were selected. The result image of this process is called detail image. Since black or white particles are small isolated regions they produce outliers in the detail image. The problem is then reduced to that of detecting outliers in the detail image. The detail image is first divided into non-overlapping square regions in which the skewness and kurtosis as measures of the asymmetry and impulsiveness of the distribution are estimated. A region with high positive skewness and kurtosis is marked as a region of interest. Then, the box plot outlier detection method is used to find the locations of the spots (black/white) in the susceptible regions. Nonlinear filters such as median filters have been previously used in order to receive the detail image. These methods were used by Chang et.al for the detection of micro-calcifications in mammograms.

2.3.2   Statistical Detection

In this method the detection is carried out in 2 steps. In the first step the image is divided into non-overlapping square regions. The images dimensions are 576x768 pixels and the size of the square regions were chosen to be 41x41. The extent of the square regions should satisfy some basic criteria, such as the dimensions should be quite large such that the regions of interest (black/white particles) not to be eliminated, while, on the other hand we should not select a very extensive square region as it is important to take into consideration the specific characteristics of the local background. In each of the areas decomposed we extract the histogram .In these regions, skewness and kurtosis, measures of the asymmetry and the impulsiveness of the distribution are

estimated. If a region has high positive skewness and kurtosis then it is marked as a susceptible region. This means, that it is quite possible to find black or white particles in these regions. In a further stage, an outlier labeling method is applied in the susceptible regions to find the locations of interest. As it is clear by the brief description of the algorithm, this procedure significantly decreases the computational complexity because instead of searching the whole image for outliers, only the regions with high susceptibility are processed by the outlier labeling method.

2.3.3 Skewness and Kurtosis Based Tests

Skewness and kurtosis are higher order statistical parameters. For a random variable X the skewness is defined as

$$\gamma_3 = \frac{E\left[(x - E[x])^3\right]}{\left(E\left[(x - E[x])^2\right]\right)^{\frac{3}{2}}} \quad \textbf{(1)}$$

And is a measure of the asymmetry of the distribution. An estimate of the skewness is given by:

$$\hat{\gamma}3 = \frac{\sum_{i=1}^{N}(x_i - m)^3}{(N-1)\sigma^3} \quad \textbf{(2)}$$

Where m and σ are the estimates of the mean and standard deviation over N observations xi (i=1…N). Skew ness is a measure of the asymmetry of the data around the sample mean. If skewness is negative, the data are spread out more to the left than to the right. If skewness is positive, the data are spread more to the right. The skewness of the normal distribution is zero. Similarly, for a random variable the kurtosis is defined as

$$\gamma_4 = \frac{E\left[(x - E[x])^4\right]}{\left(E\left[(x - E[x])^2\right]\right)^2} - 3 \quad \textbf{(3)}$$

And is a measure of the heaviness of the tails in a distribution an estimate of the kurtosis is given by:

$$\hat{\gamma}_4 = \frac{\sum_{i=1}^{N}(x_i - m)^4}{(N-1)\sigma^4} - 3 \quad \textbf{(4)}$$

Where m and σ are defined as before. Kurtosis is a measure of how outlier–prone a distribution is. The kurtosis of the normal distribution is 3. Distributions that are more outlier prone than the normal distribution have kurtosis greater than 3; distributions that are less outlier-prone have kurtosis less than 3.

If a region contains black (or white) particles then due to the impulsive nature of black (or white) particles the symmetry of histogram of the detail-image is affected. In the following figure we illustrate the histograms of the sub-regions of an image with high positive skewness and kurtosis (problematic areas occur at these locations). In the image, it is also evident that the tails of the histogram are heavier and hence the kurtosis assumes a high value. Therefore, a statistical test based on skewness and kurtosis is effective in finding regions with asymmetrical histograms. The detection problem is posed as an hypothesis testing problem in which the null hypothesis, H0, correspond to the case that no problematic spots occur in the sub-region against the alternative H1:

- *H0 black (or white) particles are not present in the sub-region*
- *H1 black (or white) particles are present in the sub-region*

(Skewness = 1.5772 ,   kurtosis = 2.666)
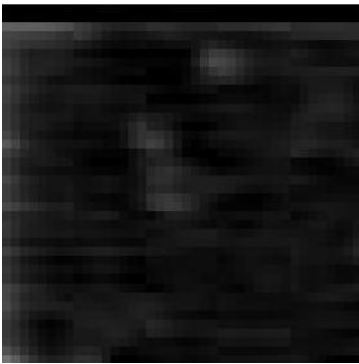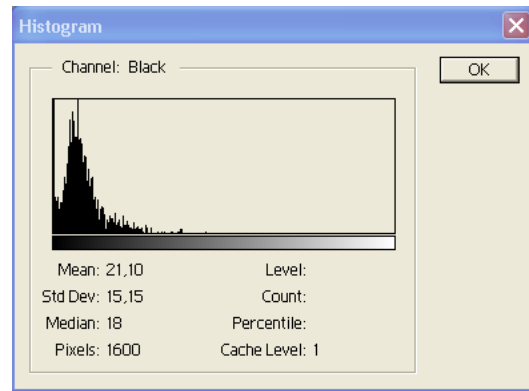
(a)   *(b)*

(Skewness = -0.0553 , kurtosis = 3.223)

(c)

(d)

Figure 2.7

This hypothesis-testing problem is reduced to the following decision rule Γ based on skewness and kurtosis,
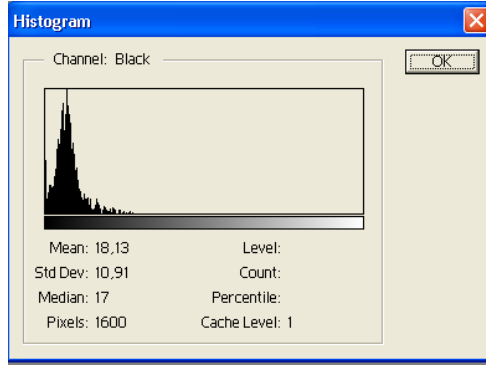
$$\Gamma(x) = \begin{cases} 0 & \gamma 3 < \text{T1} \ or \ \gamma 4 < \text{T2} \\ 1 & \gamma 3 \geq \text{T1} \ or \ \gamma 4 \geq \text{T2} \end{cases} \quad \textbf{(5)}$$

T1 and T2 are experimentally determined thresholds. Once the regions containing deteriorative particles are determined by the above test, the outlier labeling method estimates the locations of the particles. Figure 2.7 (a), (c) depicts sub-regions of an image which correspond to areas were black/white particles are and are not present respectively, while figures 2.7(b) and (d) illustrates the histograms of the specified sub-regions.

2.3.4 Box-plot Outlier Labeling

After the decomposition of the image and the calculation of skewness and kurtosis measures, the image is reconstructed and the susceptible regions are examined in order to detect the presence of black or white spots. According to this method, in each sub-region to which the detail image is decomposed we compute the histogram and from the histogram some statistical values are computed, concerning the distribution of gray pixel values. More specifically, the values computed are: lower-quartile (denoted by Q1), upper-quartile (denoted by Q3), inter-quartile range (denoted by Rf) and median. At this point we should give the statistical explanation of the terms referred above. The lower-quartile gray pixel's value determined at each sub-region is the

45

pixel value that is greater than the 25% of gray pixels value in the specific sub-region, similarly we can say that upper-quartile is the gray-pixel value which is greater than the 75% of the pixel values in the sub-image. The value assigned to the variable Rf (inter-quartile range) is computed by the difference of upper-quartile and lower-quartile. For the detection of black particles the outliers are determined to be the part of data which lay in the region (0, Q1-k*Rf) The parameter k is taken to be equal to 1.2. On the other hand, in order to detect the white particles presence we consider as outliers the data laying in the region (Q3 +k*Rf, 255).To the parameter k a value equal to 1.8 is assigned.

Black Spots   **White Spots**
*********   ******

Q1-k*Rf   Q1   Median   Q3   Q3+k*Rf

*: Outliers

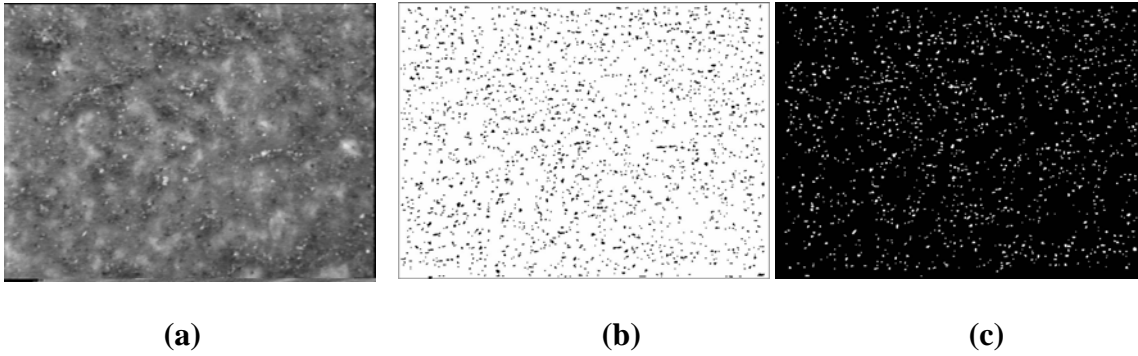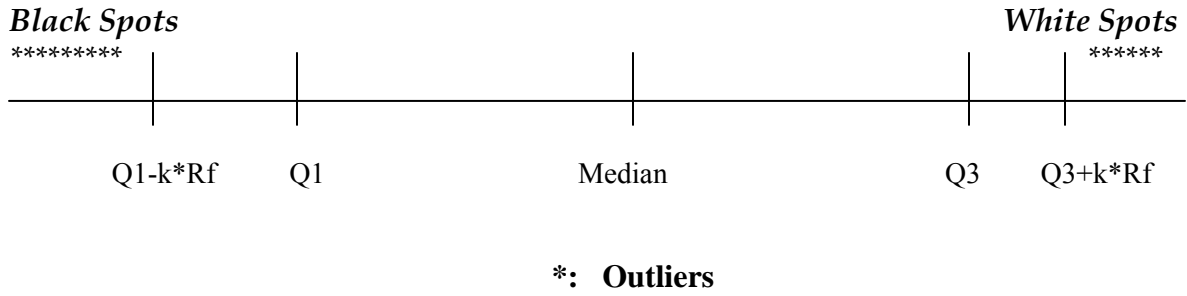| (a) | (b) | (c) |

Figure 2.8

***Figure 2.8** (a) image containing black and white particles (b) output of the detection scheme for the definition of dark spots, (c) Output of the detection scheme for the definition of white spots.*

In the following figure it is presented the flowchart of the algorithm analyzed above.
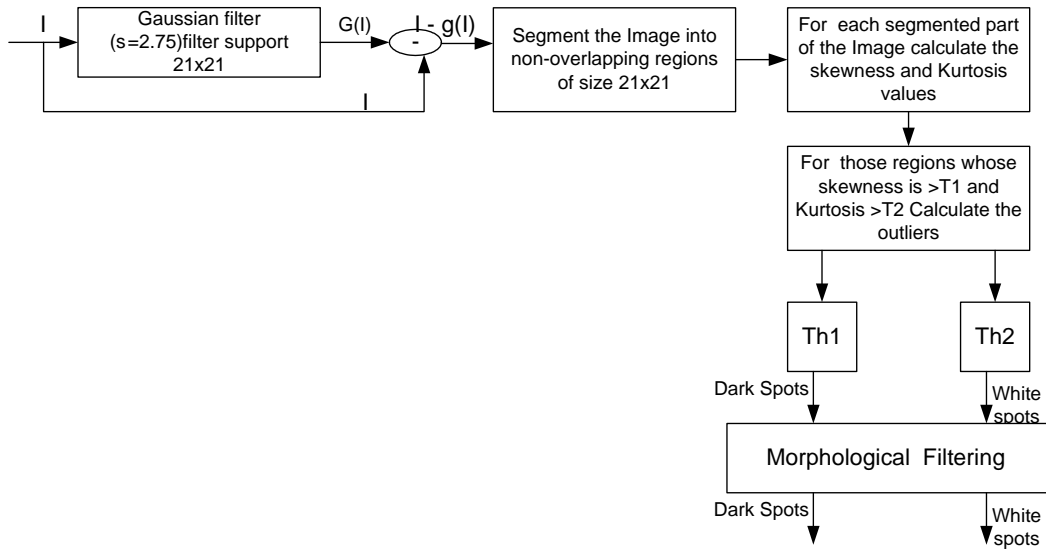
Figure 2.9

As it is depicted in figure 2.9, after the evaluation of the skewness and kurtosis measures in each sub region of the image, the sub images exhibiting high positive skewness and kurtosis are consider to be more susceptible for containing decay areas. Thus, these regions are processed with the Box-Plot Labeling Algorithm in order to extract the black\white particles. After the detection process Morphological filtering is performed in order to eliminate the noise effects and other sharp details that do not correspond to problematic areas.

In the following section the Labeling Method of extracting black/white pixels on an image depicting a stone surface is being described.

2.4   Labeling Algorithm

2.4.1 Introduction

*The labeling method of detecting decay areas is a method, which is implemented in order to reduce the false positive rate introduced by the processing of the images with the **High Pass Filtering Algorithm**. At first, the original image is high-pass filtered, and then the result image derived from the filtering process (called detail image) is being thresholded by applying some experimentally determined thresholds, as it was described in the High-Pass Filtering Algorithm (section 2.2). At a further step, a **Clustering Algorithm** was applied in order to classify all the*

discrete clusters, which define a black/white particle. In other words we could say that the Labeling Method implemented in the current study, segments a set of pixels, considered as a decay area by the High-Pass Filtering Algorithm, and assigns a label to this group of pixels. By using some rules of the imaging geometry we determine the co-ordinates of the center of each cluster. After the detection of center's co-ordinates for each cluster, this information is stored in a structure. At the specific co-ordinates (of the center of the cluster) at the detail image a window of size 41x41 is applied. The extent of the window is relative to the characteristics of the problem that we study and it was selected to be of this measure after an observation of the problem. The data concerning the decay areas evidenced that an application of a window with the above dimensions does not eliminate the decay areas while it preserves a homogeneous background. In the sub-regions defined by the window applied, the histogram is extracted and via this extraction some statistical values related to the distribution of the gray levels are evaluated. The statistical values are used accordingly in order to compute the thresholds that will be applied. At this point it should be stated that 3 methods of thresholding are used. Namely these methods are **Mean-Variance Thresholding***,* **Box Plot Thresholding** *and finally thresholding using the* **RobustFit method.**

2.4.2 Acquisition of the detail Image

As it was stated above, the first step in the implementation of the Labeling method is the extraction of the detail image. This process is performed by High Pass Filtering. A Gaussian filter is employed in order to remove all the high frequency content of the image and then the high-passed scheme is obtained by computing the difference

High-pass = Original – Gaussian (Original)

The parameters of the Gaussian filter are selected as it is described in the first section. More specifically the region of support is chosen to be equal to 21x21 and the standard deviation of the filter is determined to be equal to 2.75. The criteria according to which the above values are defined are discussed above in section 2.2. After the detail image is obtained and the thresholding of this image is performed the thresholded images were processed by morphological filtering in

order to remove abrupt changes that do not correspond to decay areas. As it is obvious the Labeling Algorithm should be considered as an extent of the High-Pass filtering Method.

In the following subsection, the procedure of classifying the decay areas into distinct clusters (labels) is described.

2.4.3 Clustering Analysis

*The **Clustering Algorithm** implemented here is based on the classification of the spots (white/black), which are present on an image. The clustering process is performed to the images containing black and white particles apparently. At first we shall consider the image, which demonstrates black crusts and how the **Clustering Algorithm** is applied at this case. At this point it may be useful to say that the structure, used to keep information for the determined clusters is a stack, in which each of the elements represents a discrete cluster. The structure used to store information for each specific cluster is a list and in turn, each of the list's components represents a pixel that is contained in the cluster. The image is traversed from left to right until the first pixel with gray value corresponding to a black particle is encountered. The specific pixel is then considered to belong to the 1st cluster, the structure that is used for storing information about the first cluster is constructed and the pixels co-ordinates are stored. Subsequently the pixel, located at its right, is examined. If this pixel corresponds to a black spot too then the current pixel is considered to belong to the same cluster as its neighbor. While traversing the first line of the image, if we encounter a black pixel we check all the clusters constructed so far and whether one of its 8-neighbors is part of a cluster, then the pixel's co-ordinates will be stored to the same cluster as its neighbor. Otherwise a new cluster is constructed and the pixel under consideration is estimated to be component of the new cluster. When the end of the first line is met we traverse the other lines in the same way. The conditions discussed above, that were related to the fact that one pixel cannot be present in 2 distinct clusters, are also valid. This process is being continued until the whole image is checked. At this point we should say that the process, which is followed in order to detect white particles on an image, is quite similar. As it was discussed in the start of this section, when the clustering of the black/white particle is completed, the centers of the clusters under consideration are evaluated.*

2.4.4 Definition of the centers of the labels

In order to determine the co-ordinates of the center of each cluster the procedure followed is described here: The list that contains the labels is traversed and for each label the co-ordinates of the center of gravity are extracted. The equations used to determine the center of each label are given below.

$$X_c = \frac{1}{N} * \sum_{i=1}^{N} x_i \qquad \textbf{(6)} \qquad\qquad Y_c = \frac{1}{N} * \sum_{i=1}^{N} Y_i \qquad \textbf{(7)}$$

N denotes the total number of pixels contained in each label, x_i and y_i denote the x and y co-ordinates of the pixels while X_c and Y_c denote the co-ordinate values of the center of each cluster. Once X_c and Y_c are determined, their values are stored into a structure (stack).

*At the following sub-sections we discuss the three methods of applying thresholds in the results of the Labeling process namely: **Mean and Variance, Box plot Outlier Method, Robust Fit**.*

2.4.5 Thresholding by using the Mean-Variance criterion

During this phase, the stack containing the centers is traversed and for each center's co-ordinates we apply a window on the detail image with extent 41x41 pixels centered at the pixel with co-ordinates (X_c, Y_c). In the sub-image defined by the window we extract its histogram and then we calculate the mean pixel's value and the standard deviation around the mean. All the pixels in the image that satisfy the equation I< (mean – 1.2*std) are considered to compose black particles. In the equation above, mean denotes the mean intensity of gray values in the sub-image into consideration while std represents the standard deviation. White particles are also detected through a completely similar process. In order the white particles to be detected the threshold applied is Th= (mean + 1.8*std). Thus the pixels which satisfy the condition I>Th are treated as constituents of the white particles. The image sequence demonstrated below shows the image data extracted at each stage of the algorithm. In order to depict how the labeling algorithm determines the center of gravity of a particular black and white particle we illustrate two cases. At the first case, it is shown black and white spots on a smooth background, and the sequence of images show

how the high-pass filtering algorithm treats these spots and then in which way the clusters are classified and the centers of gravity are extracted.
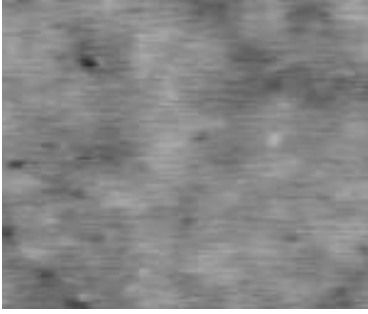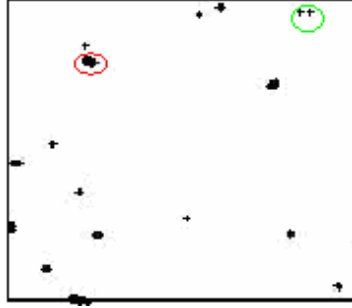

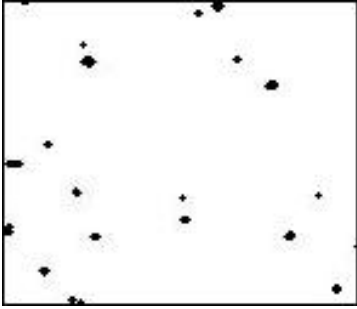| **Figure 2.10(a)** | **figure 2.10(b)** | **figure 2.10(c)** |

Figure 2.10(a) depicts region of an image that demonstrates areas covered by black particles, (b) black particles detected by the high pass filtering algorithm, (c) centers of gravities of the black particles depicted in (b) Figure 2.10(d) Black particles detected by using the mean-variance threshold

Figure 2.10 (d)

By observing the image 2.10(c) it can very easily observed that a particle seen as an entity by the human eye, is actually considered as a set of 2 particles in a very little distance between them by the Clustering algorithm. An example of this observation is found in the encircled (with red color) part of the images 2.10(b), 2.10(c). The results obtained by the application of the Mean-Variance Thresholding onto the results of the Clustering algorithm demonstrate an accurate detection of the decay areas; this can be very easily evidenced by superimposing 2.10(d) on 2.10(a). The accurate detection and the sensitivity of the method are quite reasonable as the current algorithm performs local processing, which in turn means that the false positives as well as the false negatives are reduced. An illustration of this reduction is also denoted in image 2.10(b) by the encircled (with the green color part of the image). As it can be seen the black particles determined by the High Pass Filtering algorithm (figure 2.10(b)) are more extended than the particles detected by the Mean Variance Method onto the same locations.

51

In the following images we display an analogous scheme concerning the detection of white particles.

(a)   **(b)**   **(c)**   **(d)**
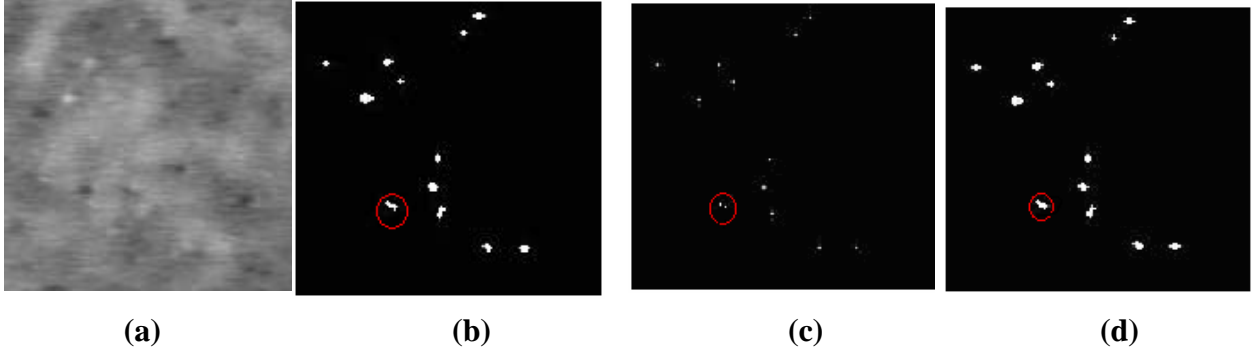
Figure 2.11

Figure 2.11(a) depicts a sub-region of an image that demonstrates areas covered by white particles, (b) white particles detected by the high-pass filtering algorithm, (c) centers of gravities of the white particles depicted in (b). (d) displays the data derived as a result of the Algorithm described here.

The observations discussed above, for the black spots are also valid for the case of white spots as well. For example we illustrate in the encircled areas (with red color) that a surface shown by the human eye as a solid white particle is in fact an area consisted of more than one distinct white areas located at a very close distance. The reduction of false positive rate cannot be seen in the above images, as the total number of white particles, which are present on 2.11(b), is the same as in the case of the image 2.11(d). It is illustrated though that the extent of the areas detected as white spots is not equal in cases 2.11(b) and 2.11(d).

It is important at this point, to refer that the results of this method, which are demonstrated, were obtained after an application of Morphological Filtering on the data extracted.

Gaussian Filter
(s =2.75) filter support
21x21

I

G(I)

-

Th1   Th2

Morphological
Filtering

Dark Spots
Detection

White Spots
Detection

Labeling Process

Find The Co-
ordinates of the
center of each Label

Black   White

/

L

For the co-ordinates
of each center go to
the L Image and
apply a window of
size 41x41

Black   White

In each window
calculate the Lower-
Quartile Upper-Quartile
and InterQuartile
Values

Th1   Th2

Morphological Filtering

Dark Spots
Detection

White Spots
Detection

Figure 2.12

*The Flowchart of the algorithm analyzed in this section is depicted in the above figure. On this figure, by Th1 we denote the thresholds applied in order to detect black particles while Th2 denotes the threshold value applied for the extraction of white particles. These variables are encountered twice in the figure .We should explain that the first occurrence of these variables corresponds to the threshold values applied at the High-Pass Filtering stage of the Labeling method. The second occurrence of variables Th1 and Th2 corresponds to the threshold value definition discussed in page **45**.*

2.4.6 Thresholding by using the Box-plot outlier method

The procedure followed in order to detect the black and white particles by using the Box-Plot outlier method is quite similar with the algorithm discussed in the previous sub section (Thresholding based on the mean and variance of gray values). Thus, at first the stack, containing the co-ordinates of the centers of clusters (black spots) is being traversed. At each pixel, which is considered to be the centre of a cluster, we go to the detail image and apply a window of size 41x41. For the sub-region defined by the square window the histogram is extracted and statistical values of the Lower-Quartile and the Upper-Quartile of the pixels gray values are computed. As it was discussed in the sub-section 2.3.4: The lower-quartile gray pixel's value determined at each sub-region is the pixel value that is greater than the 25% of gray pixel values in the specific sub-region, similarly the upper quartile of the gray pixels value is defined to be the gray value that is greater than the 75% of the of the gray pixel values in the same sub-region. After these statistical measures have been calculated in each sub-region, a threshold, which value is based on these statistical results, is applied. The threshold applied for the detection of black spots was determined to be equal to Th1 = Lower-Quartile – 1.5*Inter-Quartile (Inter-Quartile = Upper-Quartile – Lower-Quartile). All the pixels, whose values are under Th1, are considered to belong to a black particle. As for the detection of white spots, it is a process similar to this discussed here. After the stack that contains the centers of the segmented white particles is traversed, a window of size 41x41 pixels, which is centered on the co-ordinates of the centre, is applied on the detail image; the same statistical measures are calculated. The threshold was determined to be equal to Th2 = Upper-Quartile + 1.5*Inter-Quartile.

As it can be observed, the thresholds applied are statistically determined. In other words it means that their values are dependent on the distribution of gray levels. The resulting data obtained by this algorithm are reliable as the algorithm takes into account local features of the background. It should be highlighted that the method discussed at this section, as the one discussed in the previous section, were developed in order to eliminate the false positive and false negatives introduced by the high-pass filtering algorithm.

In the following images we illustrate data extracted at each stage of the algorithm .In order to depict how the labeling algorithm determines the center of gravity of a particular black and white particle we illustrate the images demonstrating the centers of gravity as they are determined by the Clustering Algorithm. On the images it is shown black and white spots on a smooth background, and the sequence of images show how the high-pass filtering algorithm treats these spots and then in which way the clusters are classified and the center of gravity is extracted. On the images (d) and (h) it can be seen the overlay of the detected black and white particles respectively onto the original image

(a)   (b)   (c)   (d)

(e)   (f)   (g)   (h)
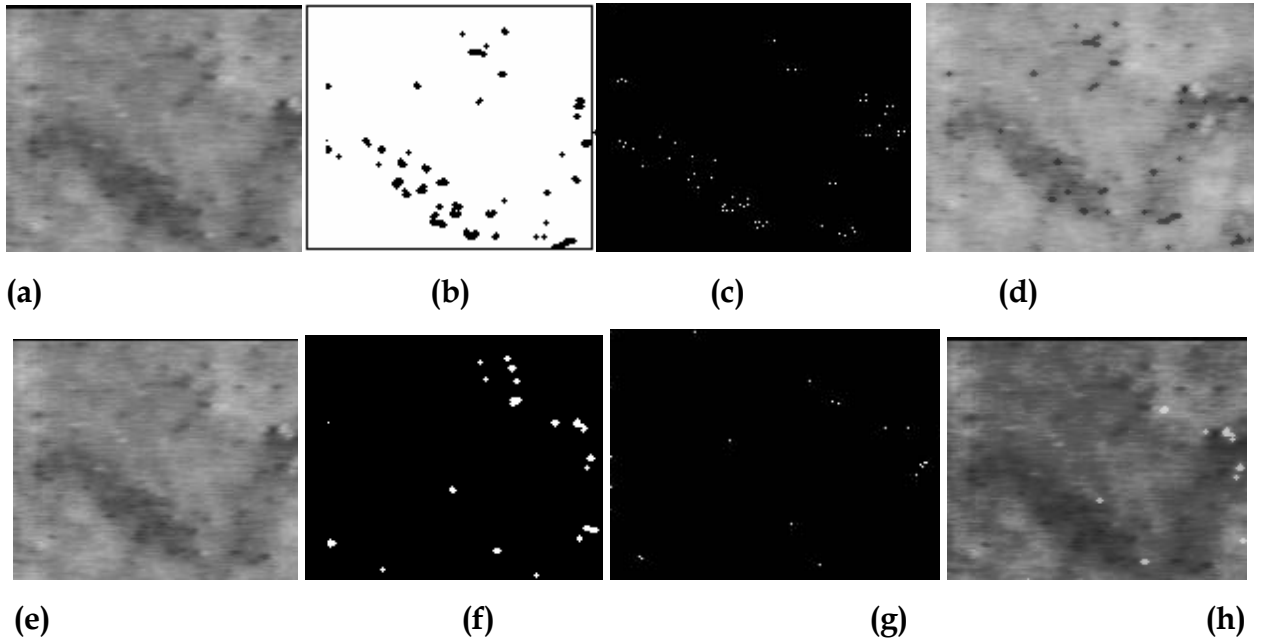
Figure 2.13

Figure 2.13(a), (e) depict a sub-region of an image that contains black and white particles. 2.13(b), (f) shows the black and white particles detected while images 2.13(c), (g) display the centers of the black and white particles respectively. Finally images 2.13(d),(h) illustrate the black and white particles overlaid on the original image.

In the following image, it is displayed the flowchart of the Boxplot Outlier Labeling algorithm, which was discussed throughout this section.
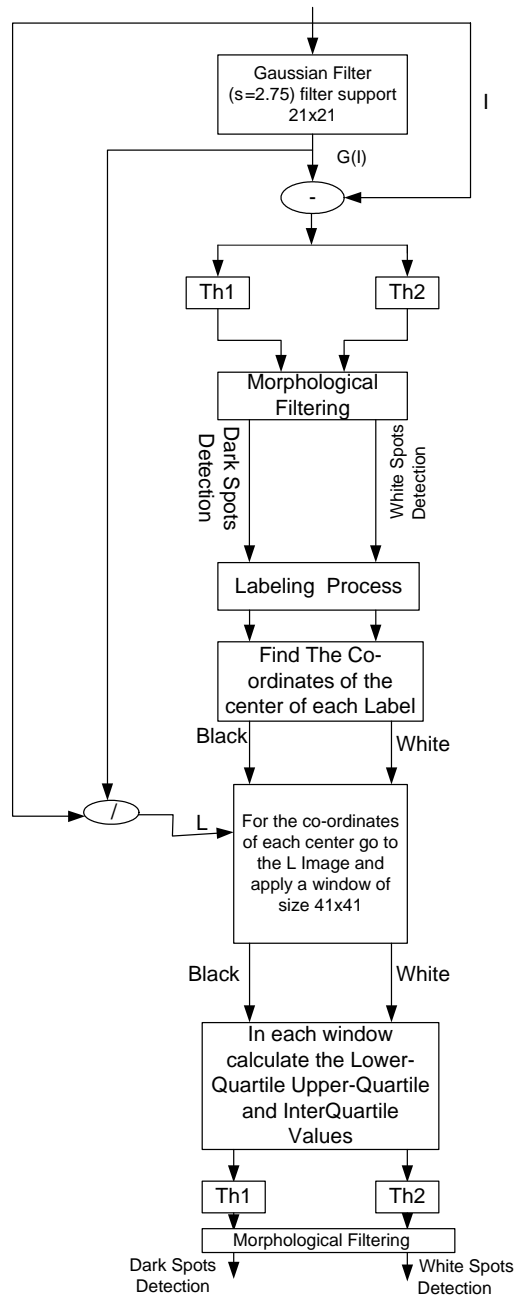
Figure 2.14

The figure above depicts all the steps followed by the algorithm in the effort to detect black and white particles. By the symbols Th1 and Th2 on the upper part of the flowchart are denoted the thresholds applied by the high-pass filtering method. As we can also observe the resulting images obtained by the high-pass filtering process, are morphologically filtered prior to the application of the clustering algorithm. The morphological filtering is performed in order to eliminate the noise effects.

2.4.7 Thresholding by using the Robust Fit method

Robust-fit method is also used in order to determine the outliers on the processing data. The steps followed by the currently discussed algorithm are similar with those reported in the above two sub-sections. More specifically for the extraction of the black particles the procedure is analyzed in the following paragraphs.

After the traversing of the stack that contains the centers of the labels considered as black particles we apply square windows on the detail image, which are centered on the co-ordinates of each of the centers of the clusters. The dimensions of the square windows were selected to be 41x41. The extent of the square windows was selected to be large enough such that the decay areas not to be eliminated. Thus this extent is dependent on the features of the surface being studied. After a square window is applied, the histogram of the sub-region defined by the window is extracted. Some statistical values are computed from the histogram, like the mean gray value and the standard deviation. Robust-fit   Method of extracting the outliers uses robust regression to fit the gray value distribution defined by the histogram with the Gaussian distribution. More specifically after the mean and standard deviation values are computed on each sub-region, we construct a normal distribution with the same parameters and then robust-fitting is used to extract the outliers. The Procedure of robust-fitting uses robust regression to fit the data of the two distributions and returns a vector b of the coefficient estimates. The robust fit function uses an iteratively reweighed least squares algorithm, with

The weights at each iteration are calculated by applying the bi-square function to the residuals from the previous iteration. This algorithm gives lower weight to points that do not fit well. In order to determine the threshold values for the detection of problematic regions, the vector containing the weights is traversed. While traversing the vector from the head to the end element, the position of the first nonzero element corresponds to the threshold denoted by the symbol Th1. All pixels which gray values are lower than Th1 are detected as pixels that constitute a black particle. The determination of the threshold Th2 is performed in an analogous way. More specifically, while traversing the same vector the position of the last nonzero element is defined to be equal to the upper threshold Th2. All pixels with gray values beyond Th2 are detected as points of white particles.

In the following figure, it is depicted the flowchart of the algorithm discussed here

Figure 2.15

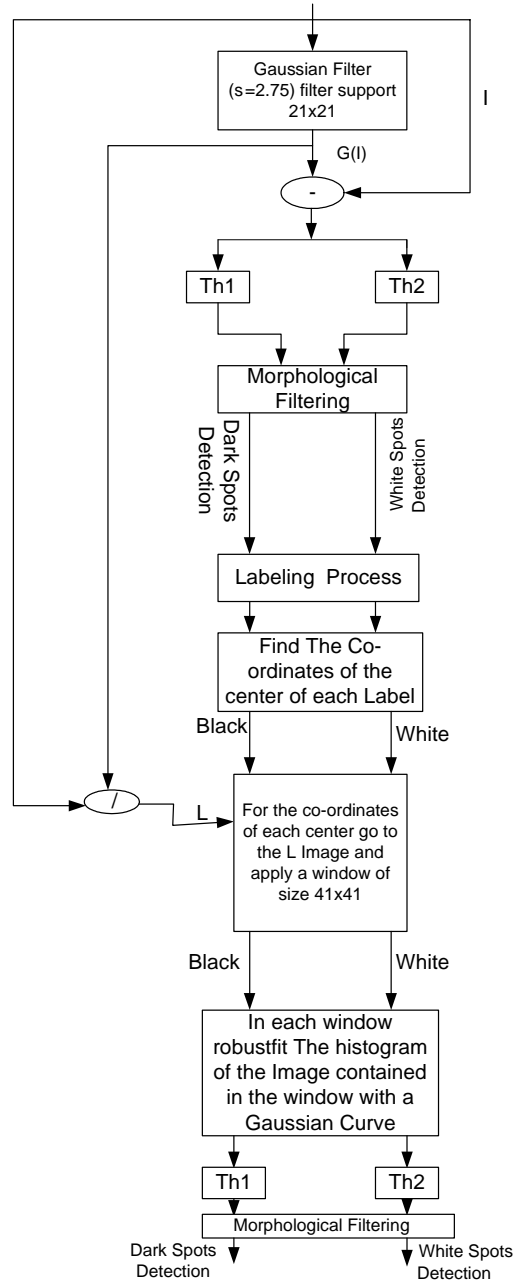As we can observe in the image above after the black and white particles have been extracted morphological filtering is performed in order to eliminate the noise effects and other sharp details which are present on the image and do not correspond to decay areas. We should mention at this point that we consider as problematic regions the labels that both of their dimensions are greater than 3 pixels.

The following images present data extracted at each stage of the algorithm .In order to depict how the labeling algorithm determines the center of gravity of a particular black and white particle we illustrate two cases. At the first case, it is shown a black and a white spot on a smooth background, and the sequence of images show how the high-pass filtering algorithm treats these spots and then in which way the clusters are classified and the center of gravity is extracted.

(a)	(b)	(c)	(d)
(e)	(f)	(g)	(h)
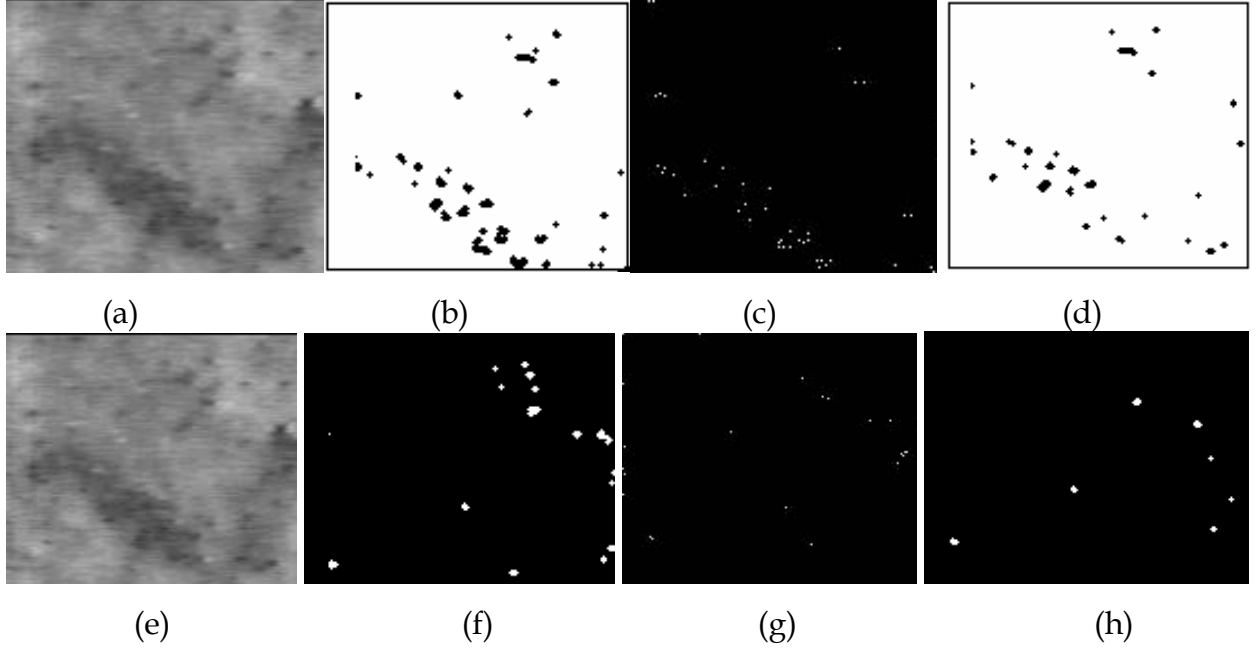
Figure 2.16

Figure 2.16(a), (e) depicts the sub-region of an image where black and white particles are present. Images 2.16(b) and (f) demonstrate the black and white particles respectively as they were detected by the high-pass filtering. The centers of black and white labels, segmented by the labeling algorithms, are shown on images 2.16(c) and (g), images 2.16(d) and (h) present the black and white particles respectively as they were defined by the algorithm currently studied.

As it can be observed, in the images 2.16(d) and (h) the black and white particles seem to be eliminated in extend and in number. This means that false positive and false negative rates are reduced.

2.5   The Gaussian Detector Algorithm

2.5.1   Introduction

The Gaussian Detector Algorithm can also be described by the term Weighted difference of Gaussians. The process of developing the Gaussian detector starts by acquiring the detail image

as it is described in the sub-section 2.4.2. At a further step 2 Gaussian filters with different kernels were applied to the detail image and a weighted difference of the two Gaussians is evaluated. Next the thresholds are determined onto the image depicting the difference between the two Gaussian kernels. The threshold values are taking into consideration the distribution of grey levels on the difference image. Thus at first the mean of the grey pixel value and the standard deviation around the mean pixel value are calculated. The process of determining the threshold values consists of two successive steps. At the first step a threshold value Th1=k1*std1 is derived and the pixels that satisfy the condition p(i,j)<Th1 (for the detection of black spots) or the condition p(i,j)>Th1 (for the detection of white spots) are used for the evaluation of a standard deviation std2 which in turn is used for the computation of a second threshold value Th2 = k2*std2.

2.5.2 Implementation Analysis

The Gaussian Detector consists of several steps. At first the original image f(x, y) is low-pass filtered using a Gaussian kernel with standard deviation σ equal to 4 pixels.

$$f1(x, y) = f(x, y) - G_4[f(x, y)]. \quad \textbf{(8)}$$

The difference of Gaussian Filtering consists in the subtraction of one smoothed version of an image from another having a different degree of smoothing. Two Gaussian kernels with different standard deviations are used to smooth the image. The standard deviations of the Gaussian kernels are chosen to reflect the dimensions of black and white particles and the inter-particle distance. The weighted version of Gaussian method is used assigning a weight of 0.8 to the kernel of larger width for the detection of black spots while the inverse process is followed for the detection of white particles. This procedure is applied to the subtracted image f1. So the two equations that hold for the detection of black and white particles respectively are addressed by the following relationships.

For black particles detection

$$f_2(x, y) = 0.6 \times G_6[f_1(x, y)] - G_{0.25}[f_1(x, y)] \quad \textbf{(9)}$$

For white particles detection

$$f'_2(x, y) = 0.8 \times G_{0.25}[f_1(x, y)] - G_6[f_1(x, y)] \quad \textbf{(10)}$$

The image resulting from the Gaussian filters f2(x, y) is processed by following the procedure described below. At first the histogram of the image f2(x, y) is extracted and the standard deviation is computed. At a further step, a first threshold equal to k1 times the standard deviation is applied. The standard deviation is recalculated, by using only the pixels that are under the initial threshold. The final threshold was set as k2 times the recalculated standard deviation. As we can very easily understand the process followed for the determination of white particles is quite similar except for the fact that in order to recalculate the standard deviation the pixels used are those which are beyond the threshold value k1*std1. At this point we should say that k1 and k2 should be selected in order to minimize the false positive and false negative rate. According to the laboratory though, it is stated that if the standard deviation is greater than 1 then k1 and k2 should belong in the range [1, 3]. In our application for the detection of white spots the k1 and K2 values were selected k1=1.5 and K2=1.5 while for the detection of black spots the k1 and k2 where selected to be 2 and 3 respectively. As it is reported in the literature the Gaussian detector is a good detector but does not preserve the shape of the spots. This in turn means that reliable information can be extracted about the exact location where a decay area is laid but it does not provide reliable information concerning the particle's shape.

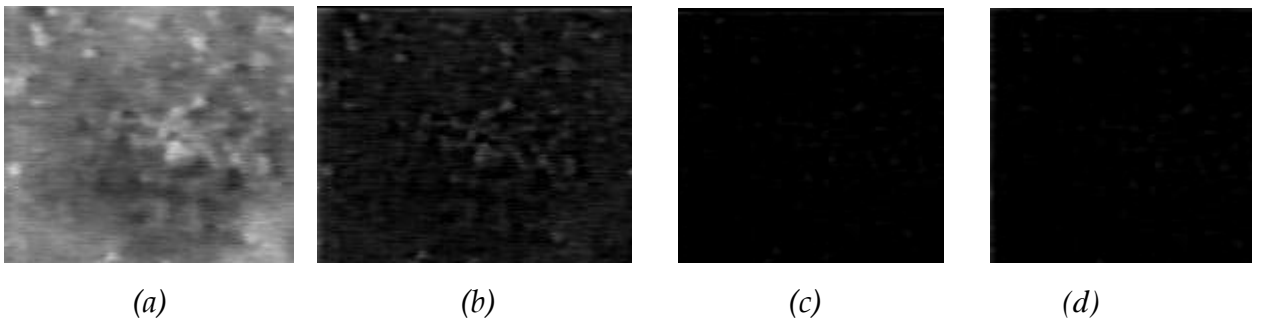*In the following images we present the resulting images of applying the weighted Gaussians difference.*

(a) (b) (c) (d)

Figure 2.18

In figure 2.18(a) we observe a sub-region of the original image and in figures (b), (c), and (d) it is depicted the schemes f1, f2, f2' respectively.

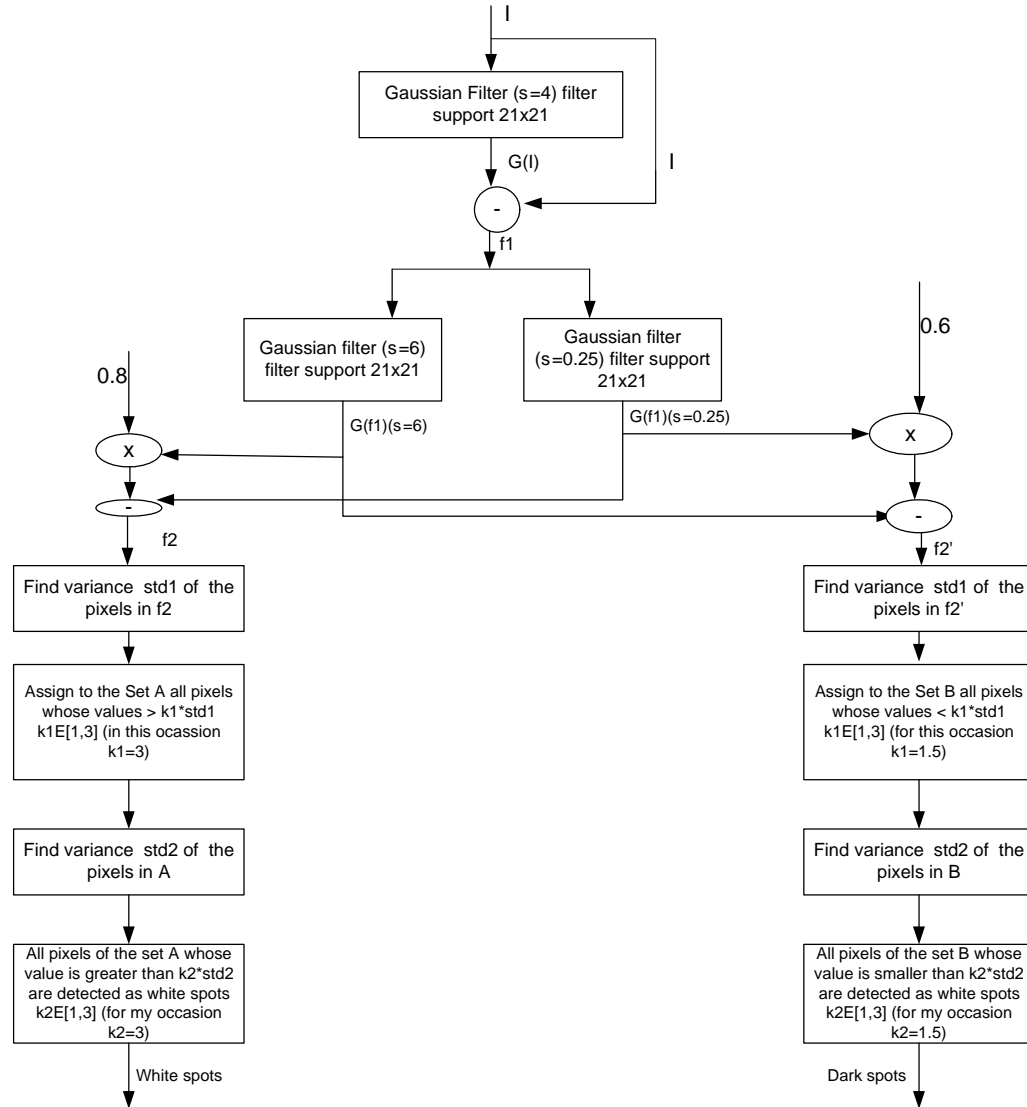*In the following figure it is displayed the Flowchart of the Gaussian Detector.*

I

| Gaussian Filter (s=4) filter support 21x21 |

G(I)   I

-

f1

| Gaussian filter (s=6) filter support 21x21 | | Gaussian filter (s=0.25) filter support 21x21 |

0.8   G(f1)(s=6)   G(f1)(s=0.25)   0.6

x   x

-   -

f2   f2'

| Find variance std1 of the pixels in f2 | | Find variance std1 of the pixels in f2' |

| Assign to the Set A all pixels whose values > k1*std1 k1E[1,3] (in this ocassion k1=3) | | Assign to the Set B all pixels whose values < k1*std1 k1E[1,3] (for this occasion k1=1.5) |

| Find variance std2 of the pixels in A | | Find variance std2 of the pixels in B |

| All pixels of the set A whose value is greater than k2*std2 are detected as white spots k2E[1,3] (for my occasion k2=3) | | All pixels of the set B whose value is smaller than k2*std2 are detected as white spots k2E[1,3] (for my occasion k2=1.5) |

White spots   Dark spots

Figure 2.17

2.6   Detection and Segmentation by Morphological Operations

2.6.1 *Introduction*

*In the current section it is analyzed the process of detecting the black and white particles by using morphological operations. The **top hat** transform is used for the detection of white particles while **bot hat** is used for white particles detection. As a structuring element it is*

62

*employed a circle with a diameter of 13 pixels for the processing with both the **bot hat** and the*
***top hat** operations. The procedure of applying thresholds on the result images is similar with the*
*thresholding procedure followed in the case of the **Gaussian Detector.***

2.6.2 Implementation Analysis

As it is reported in section 2.1, where the theoretical background of the morphological operations
is analyzed: the two basic morphological operations are erosion and dilation. These two
operations are defined as follows:

$$M \ominus B := \min B(x - m1, y - m2) \, \forall (m1, m2) \in M \qquad \textit{(11)}$$

$$M \oplus B := \max B(x + m1, y + m2) \, \forall (m1, m2) \in M \qquad \textit{(12)}$$

Where $B(x, y)$ denotes an image with 1<x<n1 and 1<y<n2 and M is a structuring element.
Dilation and erosion are complementary operations in the sense that a dilation of the background
is the same as erosion on the object. $M \ominus B = (M \oplus B^c)^c$. *By combining erosion and dilation,*
the important morphological filter operations opening and closing are formed:

$$M \circ B := M \oplus (M \ominus B) \qquad \textit{(13)}$$

$$M \bullet B := M \ominus (M \oplus B) \qquad \textit{(14)}$$

As it is obvious opening and closing are also dual operations and so therefore dark and white
particles are treated differently by these operations. The top-hat transform of an image is defined
as

$$R := B - (M \circ B) \quad \textit{(15)}$$

While the bot-hat is defined as $\qquad R := B - (M \bullet B) \quad \textit{(16)}$

The top-hat transform enhances white particles that have size smaller than the structuring
element. The structuring element M is defined to be a circle of 13 pixels in diameter. Similarly
the bot-hat transform is used in order to detect the white particles. The structuring element in
the case of the white particles detection is also a circle of the same diameter. At a further step, the
histogram of the result image (the one which came out after the bot hat and the top hat
transforms) is extracted and we calculate the standard deviation. For the detection of black spots,
after the calculation of standard deviation on the image resulted from the bot hat transform, an
initial threshold is applied which is equal to k1 times the standard deviation std1. The standard
deviation is recalculated considering only the pixels that are beyond the initial threshold. Finally

a threshold equal to k2 times the recalculated standard deviation is applied. And all the pixels whose values are greater to the thresholds value are considered to compose the black particles. The procedure used to determine the white particles is quite similar but in this case the image studied is the result of the top-hat transform. In both cases the images obtained after the thresholding are morphologically filtered in order to eliminate the noise and other sharp details.

In the following images, it can be observed a part of the original image where black particles are present, as well as the shape of the problematic region as it was determined by the bothat transform.
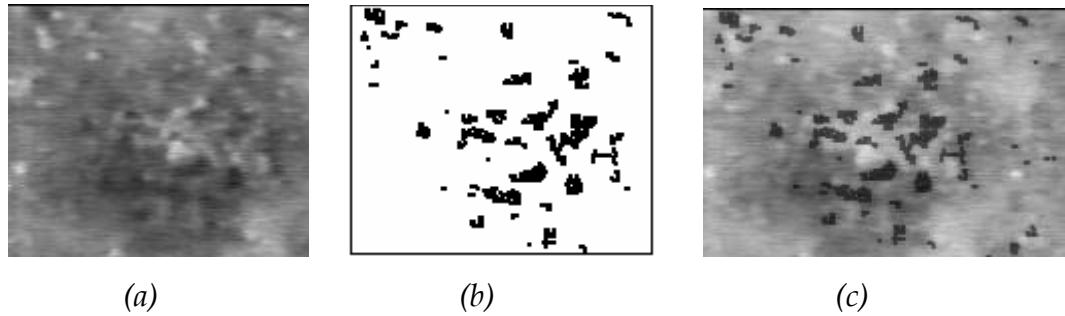

(a)   *(b)*   *(c)*

Figure 2.19

Figure 2.19(a), depicts a sub-region of the original image which contains black particles, (b) illustrates the black particles as they were detected by the procedure reported in this section and finally image 2.19(c) shows 2.19(b) overlaid on figure 2.19(a).

As it can be seen, morphological filtering managed to detect the regions considered as black particles but the locations of these regions are not reliable. This assessment comes from the fact that as we can observe neighbouring black particles are merged. Thus the problematic regions are displayed to have a greater extent than the extent that they really have. In the following sequence of images we can see how the white particles where defined by the algorithm discussed here.
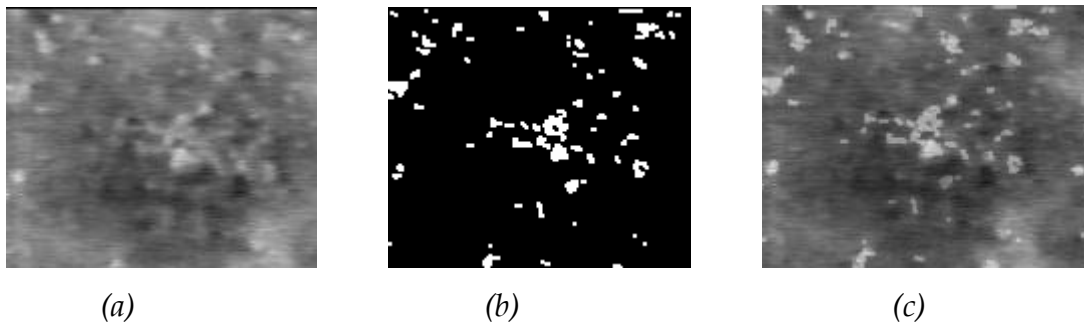

(a)   *(b)*   *(c)*

Figure 2.20(a) shows a sub-region of the original image containing white particles, figure 2.20(b) displays the white particles detected by the algorithm and 2.20(c) depicts the white particles, which were detected, to be overlaid onto the sub-region of the original image.

2.7 Conditional Thickening Method

2.7.1 Introduction

*As it was discussed in section 2.5 the procedure of detecting black and white particles by using the Gaussian detector is very reliable, however the shape of the spots is distorted: the boundary of the individual spots is smoothed. On the other hand morphological filter preserves the shape of the spots but gives a higher false positive rate. The combination of the results of the two methods guarantees both preserved shape and a low false positive rate. The images derived from the methods discussed in the two previous sections (sections **2.5** and **2.6**), were combined by a **Conditional Thickening** operation. This morphological operation extends a spot detected by the Gaussian Detector until the boundaries of the spot detected by the morphological operations are reached. Spots merged by the morphological operations are separated and the shape of the particles is preserved.*

2.7.2 Implementation Analysis

The shape of the spots determined with the morphological method is better preserved than, after the detection by the Gaussian detector at the price of more false positives occurrences of spots and merged regions that should be isolated. In order to reconstruct the shape of the spots optimally, both methods are combined. With the Gaussian detector, which was discussed at first, the spots are detected and their topology is determined. The idea, to exploit the strength of both concepts, is to detect the spots with the Gaussian detector and expand them but not let them merge or grow beyond the size given by the result of the morphological filter operation.

For this purpose, a morphological conditional thickening is applied. The operator $\otimes$ of X relative to Y with the pair of structuring elements (M1, M2) is defined as follows:

$$(M1, M2) \otimes XY = Y \cap \left(X \cup \left((M1 \ominus X) \cap (M2 \ominus X^C) \right) \right) \quad \textbf{(17)}$$

For the segmentation of the black and white particles, the structuring element M has the following structures:

$$
M_{1,1} = \begin{matrix} 1 & 1 & 1 \\ 0 & 0 & 0 \\ 0 & 0 & 0 \end{matrix} \quad
M_{1,2} = \begin{matrix} 0 & 0 & 0 \\ 0 & 1 & 0 \\ 1 & 1 & 1 \end{matrix} \quad
M_{2,1} = \begin{matrix} 0 & 0 & 0 \\ 0 & 0 & 1 \\ 0 & 1 & 1 \end{matrix} \quad
M_{2,2} = \begin{matrix} 0 & 0 & 0 \\ 1 & 1 & 0 \\ 0 & 1 & 1 \end{matrix}
$$

and every rotation of these matrices around 90^0.

The result of the conditional thickening of X onto Y with the structuring element M is the conjunction of the partial results of the equation above for every pair (M_{i1}, M_{i2}).

$$E = \bigcup\nolimits_{i=1\ldots8} M_i \otimes XY$$

This equation is applied for X=E until E does not change any more. The special property of M is that X increases until the boundaries of Y are reached or two subsets of X are separated through a line of one pixel in width. E is consequently always a subset of Y and contains as many objects as the intersection of X and Y. A conjunction of two objects of X is prevented by the structuring element M because it extends X only with pixels of Y not disturbing the topology of X. For the problematic regions detected by the current algorithm this means that the spots detected by the Gaussian detector are extended by topologically unimportant pixels and that the results is always intersected with that of the spots detected with the morphological method. In (17), X represents the result of the detection process and Y represents the result of the reconstruction giving the shape of the spots. The intersection in each step assumes that after the conditional thickening, these remain spots that are in both X and Y. The intersection step determines therefore the place and the number of the black\white particles, Y determines the shape, and the structuring element M prevents the confluence of several spots.

In the following sequence of images the results derived from the conditional thickening operation are illustrated. For space convenience the images, which are displayed, depict only a sub-region of the image, which contains black and white particles.
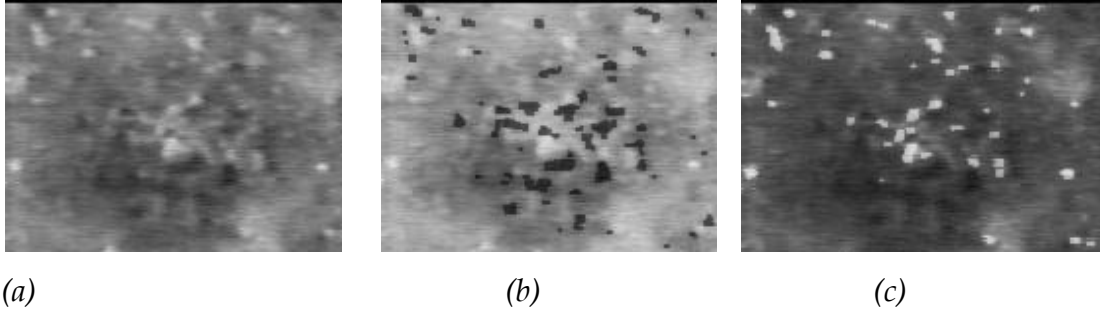
(a)	*(b)*	*(c)*

Figure 2.21

In figure 2.21(a) is shown a sub-region of the original image containing white particles, figure 2.21(b) displays the black particles overlaid onto the sub-region of the original image. And 2.21(c) depicts the white particles, which were detected, to be overlaid onto the sub-region of the original image.

2.8   Region Growing Algorithm

2.8.1 Introduction

Region Growing algorithm is applied to the image derived by a high-pass filtering of the original image. In this algorithm, a region is grown around a seed pixel by appending 4 connected pixels that satisfy the following conditions

$$p(i, j) \leq (1 - t) * \frac{(F_{min} + F_{max})}{2}$$ *In order to detect the black particles.*

$$p(i, j) \geq (1 + t) * \frac{(F_{min} + F_{max})}{2}$$ *In order to detect the white particles.*

*Where t is the tolerance parameter, and F_{min} and F_{max} are the current minimum and maximum values in the region grown that far. The value of **t** is not selected by the user; the best value is automatically determined for each segmented structure by repeating the growth with multiple values of **t** between 0.001 and 0.4.*

2.8.2 Implementation Analysis

The original image is at first passed through a high-pass filter. This means that the resulting image is obtained as the difference between the original image and a low-pass version of the original image. The low-passed image is the result of filtering with a low-pass Gaussian filter. The features of the filter (kernel and filter support regions) are chosen appropriately such that

67

the problematic regions not to be eliminated. In this application it was evidenced that the ideal value for the filter support region is 21 and the kernel was selected to be equal to 2.75. The following equation shows the process followed in order to obtain the detail image (high-pass filtered).

$$F_2(x, y) = F_1(x, y) - G_{2.75}[F_1(x, y)]$$

F1 denotes the original image while F2 represents the resulting image and σ the standard deviation of the Gaussian filter. At a further step the detail image will be traversed in order to detect regions of texture abnormality.

As in all the other algorithms, the current study attempts to determine isolated regions that correspond both to black or white particles. Thus at first we will analyze the way in which the Region Growing Algorithm operates in order to perform the detection of black particles. The procedure followed for the detection and segmentation of white particles is quite similar. The Region Growing Algorithm starts by extracting the histogram of the detail image. Then the median gray level is computed and all the pixels that are under the median gray level are selected as seed pixels. For each seed the 4-connected neighbors are checked for inclusion with the following condition

$$P(i, j) \leq \frac{(1 - t) * (F_{max} + F_{min})}{2}.$$

Where p (i,j) is the pixel being checked, Fmax and Fmin are the current maximum and minimum pixels values of the region being grown and t is the Region Growing tolerance parameter. The tolerance is varied from 0.01 and 0.4, with a step equal to the inverse of the seed pixel value. Features are extracted for each value of the tolerance. The value that introduces the least change in the features from one step to the following one is chosen as the optimal tolerance. In this study the features extracted for each region being grown with a different tolerance level are two: the centre of gravity and the size of the isolated regions. The algorithm determines the value of t that results in the minimal change in the vector of two features with respect to the previous t value in the sequence by computing a normalized distance between consecutive vectors. The vector with the minimal distance indicates the best choice of t. The process followed for the determination of regions considered as white particles is quite similar. Except for the fact the condition used to check for inclusion is

$$P(i,j) \geq \frac{(1+t)*(F_{max} + F_{min})}{2}$$

The Region Growing Algorithm was developed in order to reduce the false positives or false negatives introduced by the Image Filtering Algorithm. Its computational time though is high and this makes it difficult to be applied on images with large dimensions.

The resulting images, which depict regions considered as black or white particles are then morphologically filtered in order to reduce the noise effects on the resulting image. More specifically a region grown is treated as a black or white particle if each its dimensions are greater than 3 pixels.

Due to the fact that the process of extracting black or white particles takes into consideration the features of the background, the Region Growing algorithm is estimated to have high detection accuracy.

The following sequence of images are presented in order to be estimated the accuracy of this algorithm in detecting regions considered as degraded parts of the stonework
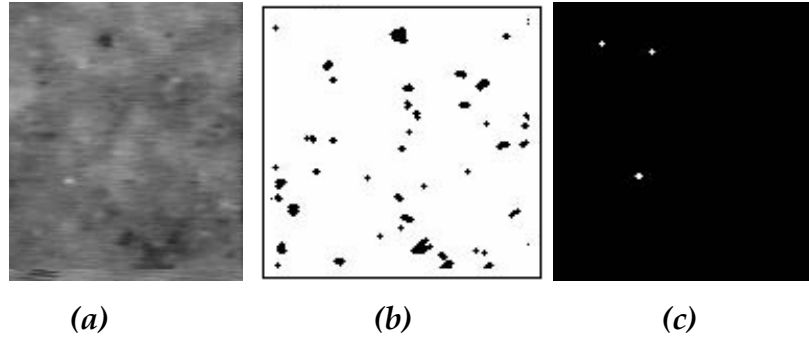

(a)   *(b)*   *(c)*

figure 2.23

Figure 2.23(a) depicts a sub-region of an image containing black and white particles while images (b) and (c) demonstrate the areas defined as black and white regions respectively by the Region Growing algorithm.

In the following figure is presented the flowchart of the Region Growing algorithm which was discussed in the current section.
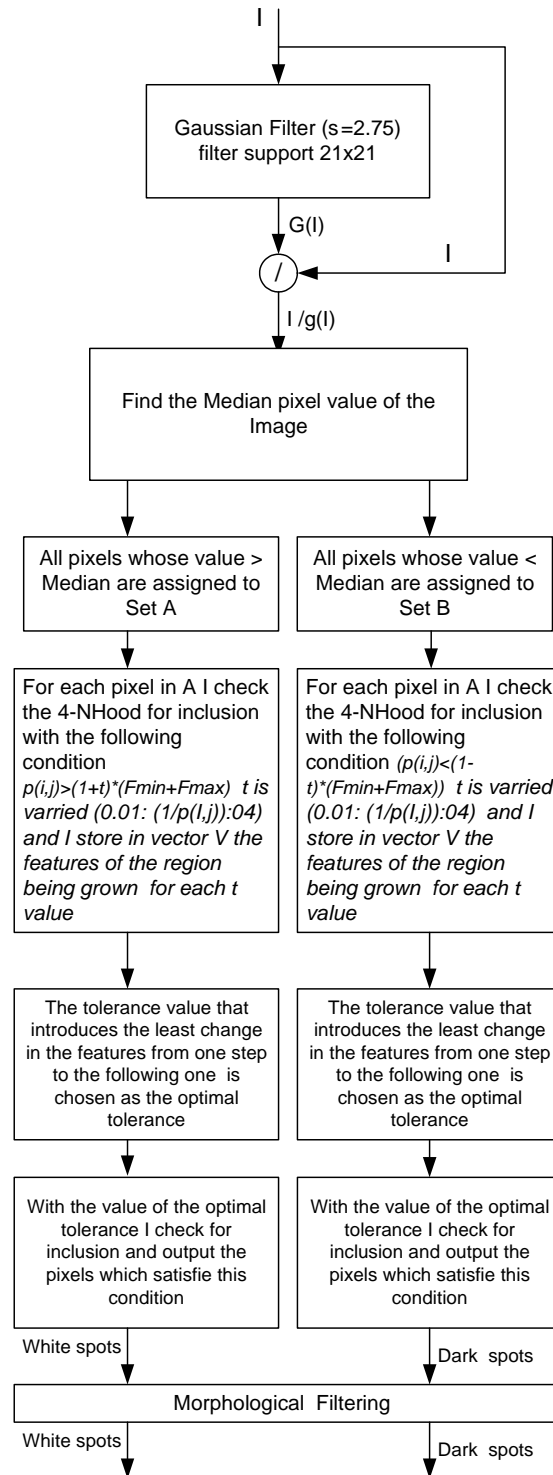
I

```
Gaussian Filter (s=2.75)
filter support 21x21
```

G(I)

/ ← I

I /g(I)

```
Find the Median pixel value of the
Image
```

```
All pixels whose value >
Median are assigned to
Set A
```

```
All pixels whose value <
Median are assigned to
Set B
```

For each pixel in A I check the 4-NHood for inclusion with the following condition *p(i,j)>(1+t)*(Fmin+Fmax) t is varried (0.01: (1/p(I,j)):04) and I store in vector V the features of the region being grown for each t value*

For each pixel in A I check the 4-NHood for inclusion with the following condition *(p(i,j)<(1-t)*(Fmin+Fmax)) t is varried (0.01: (1/p(I,j)):04) and I store in vector V the features of the region being grown for each t value*

```
The tolerance value that
introduces the least change
in the features from one step
to the following one  is
chosen as the optimal
tolerance
```

```
The tolerance value that
introduces the least change
in the features from one step
to the following one  is
chosen as the optimal
tolerance
```

```
With the value of the optimal
tolerance I check for
inclusion and output the
pixels which satisfie this
condition
```

```
With the value of the optimal
tolerance I check for
inclusion and output the
pixels which satisfie this
condition
```

White spots

Dark spots

```
Morphological  Filtering
```

White spots

Dark spots

figure 2.22

70

2.9 Post Processing

2.9.1 Computation of Statistical Measures

As it was mentioned in the first chapter of this study, further to the detection of the exact locations where black and white particles are present, it is considered as an aspect of high importance to study some features of these spots, which were defined as decay areas by the algorithms. These features are related with the number of black and white particles that were detected on each surface prior and after the chemical cleaning as well as with the percentage of the surface covered by decay areas. In order to have a broader view of the degradation effects on the surfaces under consideration we also studied the distribution of the surface sizes that are developed on the stonework. Another issue, which is also being studied on this work, is the thickness of the black and white particles. This issue is approached by a rather qualitative point of view. On this section the author considered purposive to give a report on the algorithms implemented in order to extract all the features mentioned so far.

At first we describe the procedure followed in order to determine the number and the extent of black and white particles.

2.9.2 Determination of the number and extent of the Problematic regions

On the images depicting the black and white particles that are present on the stone surfaces we apply the Clustering algorithm as it is described in the sub-section 2.4.3. Once the Clustering operation is performed, the stack contains the labels (sets of pixels considered as entities). As it is reported in the text where the Clustering operation is described each node of the stack is a list that represents a cluster. Furthermore each node of the list contains the co-ordinates of a pixel that belongs to the cluster. Thus if we want to extract the number of the particles (black /white) that were detected in the image we simply count the stack's nodes. As for the definition of the statistical measures that describe the distribution of the black/white particles surface sizes the process is more complex. The statistical measures studied in this case are median value of the surface, lower-quartile, upper quartile, min surface and maximum surface. The value assigned to upper quartile is greater than 75 percent of the values of black/white particles surface sizes; similarly lower-quartile and median correspond to surfaces values that are greater than 25% and

50% respectively of the surface values. In order to define the values that we should assign to these measures we traverse the stack and store the number of pixels encountered in each list in a temporary structure. The structure's elements are then sorted and we evaluate the values of median, upper-quartile and lower quartile of the black/white particles surface sizes.

In the next subsection it is reported the procedure used to study qualitatively the aspect of the black/white particles thickness.

2.9.3 Study of the Thickness of degraded areas

The procedure followed for the evaluation of the thickness is reported below. A mask of the same dimensions as the image is used. At first, the image depicting the detected black/white particles is scanned from up left to the right bottom. When a black/white pixel is encountered the value 1 is assigned to the element of the mask with the same co-ordinates as the studied pixel. After the whole procedure has been performed, the co-ordinates of the mask's elements with values equal to 1 correspond to problematic regions. At a further step, the mask is multiplied with the image element by element. All the non-zero results are sorted and the statistical values are extracted. The statistical measures studied at this part are the median gray value, the mean gray value, as well as the upper-quartile, lower-quartile and the standard deviation of the gray values. These values give significant information about the distribution of the gray values on the regions considered as black and white spots. As it will be reported in the next chapter, it was evidenced that the distribution of the gray levels was spread to lower values when the black crusts demonstrated a greater thickness.

3 RESULTS

In the following section an effort was made to present the results obtained from the Image Processing methods applied on the images under consideration. The way of presentation of these results allow to the reader to understand, how the problematic areas are depicted onto the images, as well as how the Algorithms developed in this work isolated these regions and studied their main characteristics. In order to describe the results obtained from the current study, it is at first considered purposive to refer to some data about the state of deterioration estimated at each of the examined samples with aid of chemical methods.

3.1 Location of Studied samples

The available images can be classified into two broad categories: Ke-images and Ks-images. The main reason of this classification is that the images were taken from regions of the monument with different deterioration patterns. This differentiation is the result of the different exposure of monument to the rain action. More specifically, Ke-images were taken from areas sheltered from the rain action whereas Ks-images represented unsheltered surfaces. The state of deterioration is greatly affected by the exposure to the rain action and in general the action of climate conditions. As it was reported in the first chapter, sheltered surfaces (surfaces protected by the rain and wind's action) develop spots thicker and darker in color. On the other hand, stone surfaces, more exposed to the combined action of climate conditions such as rain, wind, temperature etc, demonstrate different deterioration phenomena, such as thinner crust layers, discoloration due to the water flows as well as spots differing in color than those encountered on sheltered areas. At this point, the specific locations of the studied areas are reported together with the deterioration phenomenology diagnosed by the chemical analysis of the deposits. The samples belonging to Ke-images were taken from the outer line propylon, 1st from left, 4th-5th tambour. The macroscopic deterioration patterns were areas covered by extended coatings of brown to black color. An X-ray microanalysis on specimens of cannelures evidenced the existence of a gypsum layer with a thickness of 60μm. On the surface of this layer, argilo-silicate deposits were found.

*The following images illustrate the location of samples belonging to the Ke-**Surfaces***

3.1.1   Figure 3.1

(i)   (ii)

arris

cannelure   cannelure   arris

(iii)   (iv)

cannelure   arris   arris   cannelure
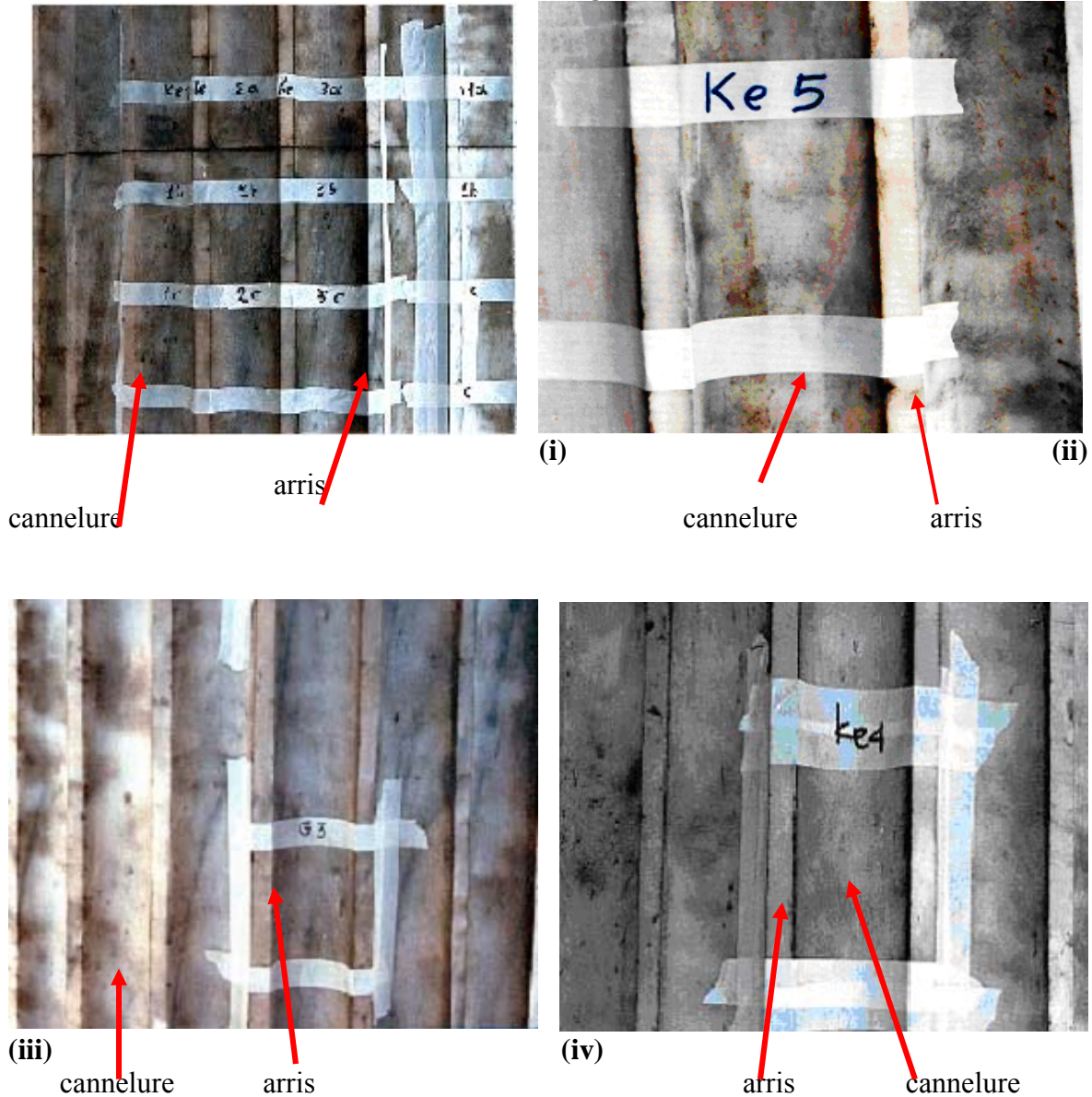
Ks-Images were taken from the outer line columns, 1ˢᵗ from right, ground floor, western direction. A brief macroscopical observation of the specimens belonging to Ks-images, rain washed areas evidenced residues of chemical treatments conducted in the past with the purpose of protecting the surfaces from weathering.

In the following image the samples belonging to Ks Surfaces are shown.

Fig 3.2
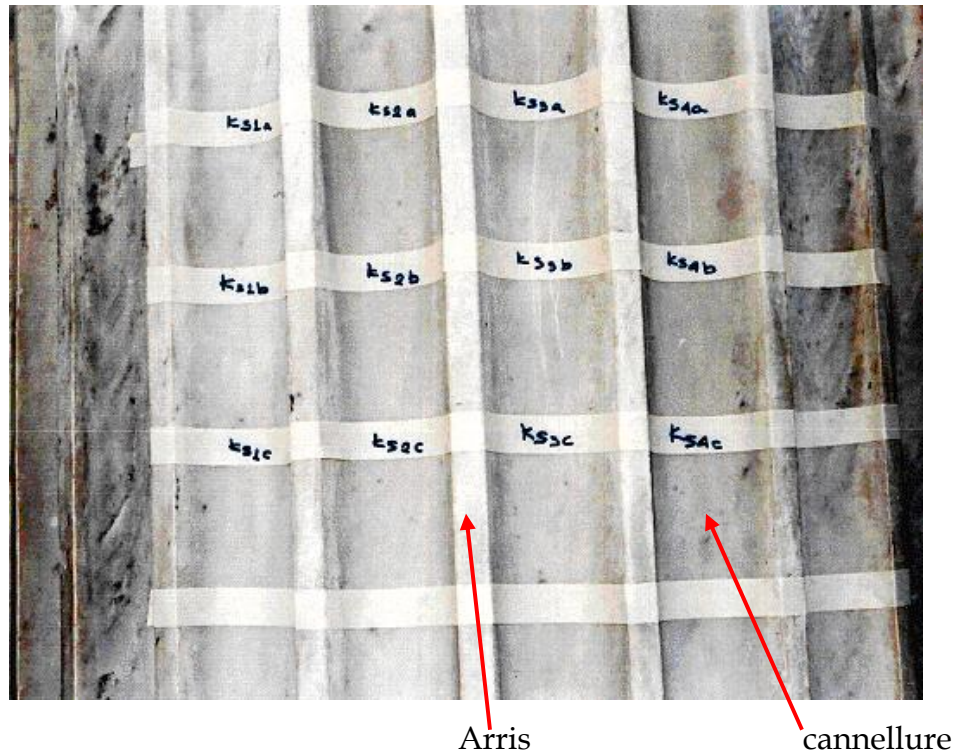
Arris   cannellure

A microanalysis of the Ks specimens belonging to arrises evidenced the presence of gypsum, hydrated argilo-silicate components, as well as traces of saturated hydrocarbons. The chemical deterioration diagnosed on the cannelure samples was quite similar, even though the deterioration effects encountered in a greater extent. A gypsum layer, lower in thickness than that observed in Ke-images exists. Variations on the type and extent of decay were observed in the samples obtained from the Ks images. More specifically, areas, more exposed to rain action, are more washed-out, demonstrating color alteration and exfoliation.

A further classification of the available images is relative to the specific area of the pillar where the images were taken from. More specifically, an issue of high importance is to study decay differences observed between samples taken from the arrises of a pillar and from the cannelures. The above discrimination is reasonable because, as it was mentioned in the first chapter, the type and distribution of pollutants varies on different areas of a pillar. Cannelures function as cavities in which pollutants; wind deposits and airborne particles (fly ash, metal oxides, dust grains etc) are concentrated

An attempt was made to detect black and white particles on surfaces located at different areas of the monument. This was done in order to check whether the algorithms implemented in this work give similar results to the corresponding of the chemical analyses. More specifically, the results of this study concern the deterioration effects in the following specimens: (1) aulakas-ravdosis x50 (Ke-images): this sample corresponds to a cannelure located on sheltered areas, (2) akmi-ravdosis x50 (Ke-images): this image represents surfaces correspond to an arris located on sheltered areas, and (3) aulakas-ravdosis x50 (Ks-images): this image corresponds to a surface of cannelure encountered on an unsheltered area.

3.2 Presentation of the Results and discussion

The images reported below are resulted from the application of algorithms developed in this work. These results are displayed in order to give the reader the opportunity to understand, which is the state of deterioration before the application of the chemical intervention methods (untreated surfaces) as well as the results of the chemical cleaning. The chemical methods employed in order to remove the pollutants from stone surfaces, are the following: Ds, Biological Paste and Gagemark.

Ds Method is a method that uses anionic resin in combination with ammonium carbonate in order to remove the pollutants. This process is applied multiple times, and at each application the parameter that changes is the duration of the application to the stone's surface. At this point it is important to mention that the time of application is associated with the type as well as the amount of the pollutants finally removed. It was experimentally proved that for the Ke-Surfaces best performance of the method was achieved with an application's duration of 40 minutes. A further observation of great importance, as far as Ke-Surfaces are concerned, efficiently removes much more gypsum in arrises than in cannelures.

Biological Paste is another chemical method for the cleaning of crusts. This method mainly uses a biological paste in order to remove the pollutants. Various applications of the method were conducted and at each case the duration of application was changed. As it came out by the iterated applications of this method, the application time of biological paste determines the quantities as well as the type of each removed pollutant. This is confirmed by the report of the effects of the specific chemical intervention method. In this report it is stated that in the case of

Ke-images a 18 day application of biological paste managed to remove the gypsum, while shorter in time applications (such as 24 hours or 48 hours of application) evidenced that traces of gypsum continue to be present.

The third chemical conservation method to be taken into consideration in the present work is Gagemark. This method uses wet micro blasting in order to remove the pollutants

The image below depicts the state of erosion, encountered on pillar's cannelure located on sheltered areas.

Figure 3.3

At this point it is important to mention that except for the detection of black particles, in this study we managed to isolate areas described here by the term "white particles". These areas exhibit some characteristics, e.g. they are visible as impulsive bright spots on a homogeneous background. In addition we can observe that the number of white particles as well as the percentage of image's surface covered by white particles is greater in the case of untreated surfaces than in the images obtained after the applied cleaning processes. A further reason that allows us to consider these regions as a deteriorated ones results by the algorithms implemented in this study, it is very easily observable that these areas are eliminated in accordance with the reduction of gypsum as it was reported by the chemical analyses. According to the author's

opinion these particles are associated with the gypsum presence, as well as the existence of calcium carbonate obtained after the re-crystallization process.

In the following sections the reader can observe the results obtained, when each one of the algorithms implemented in this study is applied on the available images. For each algorithm the results are displayed for treated and untreated cases.

The algorithms implemented in this work with the aim of detecting decay areas are the Highpass filtering Algorithm, Region Growing, Skewness and Kurtosis algorithm. In order to reduce the false negative and false positives introduced by the High-pass Filtering, 3 Labeling Algorithms were developed. In these algorithms, after the labeling process was carried out (& 2.3), 3 distinct procedures were used in order to apply the thresholds. Namely the algorithms used for threshold extraction are Mean and Variance, Boxplot outlier Method and Robust fitting. As it was discussed in the first chapter, except for the accurate detection of the specific locations where black\white particles exist, an issue of high importance is also to preserve the shape of the spots. Thus, 2 algorithms were developed: Gaussian Detector that detects efficiently the exact locations of black/white particles and Conditional Thickening Algorithm which guarantees both accurate detection and shape preservation.

3.2.1 High-Pass Filtering

Figure 3.4 illustrates the deterioration effects observed on a cannelure located at sheltered areas (Diagnosis Scheme)

<center>

(a)   *(b)*   *(c)*
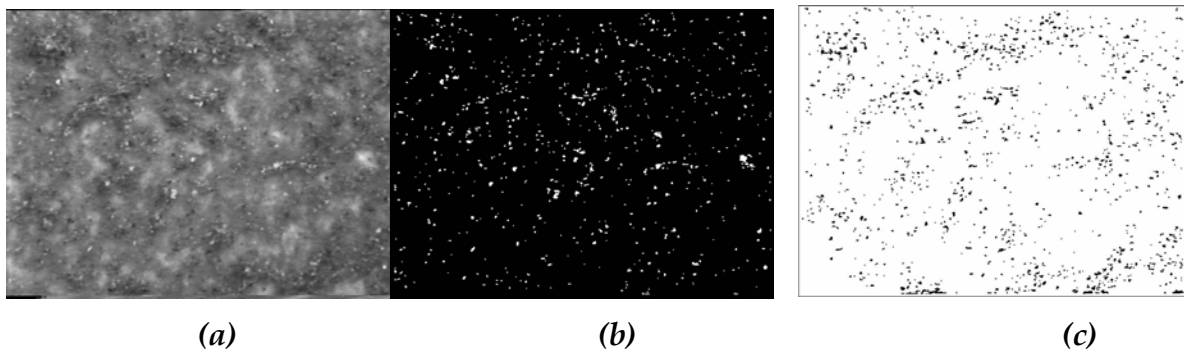
Figure 3.4

</center>

Figure 3.4(a) depicts the state of erosion before the cleaning process in a cannelure located at sheltered areas. (b) Shows the white particles detected by the algorithm (c) illustrate the locations where black spots were found.

In the following sequence of images we present how the chemical method Ds 60min managed to remove white and black particles from the cannelure discussed above.
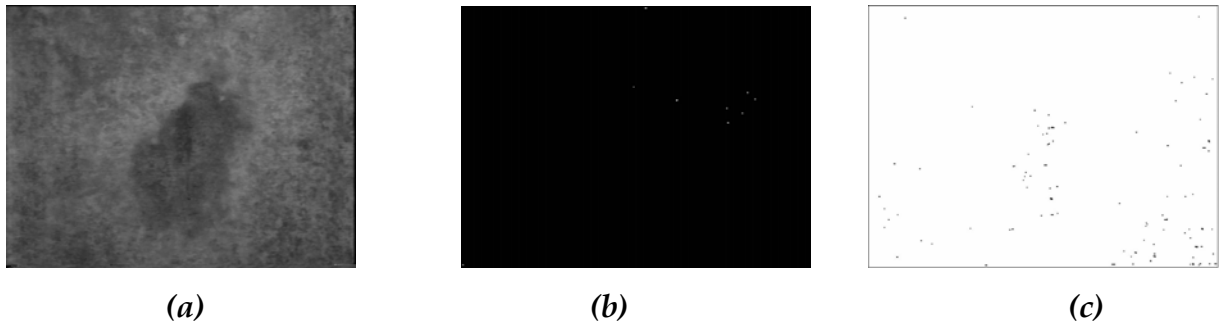

(a)	*(b)*	*(c)*

Figure 3.5

On figure 3.5(a) it is shown the area discussed above (cannelure on sheltered areas) but the image was taken after the chemical treatment with the anionic resin. Figure 3.5(b) illustrates the white spots detected by the High-pass filtering on 3.5(a).Finally 3.5(c) demonstrates the locations where black particles exist.

By comparing images 3.4 to 3.5, it is obvious that the black and white particles detected on the treated surface are less in number than those detected in the specimen before the chemical cleaning.

The images below, illustrate the results of the application of Biological paste Cleaning Method in order to clean the black crusts. These images are also reported in order to illustrate, which are the differences in the deterioration effects observed in these cases.

(a)	*(b)*	*(c)*
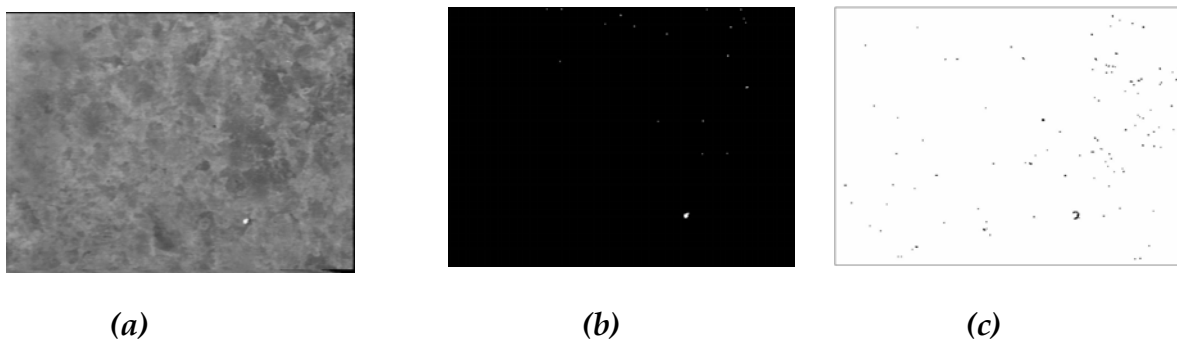
Figure 3.6

Figure 3.6(a) represents the cannelure examined above, after the restoration process with biological Paste. 3.6(b) shows the regions considered as white particles by the High Pass filtering algorithm and image 3.6(c) illustrates the dark particles detected in the image.

Finally the sequence of images reported below, illustrates the spots recognized as white and black particles in the image obtained after the cleaning of cannelure with wet micro-blasting.

| *(a)* | *(b)* | *(c)* |
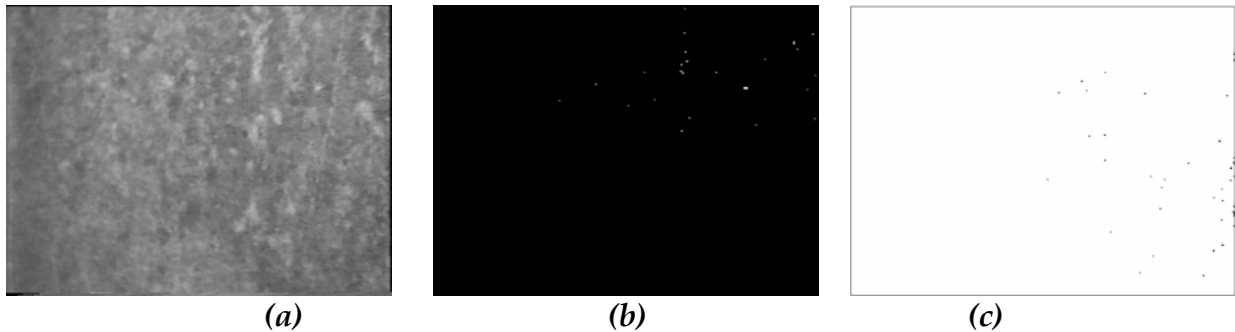
Figure 3.7

*Figure **3.7(a)** shows the image illustrating the cleaned surface by the intervention with wet micro blasting. **3.7(b)** depicts the spots considered as white particles in the image while figure **3.7(c)** shows black spots detected, by the High Pass Filtering Algorithm, on the image 3.7(a).*

By a brief observation of the images above, reported, it is obvious that the chemical intervention methods used for the conservation of stone surfaces removed the deterioration effects. The efficiency of each method though, is an important aspect. At a first view on the images, it seems that the wet micro-blasting method discussed in figure 3.7 managed to eliminate the deterioration phenomena more than the other chemical cleaning methods. This conclusion is in accordance with the assessment reported by the chemists.

As it was mentioned in the introduction of this chapter, an attempt was made to detect black and white particles on surfaces located at different areas of the monument. Our aim was to evaluate whether the algorithms implemented in this work give similar results with those obtained by the chemical analysis. The images shown below illustrate the deterioration effects observed on akmi-ravdosisx50 (arris located at sheltered area).

| *(a)* | *(b)* | *(c)* |
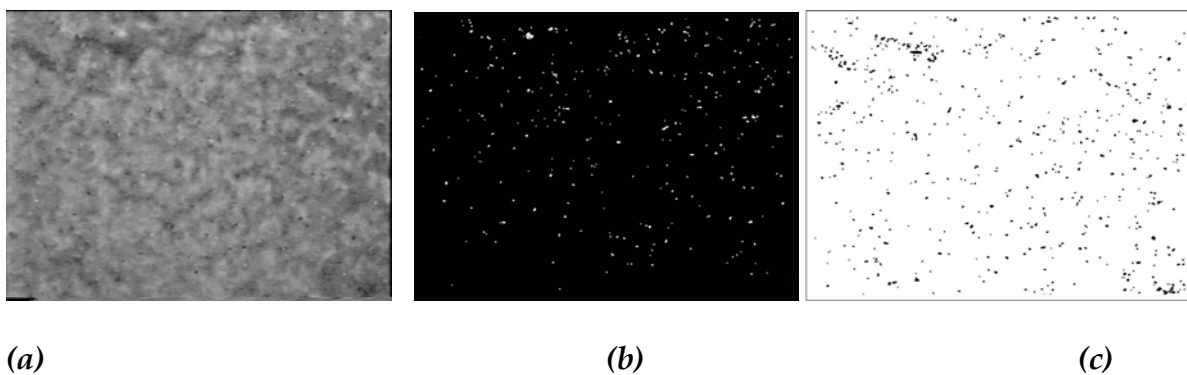
Figure 3.8

Figure 3.8(a) illustrates akmi-ravdosisx50 in the untreated scheme, 3.8(b) shows the white spots that the high pass filtering algorithm detected while 3.78(c) illustrates the existence of black particles.

By comparing the images 3.8(b) and (c) with the images 3.4(b) and (c) it can be concluded that erosion phenomena in the aulakas (figure 3.9) are more extended than in akmi (figure 3.8). This is an assessment that will be discussed in the following sections.

In the following section the results obtained after the application of Region Growing algorithm (in order to detect the problematic regions) are presented.

3.2.2 Region Growing

Figure 3.9 illustrates the deterioration effects (as determined by the Region Growing Algorithm) observed on a cannelure located at sheltered areas (Diagnosis Scheme)

(a)   *(b)*   *(c)*
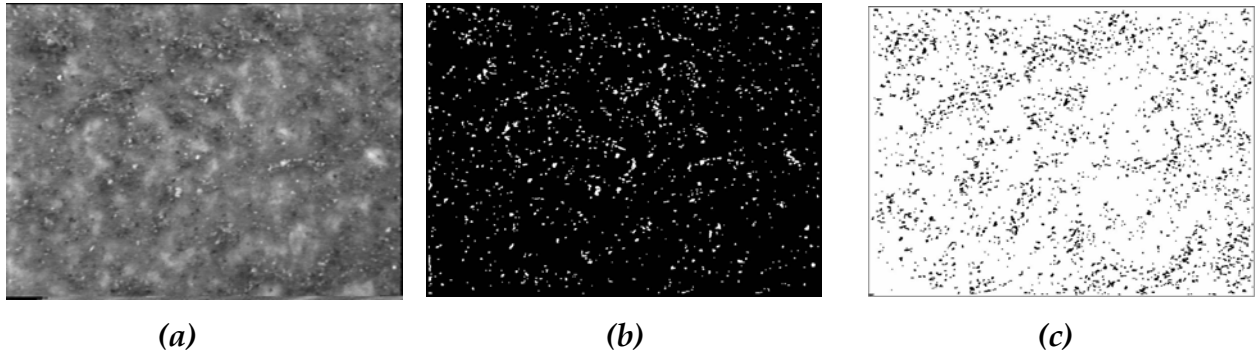
Figure 3.9

Figure 3.9(a) shows the untreated surface while images (b), (c) show white and black particles respectively.

A brief observation of the images 3.4 and 3.9 shows that Region Growing Algorithm detects more problematic regions than High-Pass Filtering. This could be explained by the fact that the Region Growing Algorithm performs local processing. As it was analyzed in the previous chapter, pixels with intensities that differ above a threshold from their neighbors are considered as problematic areas. The results extracted by this algorithm are more reliable than those obtained by high pass filtering since the specific characteristics of the image's sub-regions have been taken into consideration.

Figures 3.10, 3.11 and 3.12 demonstrate images of the same cannelure after the chemical cleaning, in which Region Growing Algorithm detected decay areas. More Specifically, 3.10

depicts the image illustrating the state of restoration after the application of the Method Ds 60 min (anionic resin in combination with calcium carbonate) while images 3.11 and 3.12 show the same surface after the application of Biological Paste and wet-micro blasting respectively.
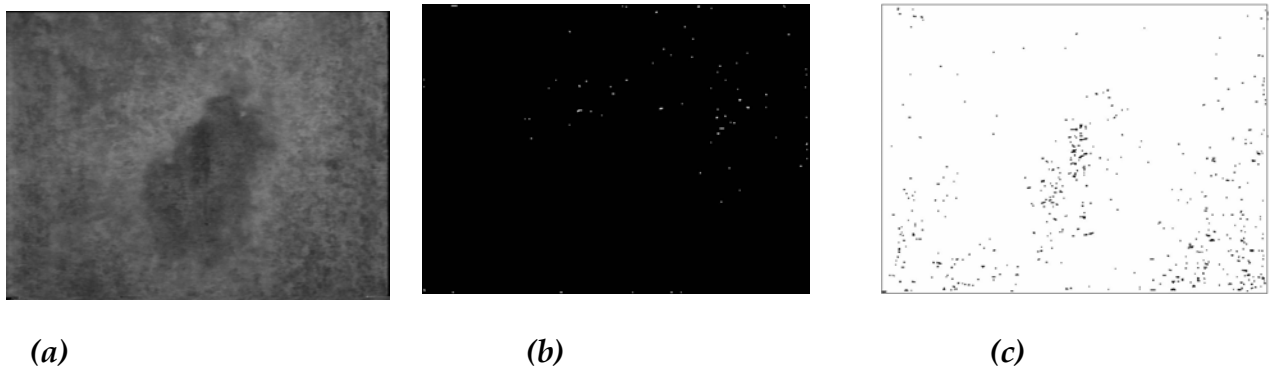

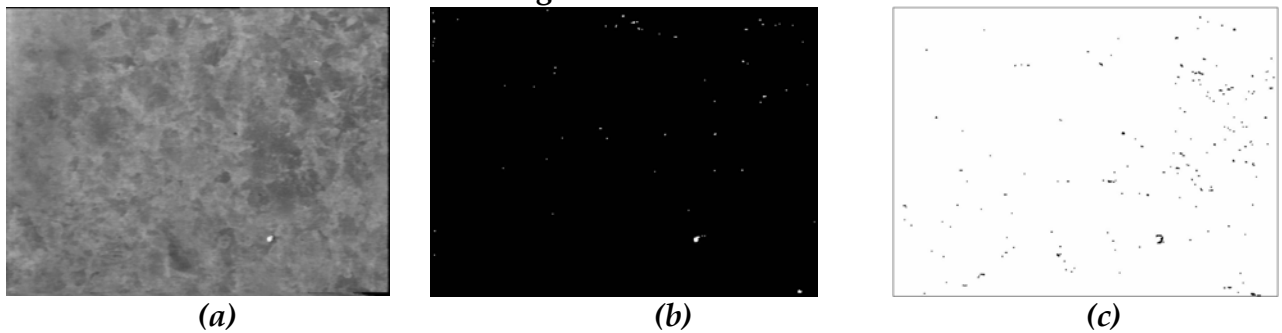*(a)*   *(b)*   *(c)*

Figure 3.10

(a)   *(b)*   *(c)*

Figure 3.11

Figures 3.10(a) and 3.11(a) illustrate the cannelure case after the treatment with Ds 60 min and Biological Paste respectively. In addition images 3.10(b) and 3.11(b) depict the white particles that the Region Growing Algorithm managed to determine. Finally images 3.10(c) and 3.11(c) display the regions considered as black particles by the Region Growing Algorithm.

Finally, the image 3.12 shows the image obtained after the application of wet micro blasting.

(a)   *(b)*   *(c)*
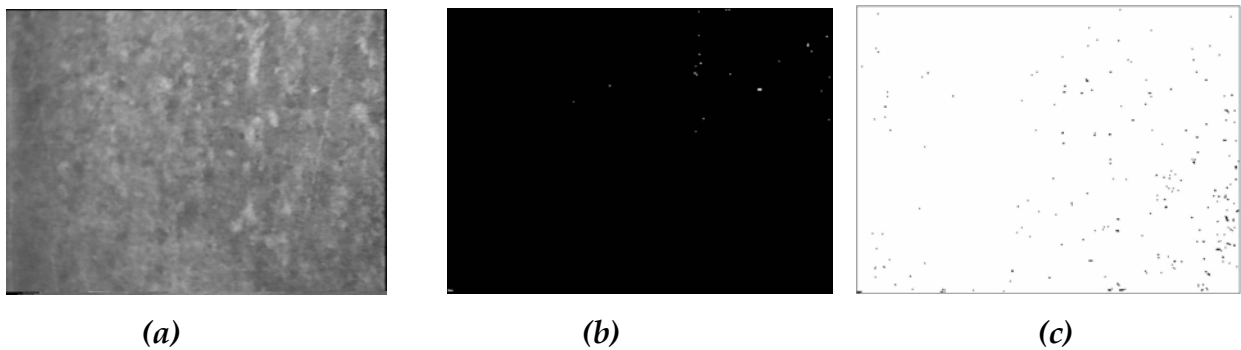
Figure 3.12

Figure 3.12(a) shows the treated surface (wet micro blasting was applied in order to remove the pollutants) while images (b), (c) show white and black particles respectively.

Another Algorithm implemented in this work is the so-called "Skewness and Kurtosis". As it was reported in the previous chapter, skewness and kurtosis are statistical variables, which values were used to define sub-regions with a high susceptibility to contain black or white particles. In the following section, images illustrating the white and black particles detected by this algorithm are reported
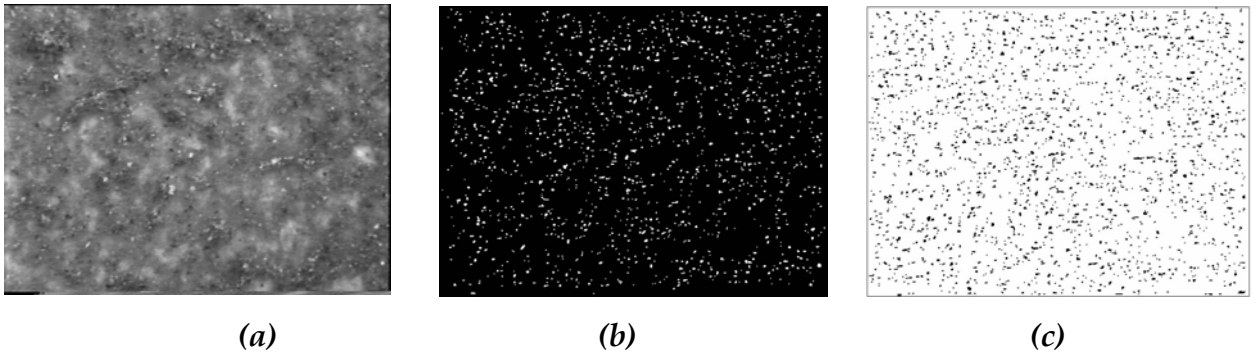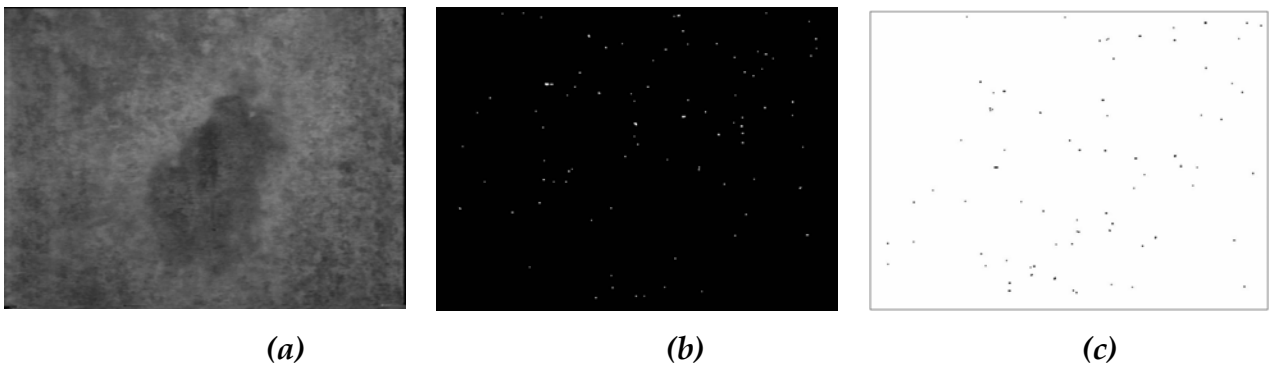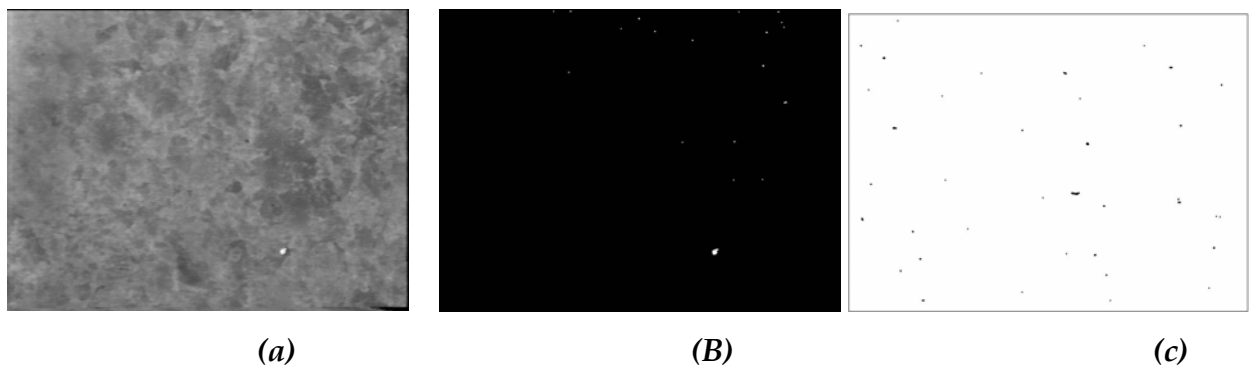
3.2.3 Skewness and Kurtosis

(a)　　　　　　　　*(b)*　　　　　　　　*(c)*

Figure 3.13

(a)　　　　　　　　*(b)*　　　　　　　　*(c)*

Figure 3.14

(a)　　　　　　　　*(B)*　　　　　　　　*(c)*

Figure 3.15

| *(a)* | *(B)* | *(c)* |
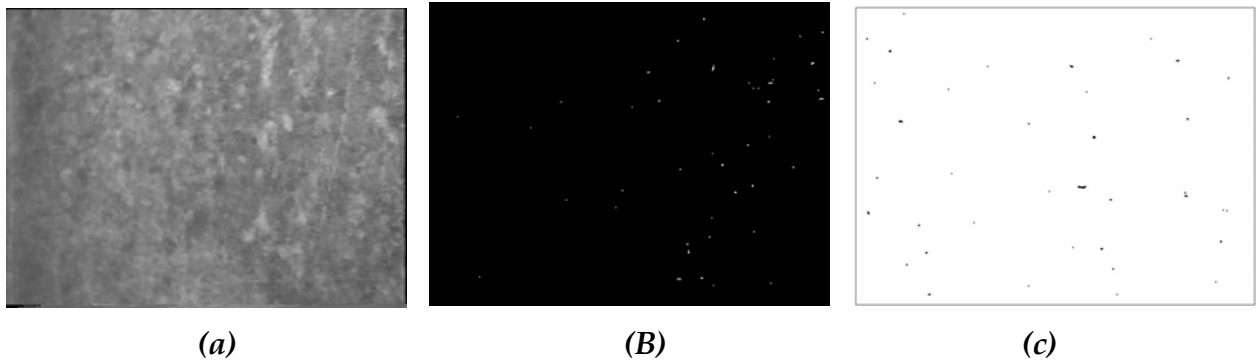
***Figure* 3.16**

Figure 3.13 illustrates the cannelure located on sheltered areas before the application of any chemical conservation method. More specifically, 3.13(b) depicts the black particles detected onto the image while in picture 3.13(c) we can see the regions defined as white spots by the Skew-ness and Kurtosis Algorithm. Image 3.14(a) shows the state of restoration after the application of Ds 60 min Method while schemes (b) and (c) display the white and black particles respectively as they were detected by the Algorithm. The image 3.15 depicts the deterioration effects detected on the stone surface after the intervention with the Biological Paste method. Figure 3.16 illustrates the case of cleaning carried out by the application of wet micro blasting

In the following section, the results obtained after the application of Labeling Algorithms on the studied images are given. These algorithms were implemented in order to remove false negatives and false positives introduced by the High Pass Filtering algorithm. Their accuracy is estimated to be better as they perform local Processing, which means that the specific characteristics of the background at each sub-region are taken into consideration.
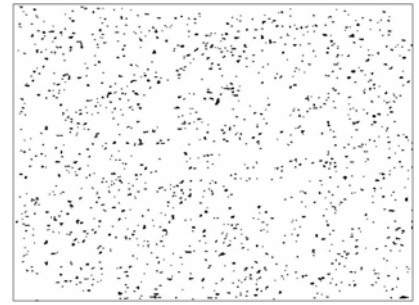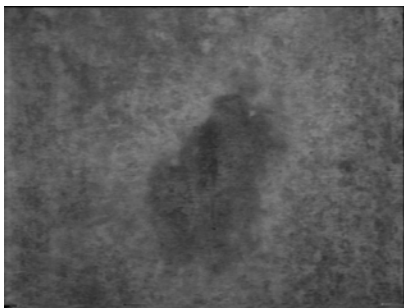
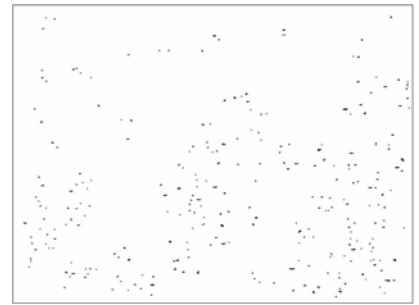### 3.2.4 Labeling Algorithms (Mean-Variance Thresholding)
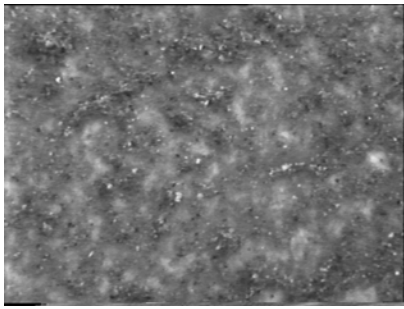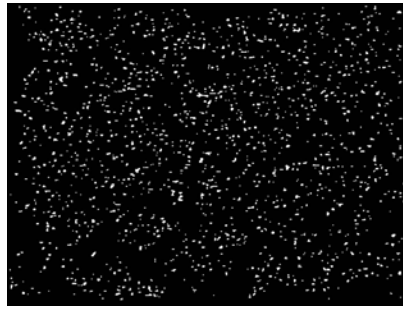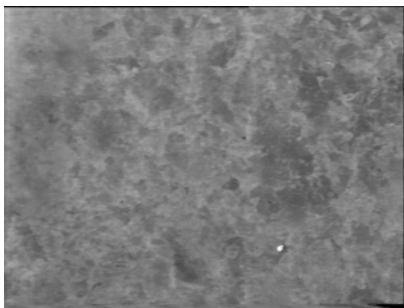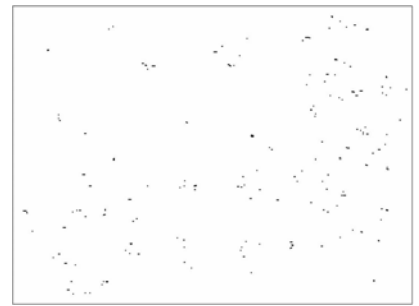

(a) *(b)* *(c)*

Figure 3.17

(a) *(b)* *(c)*
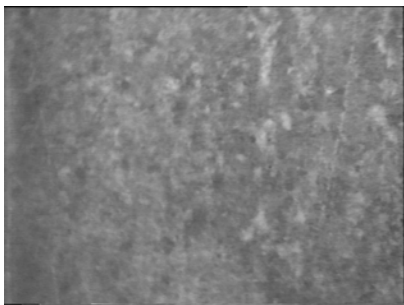
Figure 3.18

(a) *(b)* *(c)*

Figure 3.19

(a) *(b)* *(c)*

Figure 3.20

85

Figure 3.17 illustrates the cannelure located on sheltered areas before the application of any chemical conservation method. More specifically, 3.17(b) depicts the white particles detected onto the image while in picture 3.17(c) we can see the regions defined as black spots by the Algorithm.

Image 3.18(a) shows the state of restoration after the application of Ds 60 min Method while schemes (b) and (c) display the white and black particles, respectively, according to the Algorithm detected them. In addition, the image 3.19 depicts the deterioration effects detected on the stone surface after the intervention with the Biological Paste method. The figure 3.20 illustrates the case where the conservation was conducted by the application of wet micro blasting.

By comparing the results obtained by this Labeling Algorithm with those given by the High Pass Filtering Algorithm, it can be observed that the surface sizes detected by the labeling algorithm are in general smaller. This conclusion is very reasonable by considering that High Pass Filtering Algorithm usually merged neighboring decay areas. This can be observed not only on the results of this Algorithm but also in all the results, since Ds 60min Method has removed less pollutant than the other two methods (Gagemark and Biological Paste). The results are in accordance with these obtained by the chemical cleaning.

We implemented other two Labeling Algorithms in this study (Box Plot Thresholding and Robust Fit). The thresholds applied, were determined by some statistical data concerning the distribution of gray values in each sub-region. The results obtained by these algorithms are quite similar with those reported above. Nevertheless the illustration of these results is not considered necessary.

Apart from the images illustrated above, the results obtained by applying the Gaussian Detector and Conditional Thickening Method to the images under consideration will also be displayed. The Conditional Thickening Method comprises a combination of the Gaussian Detector and a detection process using Morphological Operations, as it was discussed in the previous chapter. According to the literature, Gaussian Detector is a good detector, as it determines with a high accuracy the location of problematic regions, but it cannot preserve the shape of the region. On the other hand, morphological operations preserve the shape of spots, but increase high positive rate. Conditional Thickening, as a combination of the Gaussian Detector and Morphological Operations guarantees both, preserved shape and false positive rate.
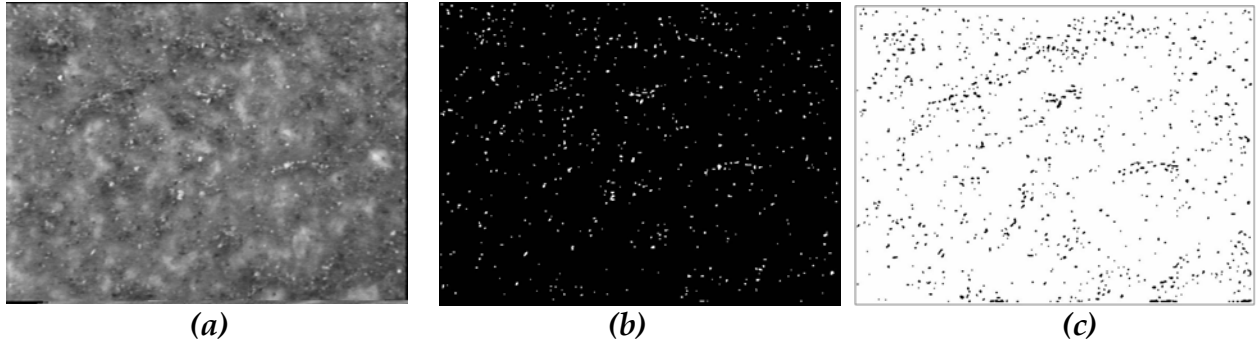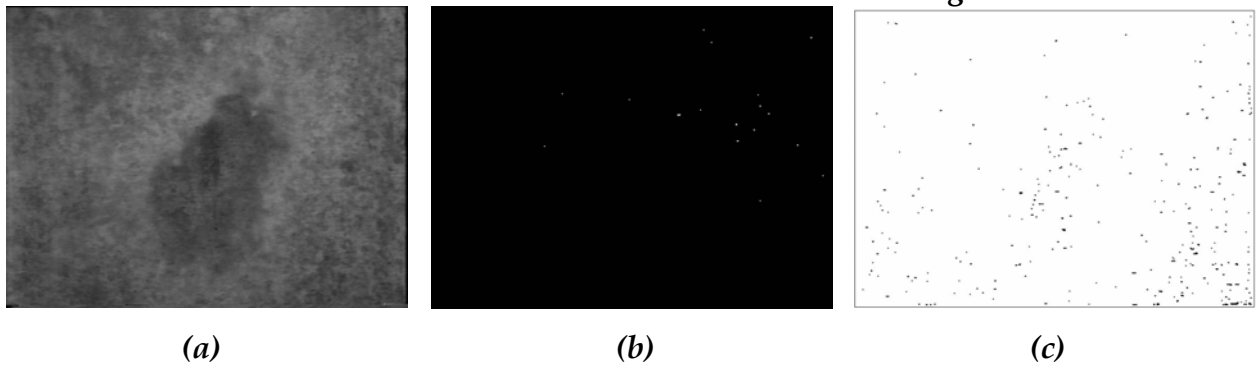
3.2.5 Gaussian Detector

(a) (b) (c)

Figure 3.21

(a) (b) (c)

Figure 3.22

(a) (b) (c)

Figure 3.23

(a) (b) (c)

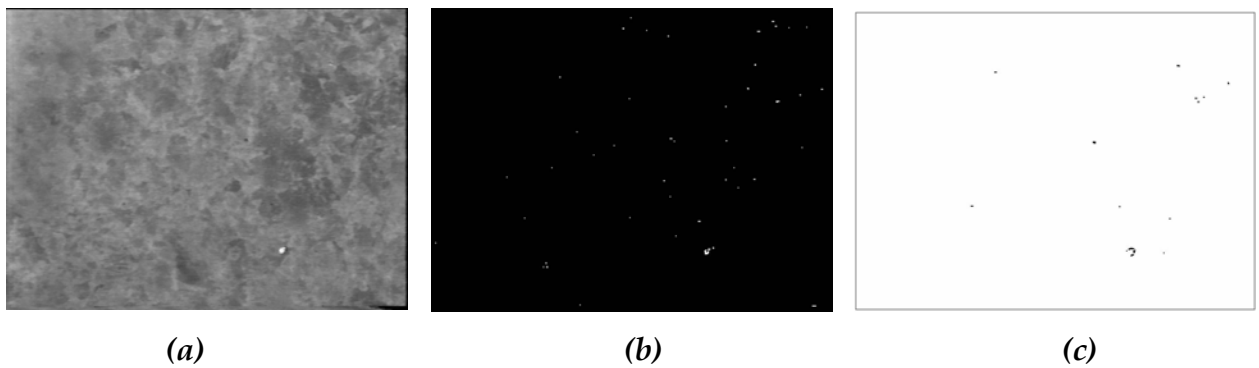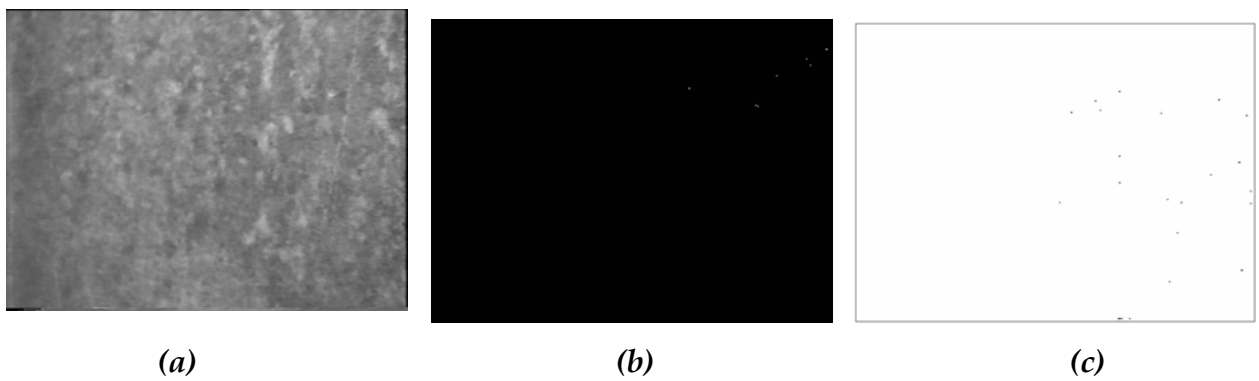*Figure 3.24*

Figure 3.21(a) depicts the studied cannelure with all the algorithms before any chemical conservation method, while images 3.21(b) and 3.21(c) show white and black particles respectively, defined by the algorithm. The image 3.22 illustrates the deterioration state after the application of Ds 60min and in schemes (b), (c) it can be observed the detected white and black particles. Images 3.23 and 3.24 show the same canellure after the intervention with Biological Paste and wet micro blasting respectively.

In the Following section, the results of the application of Conditional Thickening algorithm are displayed.
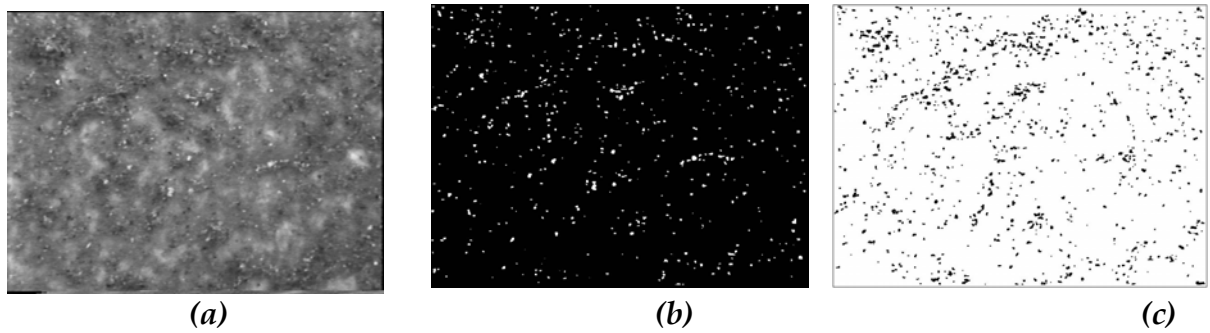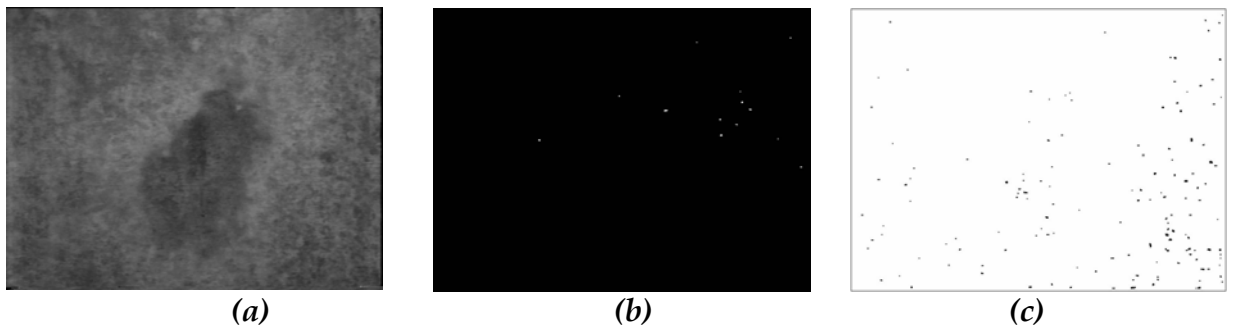
3.2.6 Conditional Thickening

(a)   *(b)*   *(c)*

Figure 3.25

(a)   *(b)*   *(c)*

Figure 3.26

(a)   *(b)*   *(c)*
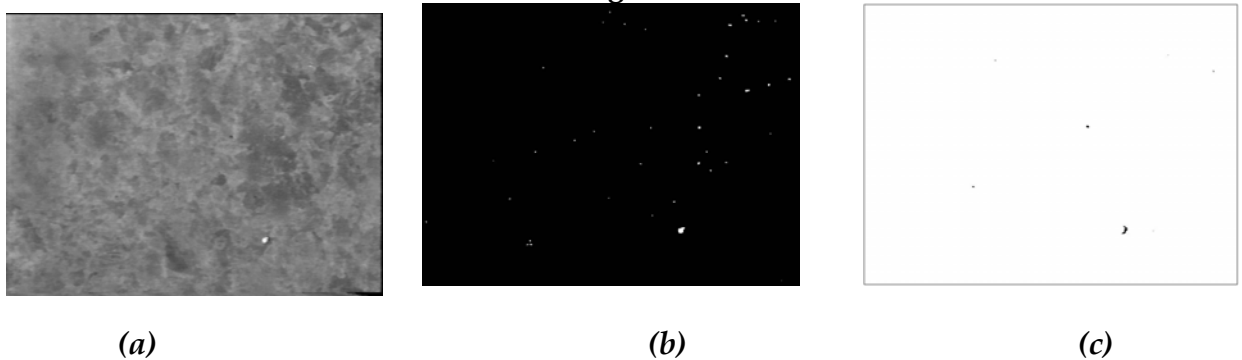
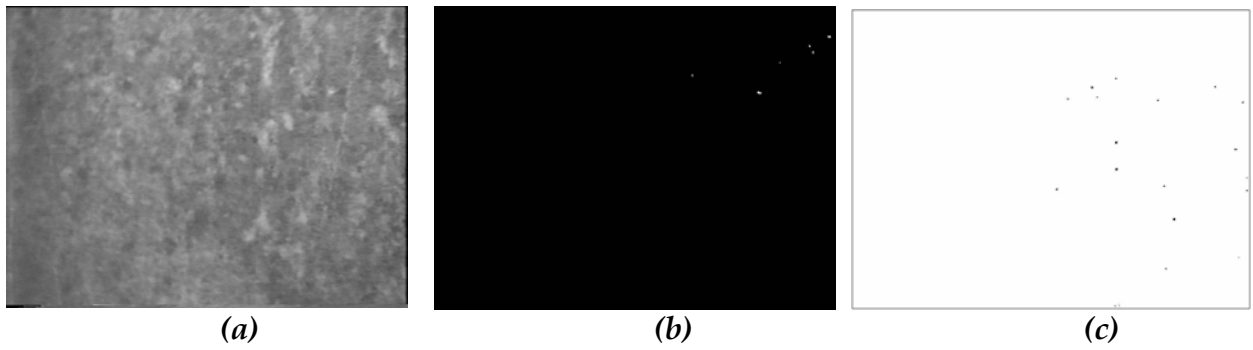*Figure 3.27*

(a)   *(b)*   *(c)*

Figure 3.28

Figure 3.25 illustrates the cannelure located on sheltered areas before the application of any chemical conservation method. More specifically, 3.25(b) depicts the white particles detected onto the image while in picture 3.25(c) it can be seen the regions defined as black spots by the Algorithm.
Image 3.26(a) shows the state of restoration after the application of Ds 60 min Method while schemes (b) and (c) display the white and black particles, respectively, according to the Algorithm detected them. The image 3.27 depicts the deterioration effects detected on the stone surface after the intervention with the Biological Paste method. The figure 3.28 illustrates the areas in which wet micro blasting was carried out.

As it is obvious by a brief observation of the images, particles detected by the Conditional Thickening Algorithm are more extended than those detected by the Gaussian Detector. Super Imposing of the results given by Conditional Thickening Algorithm on the original image evidences that it approaches the actual shape of the particles considered to be white or black spots.

3.2.7 Observations and discussion on the result images

By observing the images reported above it can be seen that the spots detected as decay areas vary in number, in extent as well as in the shape that they exhibit. Furthermore, it can be easily deduced that some algorithms respond in a similar way. At this point it should be highlighted that after a comparison on the result images, it was evidenced that the vast majority of the black/white particles were detected by all the algorithms (Especially those that are larger in size and are located on inhomogeneous background). In an attempt to study the efficiency of the algorithms developed in this work, it can be argued that High-pass filtering algorithm does not take into consideration the local characteristics of the background and it introduces many false positive and false negative spots. This argue, could be proved by overlying an image

89

depicting black\white particles onto the original image. Such an experiment would evidence that high-pass filtering merges decay areas and cannot approach efficiently their shape. Furthermore, the result images obtained by different algorithms demonstrate a similarity. As an example of this fact it could be mentioned the case of the 3 Labeling Algorithms. By observing their results, it is obvious that these algorithms detected almost the same decay areas. More Specifically, their results exhibit similarities not only to the specific points, which were determined as decay areas, but also to their shape. The results obtained by these algorithms are more reliable as they were constructed in order to reduce the false positive rate introduced by the High pass filtering algorithm. The regions, which were determined as black or white particles by the labeling algorithms are smaller in size. Another observation that can be made on these results is that decay areas, which are considered as an entity by the High-pass Algorithm, are split into 2 or more sets of pixels by the Labeling algorithms. Region growing process is an algorithm that guarantees low false positive rate but increases the computational time. The results obtained by the Region Growing Algorithm and the Skewness and Kurtosis Algorithm show some similar features concerning especially the number of the black/white particles defined by the two algorithms. Finally the last 2 algorithms, Gaussian detector and Conditional thickening were developed in order to detect the decay areas at the correct locations while preserving the shape of these areas. More specifically, by observing the images presented above, it can be observed that Gaussian detector defines more distinct spots as black/white particles but it does not preserve their shape. Thus it can be argued that the Gaussian Detector manages to determine efficiently the co-ordinates of an image where black or white particles are present but it cannot approach their shape. On the hand Conditional Thickening Algorithm guarantees both accurate detection and shape preservation.

Another aspect that should be reported at this point is the efficiency of the chemical cleaning methods studied in this survey. At first it should be stated that the number of black\white spots detected in the images, which show the deterioration state before the chemical cleaning, are greater in number than in the images that depict the degradation patterns on the treated surfaces. (This is very obvious if for example image 3.25(c) is compared to the image 3.26(c)). Furthermore by comparing the images 3.4(b),(c) to the images 3.8(b),(c) respectively , it can be argued that in the image 3.8(b)/(c) less particles were defined as decay areas than in the images 3.4(b)/(c). By this observation it becomes evident that in the arris located on sheltered

regions (image 3.8) less black/white particles are present. This conclusion is in accordance with the results obtained after the chemists examined the stone surface. An attempt to compare chemical cleaning methods according to their efficiency would be rather dangerous. A brief observation though of the images depicted above enforces the author to consider the Ds 60min method as the cleaning process that removes less pollutant. The assessment stated above was made by comparing the images 3.26 (b) and (c) with the images 3.27(b),(c) and 3.28(b),(c) where it can be observed that more decay areas prevail in the images 3.26(b) and (c) than in the other. This observation is also confirmed by the results obtained after the deterioration phenomena were studied by the chemists. Finally in the images presented in the previous sections of this chapter it is shown that the wet micro blasting method removes the deterioration effects more efficiently. This conclusion is based on the number of detected black/white spots in the images depicting stone surfaces after the chemical cleaning methods. All these observation reported in this section are also depicted on the diagrams presented below.

3.3 Diagrams depicting the number of Black and white Spots that exist on Stone Surfaces

*Apart from the images reported above, it was considered essential to present some diagrammatic results illustrating the state of deterioration diagnosed on the untreated surfaces, as well as the efficiency of each conservation method. The diagrammatic results concern 3 of the available specimens. More specifically, from the Ke-Images we are studying the samples **aulakas-ravdosisx50** and **akmi-ravdosisx50**. From these two samples the first one belongs to a cannelure located at a sheltered area while the second belongs to an arris at a sheltered area. As far Ks- images are concerned, the diagrammatic data represent a cannelure located at a unsheltered area (**aulakas-ravdosisx50**). These surfaces were studied before and after the application of chemical cleaning.*

The diagrams shown in the following section depict the number of black and white particles detected on the surfaces under consideration. The order in which the results are presented gives the opportunity to the human eye to compare deterioration effects on the 3 surfaces. At first, the diagram below represents the number of black spots detected on the cannelure located at sheltered areas (Ke-Images). We define this surface by the term aulakas-ravdosisx50.

Number of Black
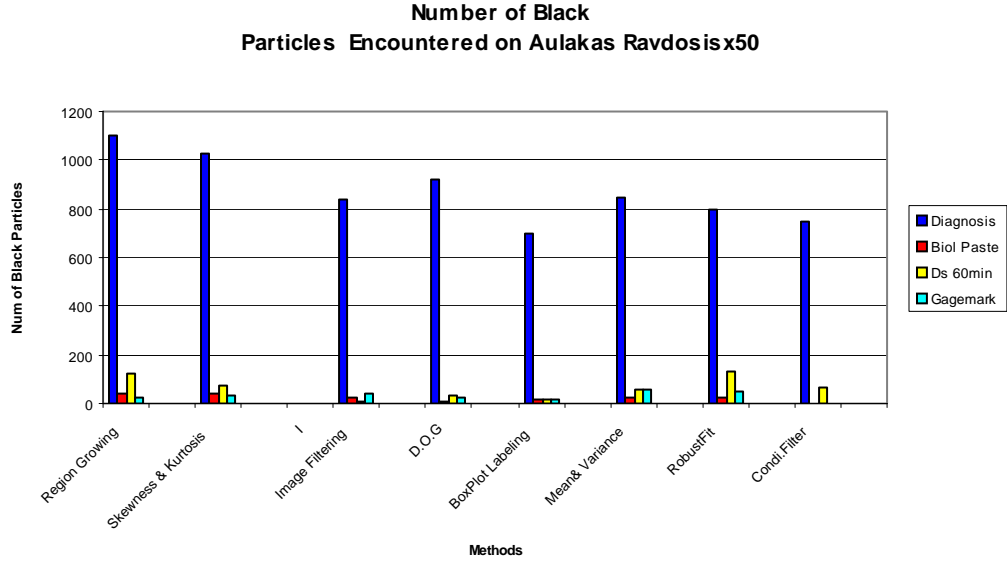**Particles Encountered on Aulakas Ravdosis x50**

Figure 3.29

As it is obvious by observing the figure above, all the algorithms applied, detected less black particles on the studied surfaces after the chemical cleaning. A better reading of the diagram evidences that there are some algorithms with similar response. We can see for example, that the number of black particles detected by the Region Growing and Skewness and Kurtosis are similar. A similar assessment is valid for the case of the three labeling Algorithms (Mean-Variance, Box Plot, Robust Fit). Furthermore the number of black particles detected by the High Pass Filtering is similar with the regions defined as black particles by the Gaussian Detector (DOG).

The following figure, illustrates the number of black spots detected on a pillar's arris located on a sheltered area. In figure 3.31 the number of black particles detected on a cannelure located on an unsheltered area is shown. We define the arris discussed above by the term 'akmi-ravdosisx50 (Ke-images)' and the cannelure located on the unsheltered area by the term 'aulakas-ravdosisx50 (Ks-Images)'.
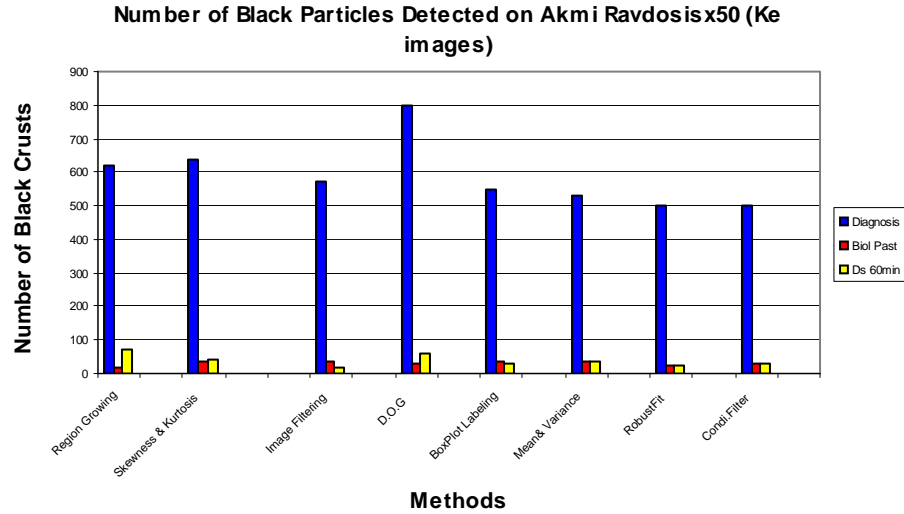
Number of Black Particles Detected on Akmi Ravdosisx50 (Ke images)

Figure 3.30

Number of Black Particles detected on aulakas ravdosisx50 (Ks Images)
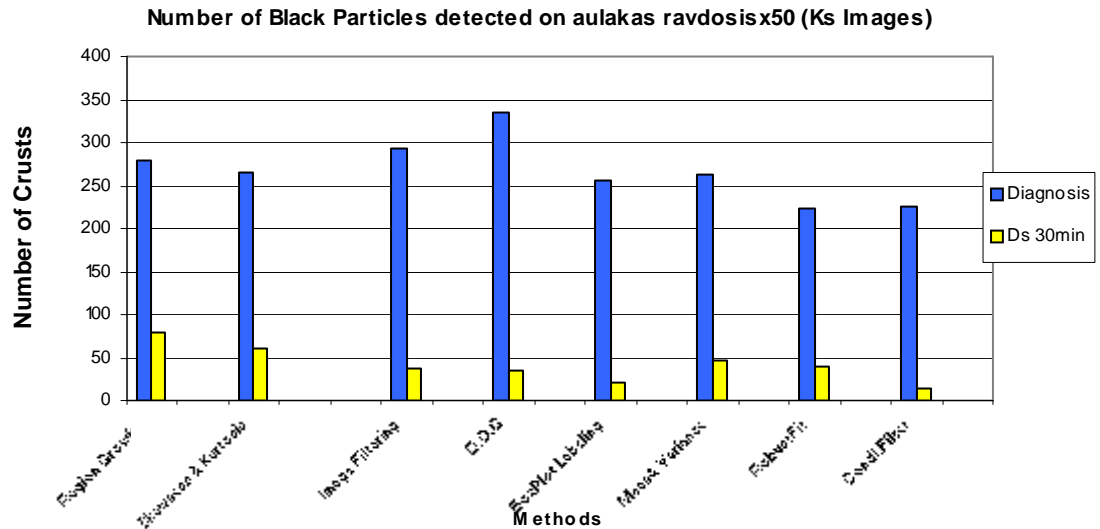
Figure 3.31

It can be observed that the number of problematic regions defined as black spots are more in the diagram 3.29 (cannelure located on sheltered areas) than in the other two. This result was expectable because of the different climate conditions to which the surfaces are exposed. As was stated above, more extended black crusts were observed on cannelures at sheltered areas comparing to the cannelures and to arrises located at unsheltered areas.. In addition, the diagrams of figures 3.30 and 3.31, show that more black particles were encountered in figure 3.30, than in 3.31. This is also explainable by the fact that the main erosion phenomena prevailed on exposed surfaces, are discoloration and foiling, because of the removal of black spots and gypsum by the rain's action. Trying to compare the response of the algorithms used in detecting

93

black particles at both cases, it can be argued that Region Growing and Skewness and Kurtosis Algorithms determined almost the same number of regions as black particles. The same fact is observed for the case of the three labeling Algorithms. The number of black particles determined is similar. In the figure 3.30 it can be seen that D.O.G algorithm (Gaussian Detector) detected more black particles than the other algorithms. This does not mean that this algorithm has the worse response in detecting black particles. It can be simply explained by taking into consideration that this algorithm has the drawback of not preserving the shape of black particles. Thus a region considered as an entity by the other algorithms, is broken into two or more sets of pixels (spots) by the Gaussian Detector. In general the number of spots detected by the algorithms in figures 3.30 and 3.31 are similar (except for the D.O.G algorithm on image 3.30). An effort to assess the efficiency of the chemical conservation method by reading the diagrams above reported would be rather dangerous. According to the author opinion though Ds 60min (application of anionic resin in combination with ammonium carbonate) seems to remove less decay regions. This can be observed in the diagrams 3.29 and 3.30, where the number of black particles detected after the application of Ds is greater than in the other schemes. Such an estimation was also obtained by the chemical analysis of the treated specimens.

In the following figures, the number of white particles detected on the three surfaces is reported. At first, the diagram depicting the number of white spots detected on the cannelure located at sheltered area is given.
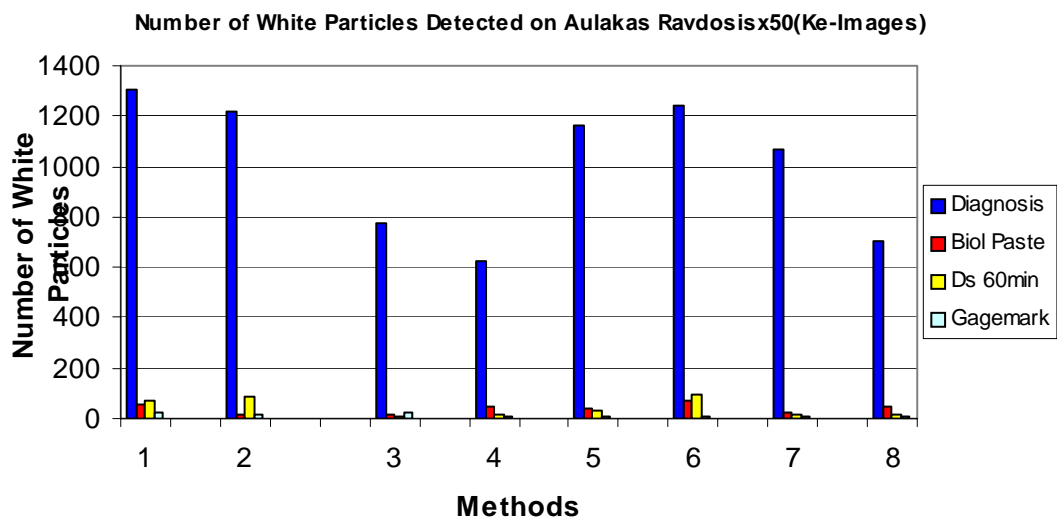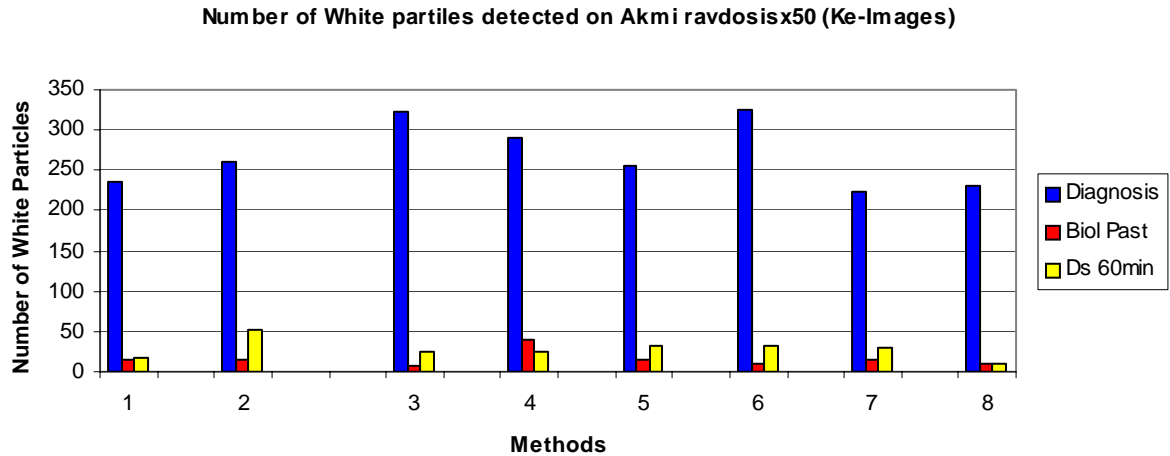

Figure 3.32

Number of White partiles detected on Akmi ravdosisx50 (Ke-Images)

figure 3.33

Num of White crusts detected on Aulakas Ravdosisx50(Ks images)
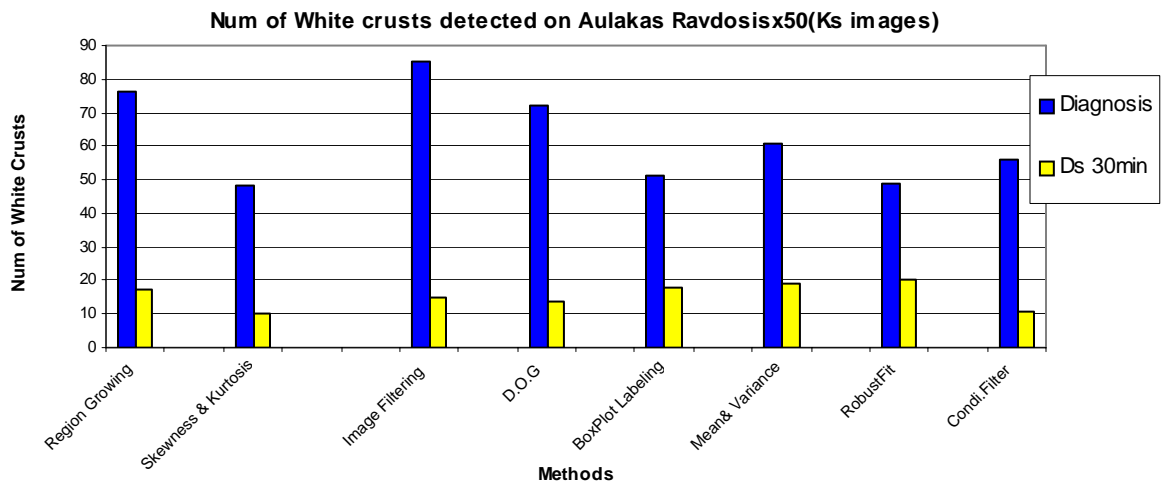
figure 3.34

By observing the 3 diagrams above reported it can be argued that the conclusions made for the detection of black spots are also valid in the case of white particles. In the surfaces before the application of any chemical conservation method more white particles are present than in the corresponding after the cleaning. It can also be seen that more white spots were detected in the diagram 3.32 than in diagrams 3.33 and 3.33. Trying to find the mean particle number detected at each case (on the untreated scheme) we would find that the mean number of white particles detected is around 1000 (figure 3.32) while in fig 3.33 the same number is around 275 and in figure 3.34 it would be around 60. These results are quite reasonable as gypsum layers prevail in areas not exposed to rain. Specimens less exposed to rain action are represented by the data of figure 3.32. In the above diagrams it can be seen that the total number of white particles detected both by the Region Growing Algorithm and those defined by the Skewness and Kurtosis

Algorithm are similar. In addition, the results obtained by the three labeling algorithms indicate that the Mean-Variance Algorithm define more spots as white particles than the other two (Robust Fit, Box Plot).

3.4 Diagrams depicting the percentage of coverage with Black Spots on Stone Surfaces.

Except for studying the total number of black and white particles it was also considered important to know the percentage of the total surface covered by decay areas (white or black particles). Thus it was estimated to be essential the presentation of diagrammatic data concerning this issue. In the diagrams illustrated below it becomes evident how the percentage of surfaces covered by pollutants is changed over cleaned and un-cleaned surfaces. These diagrams demonstrate the extent of the decay area in the image. According to the authors opinion these diagrams give a clearer answer about the state of deterioration encountered on each specimen.

The first diagram shown below depicts the percentage of surface covered by black spots in case of the cannelure located at sheltered areas.
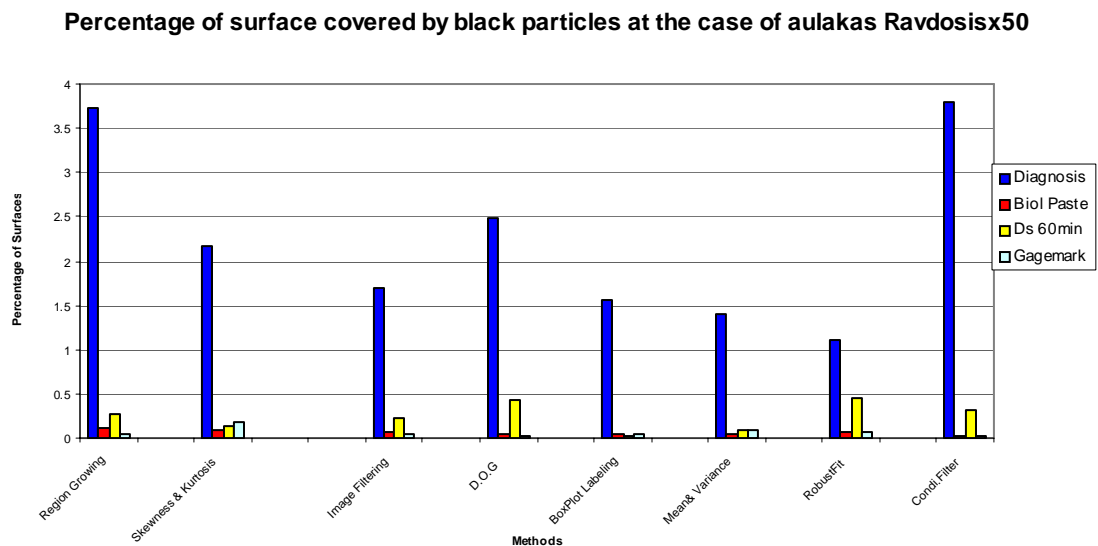
Percentage of surface covered by black particles at the case of aulakas Ravdosisx50

Figure 3.35
At the next figure we can see the case of the arris located at the same region

Percentage of surface covered by black particles at the case of akmi Ravdosisx50
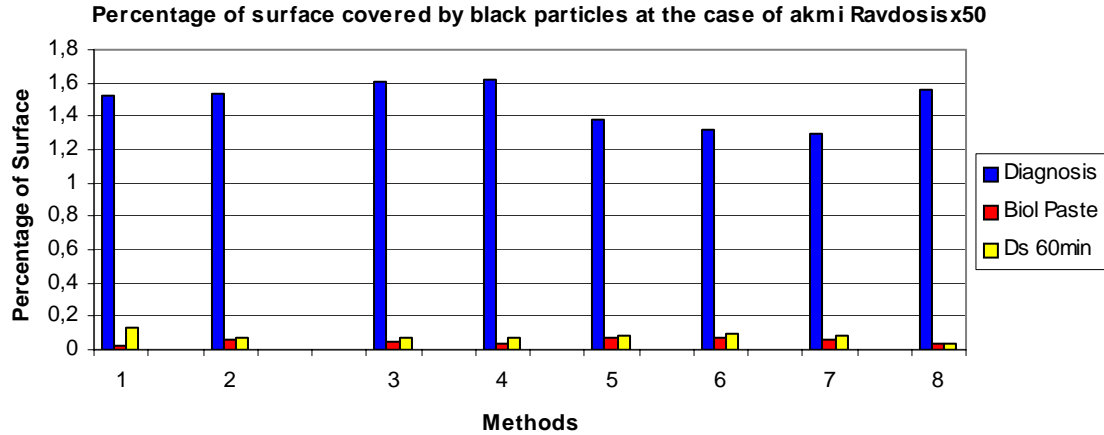
Figure 3.36

At the next figure we can see the case of a cannelure located at the unsheltered areas.

Percentege of the Surface Covered by Black Crusts
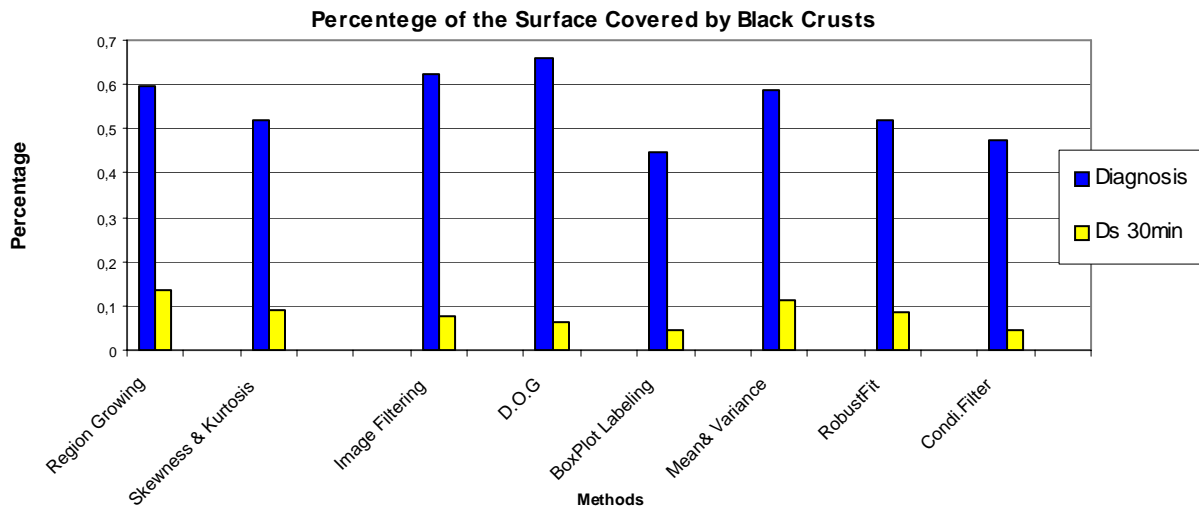
Figure 3.37

By comparing the figures above it can be stated that, in general, protected cannelure surfaces are covered by black particles to a greater extent. The percentage of surface covered by black spots, according to the algorithms determined it seems to vary (especially in the case of the diagram 3.35). This can be explained by the fact that these algorithms demonstrate a different accuracy in preserving the particles shape. It is obvious that the first cannelure is related to more deterioration patterns (in the untreated case). To evidence this, it can simply be compared the percentage of surface covered by black spots, as determined by the Conditional Thickening Algorithm, which performs better shape preserving. In the diagram 3.35 the percentage of surface covered by black particles, as this was determined by the Conditional Thickening Algorithm, (protected cannelure) is 3.8057 while in the diagram **3.36** (arris located at sheltered

*area) is equal to 1.5582 and finally in the last diagram this value is 0.473. In order to extract more reliable results concerning the erosion degree observed in the studied surfaces, the mean value of the surfaces percentage covered by black particles (in the untreated cases) was calculated. The values were the following: for the case of the diagram 3.35 the mean value of the surface percentage covered by black spots was equal to **2.2415%**, for the diagram 3.36 the same value was equal to **1.4834%** while for the last diagram the mean value was **0.5529%**. The results obtained are in accordance with the chemical evaluation of the deterioration effects. The cannelure located at sheltered areas demonstrates more deterioration phenomena than the other two specimens; the arris (located also at sheltered region) is more eroded than the cannelure located on an unsheltered area. The results of the diagrams reported above indicate that Conditional Thickening algorithms determine a higher percentage of surface covered by black spots than the other algorithms (in the untreated surface). This conclusion is not valid for the case of the last diagram because very few regions were detected as problematic.*

The percentage values discussed are presented in the table below.

Table 1

	Diagram-4.35 *(aulakas-ravdosisx50 located at sheltered areas)*	*Diagram-4.36* *(akmi-ravdosisx50 located at sheltered areas)*	*Diagram-4.37* *(aulakas-ravdosisx50 located at unsheltered areas)*
Percentage of the surface covered by black particles (as it was determined by the Conditional-Thickening Algorithm)	*3.8057%*	*1.5582%*	*0.474%*
Mean value of the percentage coverage (The mean value was computed by the results of all the algorithms)	*2.2415%*	*1.4834%*	*0.5529%*

In the following section the diagrams depicting the coverage of white spots and the surfaces under consideration are presented, in the same as this followed for the above diagrams.

3.5 Diagrams depicting the percentage of coverage with White Spots on Stone Surfaces.

The diagram of figure 3.38 demonstrates the percentage of surface covered by white particles in the case of the cannelure located at sheltered areas.

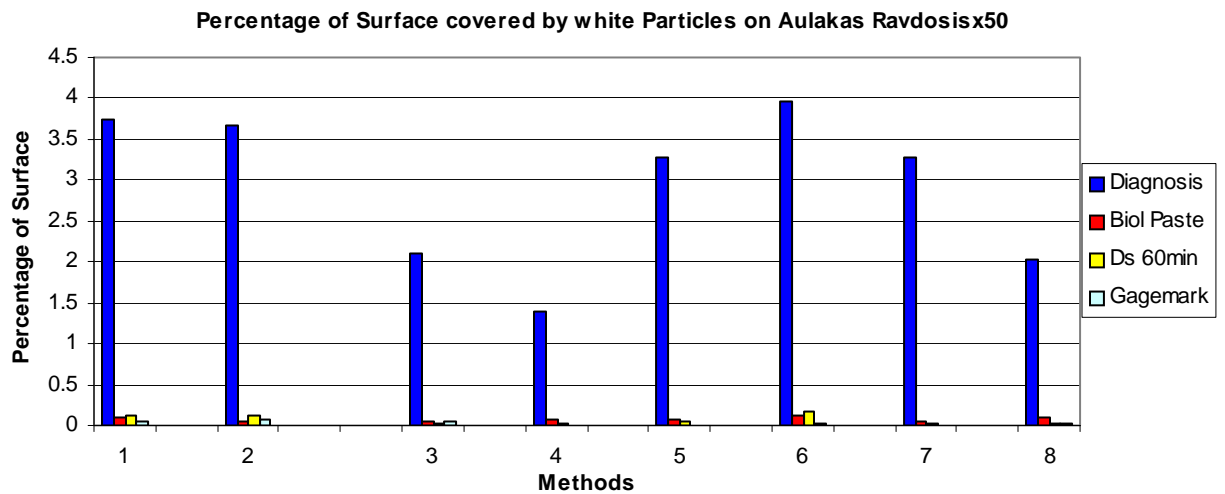**Percentage of Surface covered by white Particles on Aulakas Ravdosis x50**

Figure 3.38

In the figure 3.39 the case of the arris located at the same region is depicted.

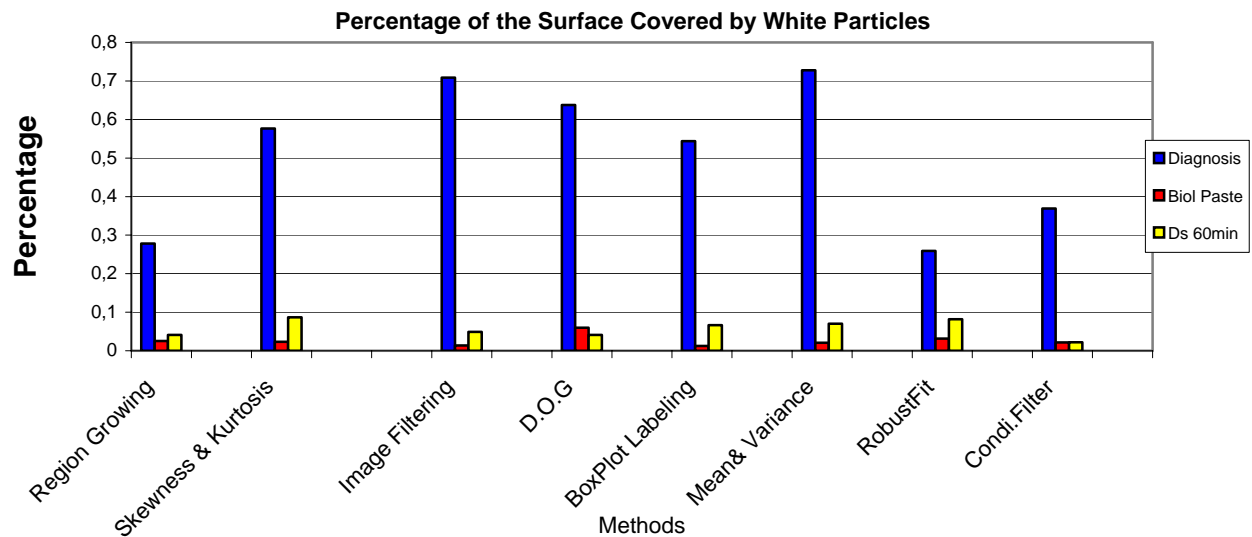**Percentage of the Surface Covered by White Particles**

Figure 3.39

By comparing the diagrams it can clearly be seen that white particles are more extended on the cannelure surface. More specifically, Mean-Variance determined the maximum surface percentage of the arris covered by black spots is equal to 0.7277%, while D.O.G in diagram 3.38 showed that the minimum percentage of white particles is 1.49. Thus the results extracted by this study are completely compatible with the chemical evaluation of the problem which reported that more gypsum crystals were detected on the cannelures of (Ke-Images) than on arrises.

At the next figure it can be seen the case of a cannelure located on the unsheltered areas.
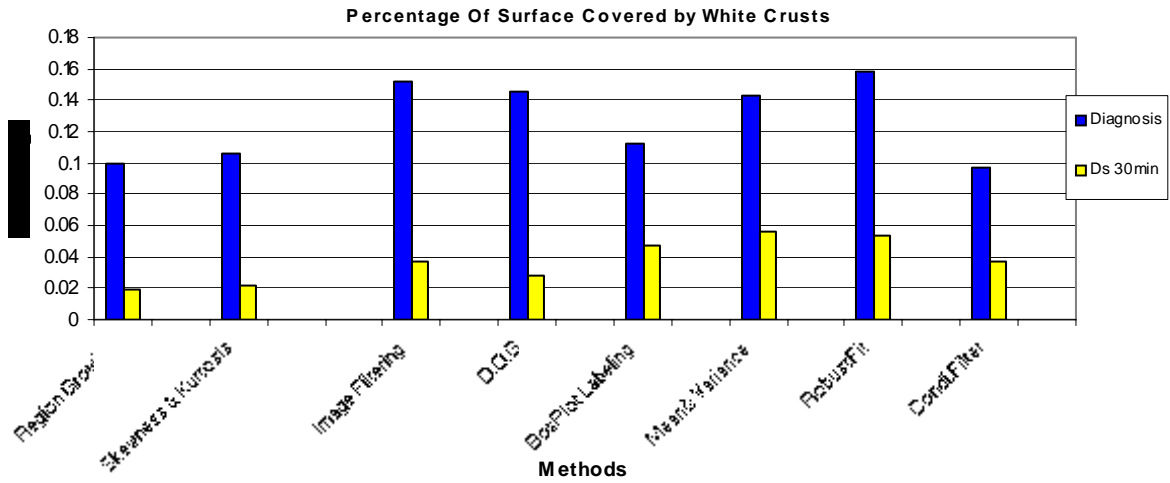
Figure 3.40

*The diagram 3.40 evidences that on unsheltered areas the presence of either gypsum or calcium carbonate is less extended (as stated above gypsum and calcium carbonate are represented as white particles in the images studied here). As it can be observed the higher percentage of surface covered by white particles is determined by the Robust Fit Labeling Algorithm (equal to 0.16%), while in the other diagrams this value is higher. For example in the first diagram, the mean surface percentage covered by white particles is **2.935015%,** while this value in the case of unsheltered areas is equal to 0.51263%.*

3.6 Distribution of Surface Sizes of Black Particles

An aspect of high importance for the current work is to study the extent (in pixels) of the black particles, which were detected in the images. Further to the extent an attempt was made to

100

determine some statistical data that could help in the description of the problem and the comprehension of the way that the chemical conservation methods function. We display below some statistical data depicting the distribution of surface sizes of black/white particles. This process was carried out in order to understand how the distribution of surface sizes is affected by the chemical cleaning methods applied to untreated surfaces, as well as to observe how this distribution vary among the results obtained from the different algorithms.

In order to illustrate the distribution of surface sizes, depicting the extent of black or white spots, it is essential the definition of some measures used in this illustration. The definition of these measures is analyzed below.

Maximum surface: *Its value corresponds to the extent of the particle with the greater surface among all the black/white particles encountered in the image.*

Minimum surface: The *value assigned to this variable is the acreage of the black/white particle with the least surface.*

Median: *Median as well as lower and upper quartiles are computed in order to provide information about the shape of the data as well as its location and spread. The value returned by median is greater than 50 % of the black/white particles surfaces values.*

Lower Quartile. *Lower quartile returns a value that is greater than 25 % of the values of black/white particles surfaces.*

Upper Quartile: *The value assigned to upper quartile is greater than 75 % of the values of black/white particles surfaces.*

In the figure below it can be seen the distribution of black particles surfaces size detected in the case of the cannelure located on sheltered areas (untreated case). The following figures display the distribution in the surface of the same cannelure after the application of the chemical cleaning.

Surface Measures of Black Particles Detected on Aulakas Ravdosisx50(Diagnosis)

figure 3.41

Surface sizes of blck crusts detected on aulakas ravdosisx50 (Ds 60min)

Figure 3.42

Surface Measures of Black Particles Detected on Aulakas Ravdosis x50(Biological Paste)

Figure 3.43

Surfaces of Black Particles Detected on Aulakas
ravdosisx50(Gagemark)
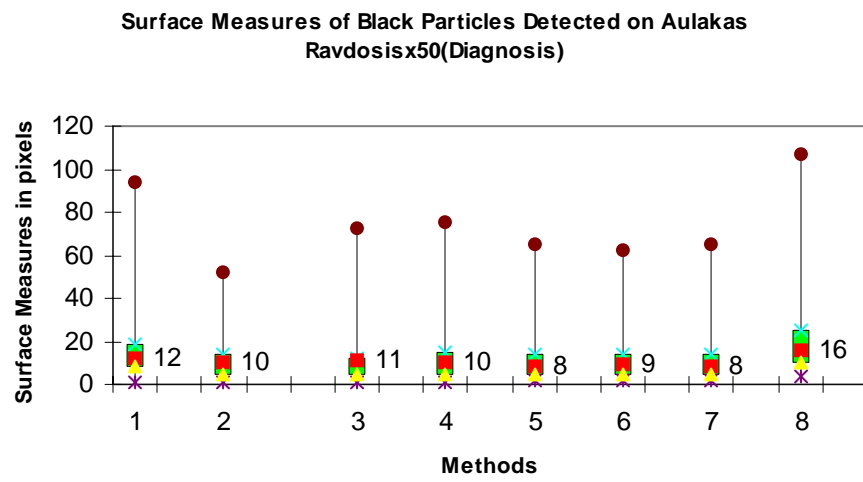
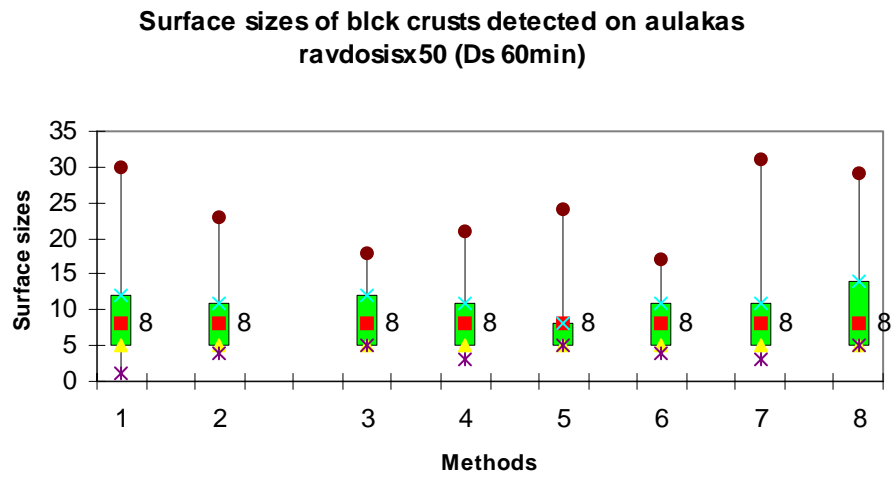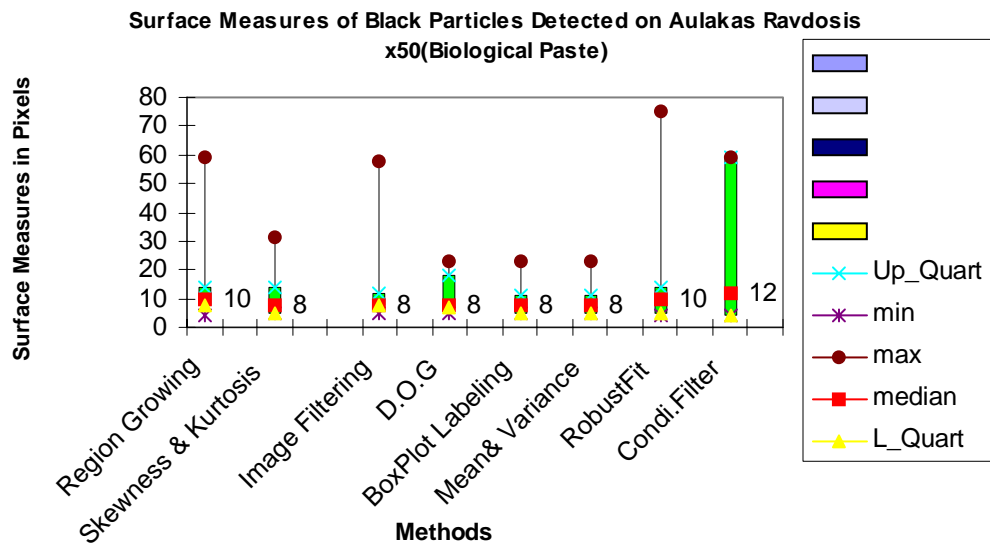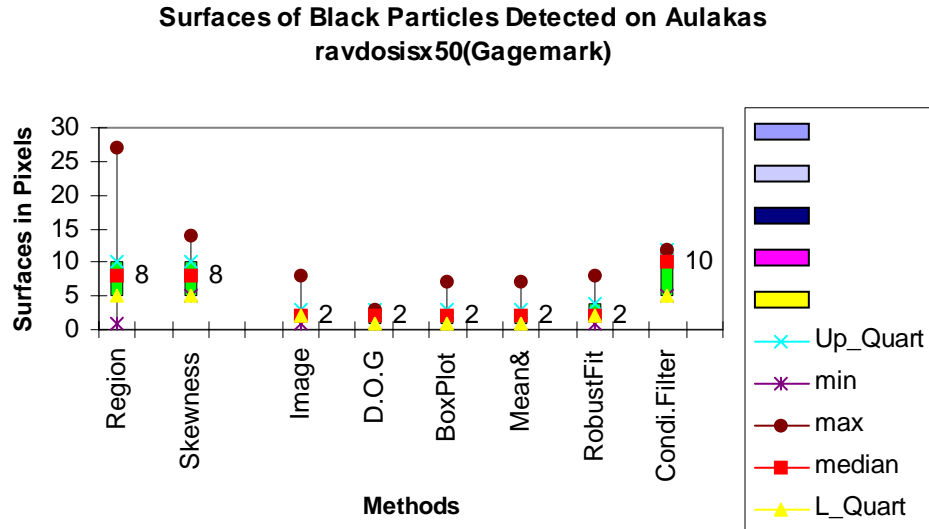*Figure 3.44*

The data labels in the diagrams represent the median value

The above diagrams demonstrate that Conditional Thickening Algorithm detects regions with acreage sizes, exhibiting a spread around greater values than the other Algorithms. Some data are reported as evidence the distribution of black particles sizes on diagram 3.41. We can see that Conditional Thickening Algorithm determined the Lower-Quartile of the particles acreages is equal to 8, Up Quartile was defined to be equal to 22 while according to the same algorithm, median was computed to be 13. While other algorithms such as the Skewness and Kurtosis defines the lower quartile to be equal to 5 in the upper quartile is assigned the value 15 and median is defined to be equal to 10. The same condition is valid for all the other algorithms studied in this work. In a further effort to study these results, it can be observed that some algorithms respond in almost the same way in the definition of black particles size. Thus, the diagrams 3.41-3.44 point out that Image Filtering, the Gaussian Detector (D.O.G), as well as the 3 Labeling Algorithms (Box Plot, Mean Variance, Robust Fit) exhibit a similar distribution of the surface of black particles. On the other hand, Region Growing and the Conditional Thickening Algorithms detect black regions that are spread in higher values.

A further observation is that the distribution of black particle sizes is spread in lower values in the figure depicting the state of erosion after the application of the chemical cleaning. This characteristic, according to the author's opinion, may reflect that chemical cleaning of stone

surfaces not only removes black particles but also eliminates the extent of black areas. It means that the black particles observed on the cleaned surfaces are not only less in number, but also smaller in size than the dark spots encountered on the corresponding untreated surfaces.

In the following diagrams it can be observed the distribution of black surface sizes detected on an arris located on a sheltered area. As it was earlier stated, this surface is labeled by the name 'akmi-ravdosisx50'.

Surface Measures of Black Particles Encountered on Akmi Ravdosisx50(Diagnosis)
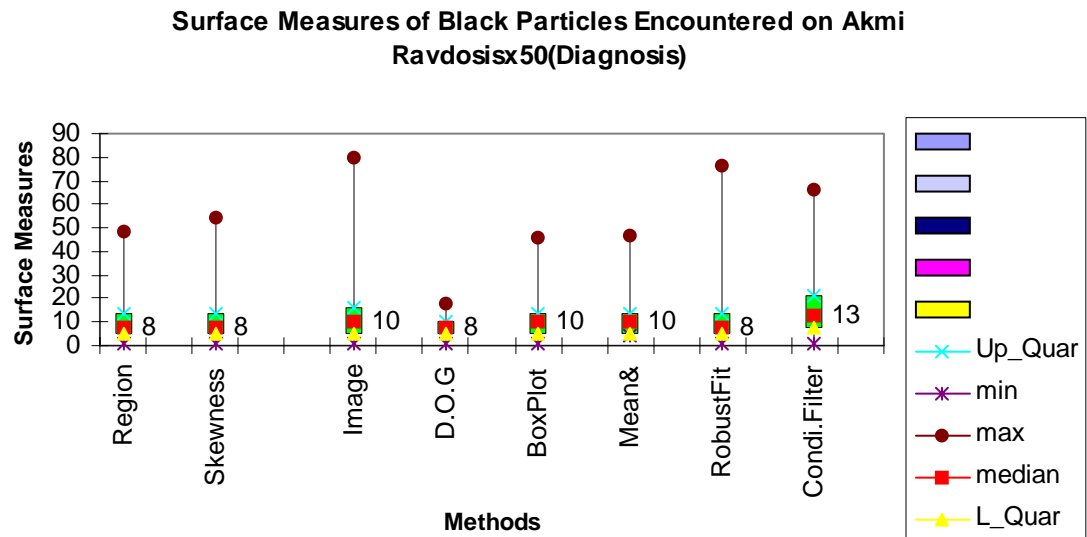
Figure 3.45

In figure 3.45 it can be seen the distribution of black spot sizes for the case of the arris located on sheltered areas. By comparing diagram 3.41 with diagram 3.45 it can be observed that decay areas detected in the cannelure located on sheltered areas, demonstrate surface sizes with higher values than black spot surface values represented in diagram 3.45. This statement may be rather dangerous but according to the author's opinion it evidences the presence of more extent black particles on cannelures surfaces. For example we can refer to the case of the surface distribution given by two Algorithms: Gaussian Detector and Conditional Thickening.

The data are presented in the following table in order to be more easily comparable. At first, the data obtained by the Gaussian detector algorithm are displayed.

Table 2
Gaussian Detector

	Lower-Quartile	Upper-Quartile	Median
(Diagram 4.41) cannelure located at sheltered areas	5	15	10
(diagram-4.45) akmi located at sheltered areas	5	10	8

At next, the data obtained by the application of the Conditional Thickening Algorithm are displayed

Table 3
Conditional Thickening Algorithm

	Lower-Quartile	Upper-Quartile	Median
(Diagram 4.41) cannelure located at sheltered areas	10	25	16
(diagram-4.45) Akmi located at sheltered areas	8	21	13

As we can understand surface sizes of black spots are spread at slightly higher values in the case of the cannelure. This observation may reflect the existence of more extended problematic regions at the cannelures.

In the following diagrams we display the distribution of black particles surface measures detected on arris surface after the chemical treatment.

Figure 3.46

Surface Measures of Black Crusts Encountered on Akmi Ravdosisx50-2(Biol Paste)
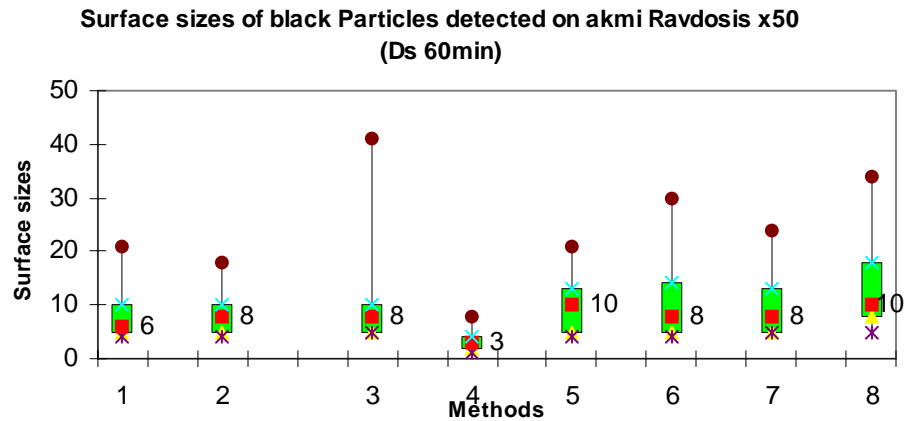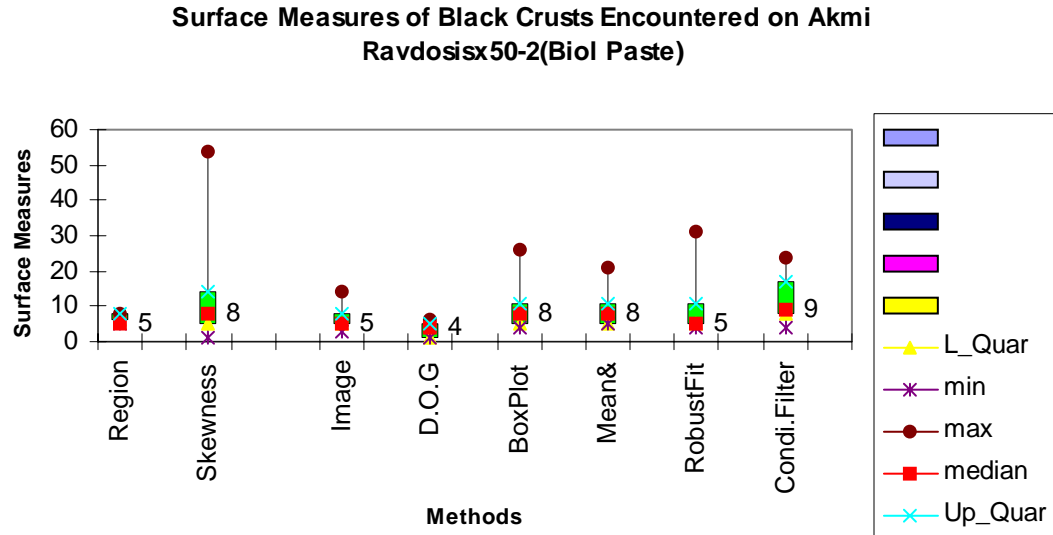
Figure 3.47

In the diagrams 3.45-3.47 it can be observed that the Gaussian Detector (D.O.G) detects black spots, with surface sizes, spread at lower values. This fact is reasonable because Gaussian detector is reported in the literature as a detector that can efficiently determine the specific locations on an image where a decay area exists, but it does not preserve the shape of the detected decay areas.

In the following diagrams the distribution of black particles surface sizes detected on cannelure surface (the cannelure is located at unsheltered areas), prior and after to the chemical treatment, are displayed.

Surface sizes of Black Crusts Detected on Aulakas Ravdosisx50(Diagnosis) (Ks Images)

Figure 3.48

Surface Measures of Black Particles Detected on Aulakas Ravdosisx50(Ds 30min)

Figure 3.49

Surface Measures of Black Crusts Detected on Aulakas Ravdosisx50(Ds 30min)
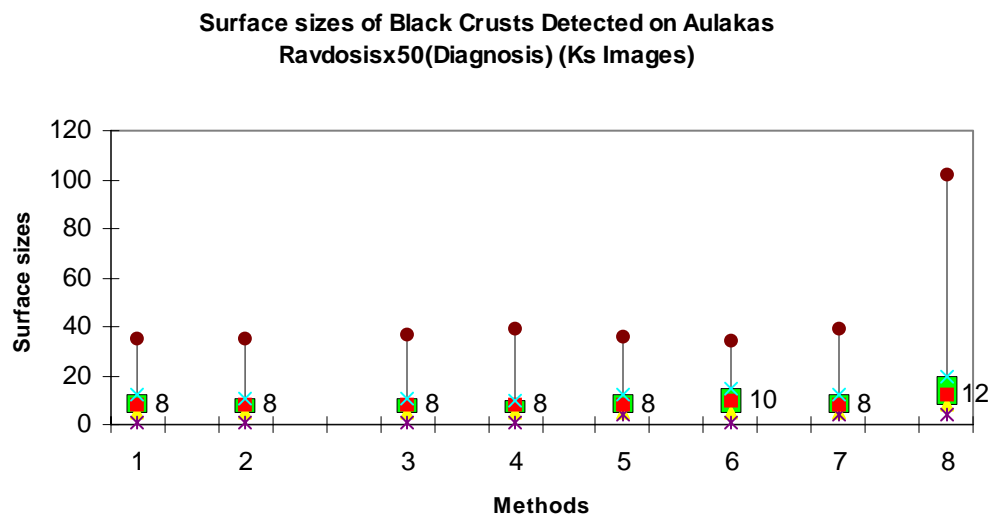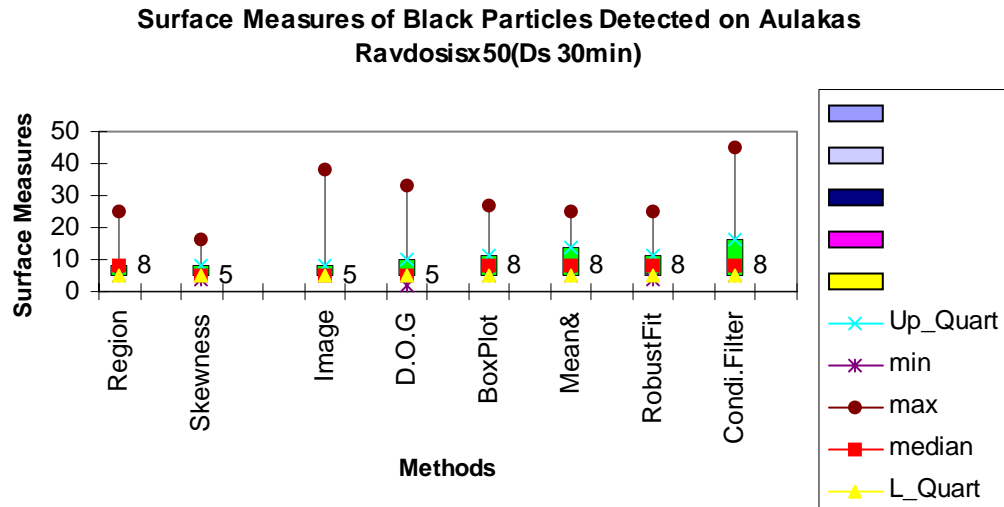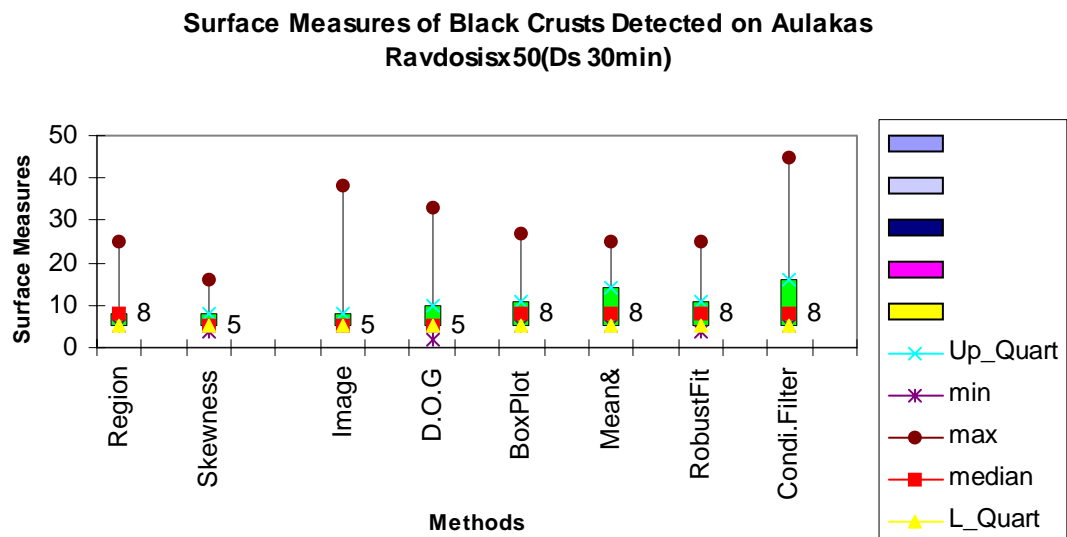
Figure 3.50

An important point that should be noted is that the black particles encountered on the Ks images are less extensive than those in the Ke images both, at diagrams 3.41 and 3.45. This is quite explainable taking into consideration the data obtained after the deterioration diagnosis on Ks images. According to these observations, on the stone surfaces it was defined a layer of gypsum with low amounts of particles that constitute the black spots.

3.7 Distribution of Surface Sizes of White Particles

As it was earlier evidenced, white particles occurring on stones surfaces exhibit some similar characteristics to those reported for black spots. Thus, in the following section it can be seen the distribution of white particles surfaces size. The surfaces studied here are the same as those mentioned above. More specifically, at first we display the case of the untreated cannelure located on a sheltered area and next, all the images of the same region after the chemical cleaning methods. In the same order the sequence of images concerning the cases of the arris located on sheltered area and the cannelure located on unsheltered areas (Ks images) are shown.

Surface Measures of White Particles Detected on Aulakas Ravdosisx50(Diagnosis)

Figure 3.51

Figure 3.52

Surface of White Particles Encountered on Aulakas ravdosisx50 (Biological Paste)

Figure 3.53

Surface Measures of White Crusts Detected on Aulakas Ravdosisx50(Gage
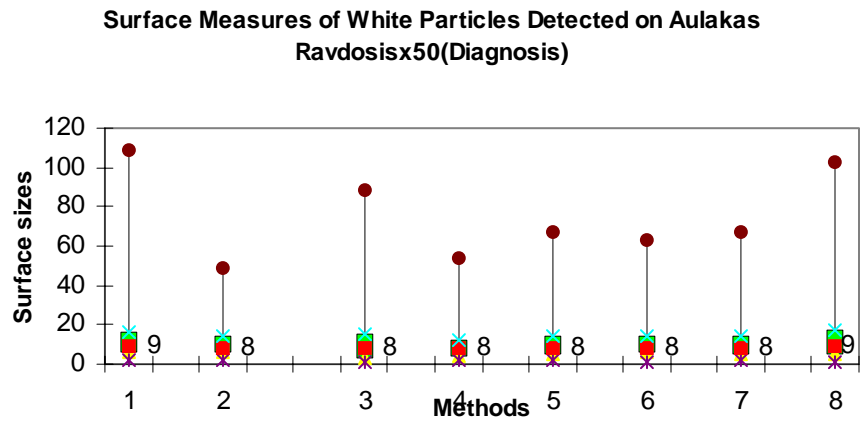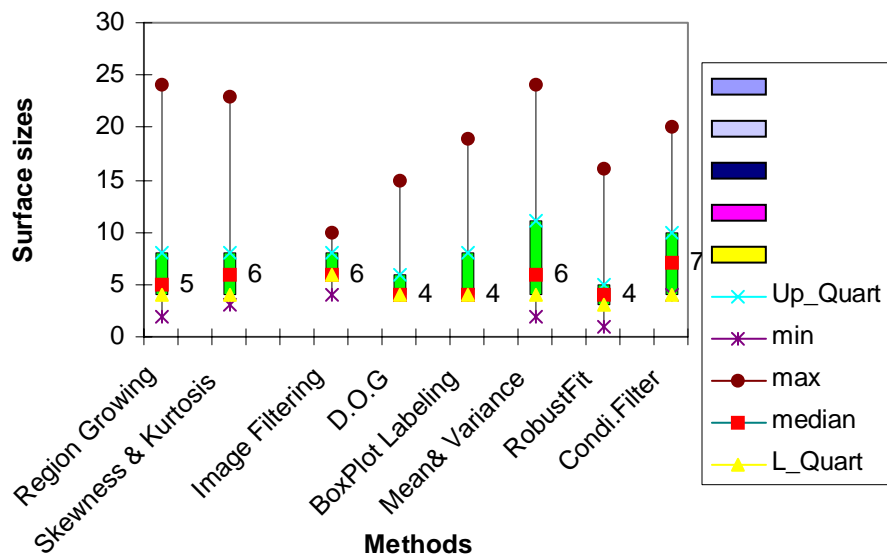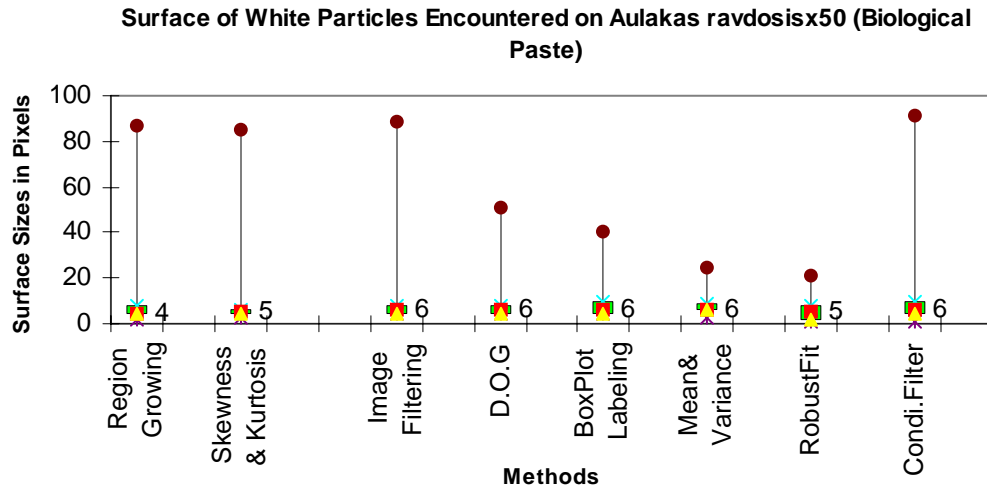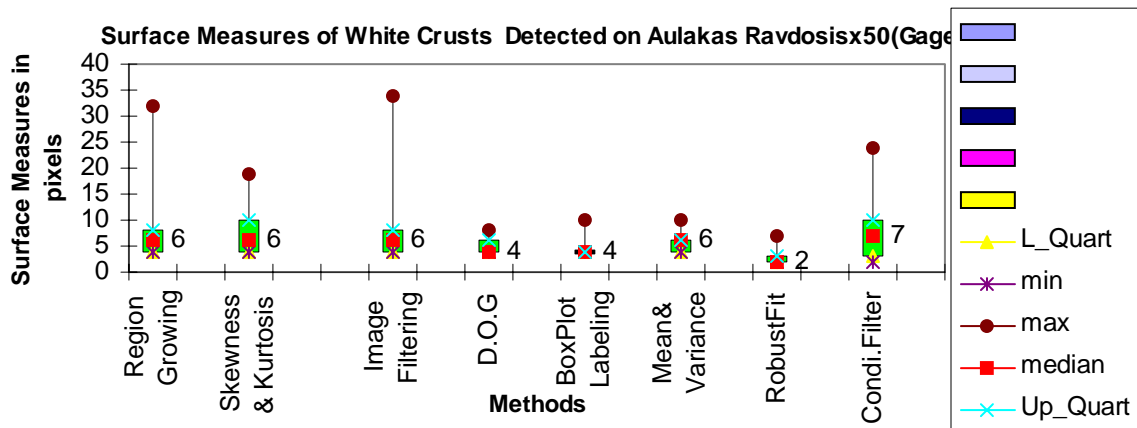
Figure 3.54

In the case of white particles detected on the cannelure, which is located on a sheltered area (diagram 3.51), it can be observed that all the algorithms applied demonstrate a similar distribution of surface sizes. The algorithms determined that the median surface size is equal to 8. The same characteristic can be observed in the following diagrams (3.52-3.54)

In the following figures it can be observed how the surface sizes, detected on the arris located on sheltered areas, are distributed.

In the figure below is reported the surface distribution of the untreated surfaces.
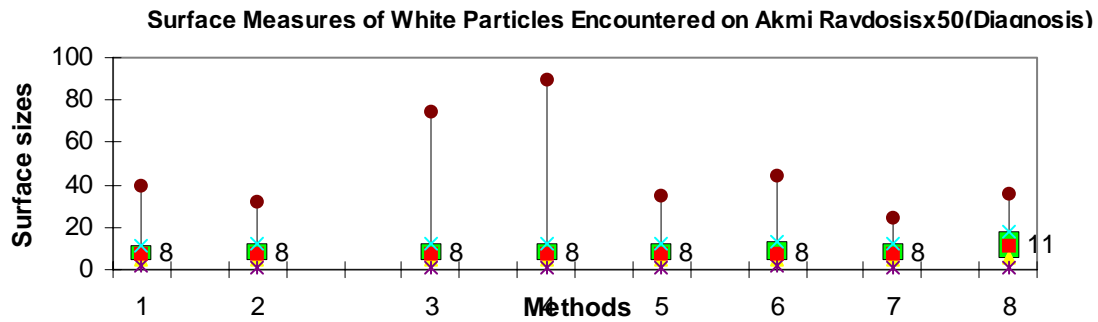
Figure 3.55

The following figure demonstrates how the above studied distribution is affected after the chemical cleaning with the method Ds 60min, while in diagram 3.56 the same distribution after the intervention of the Biological Paste Method is displayed.
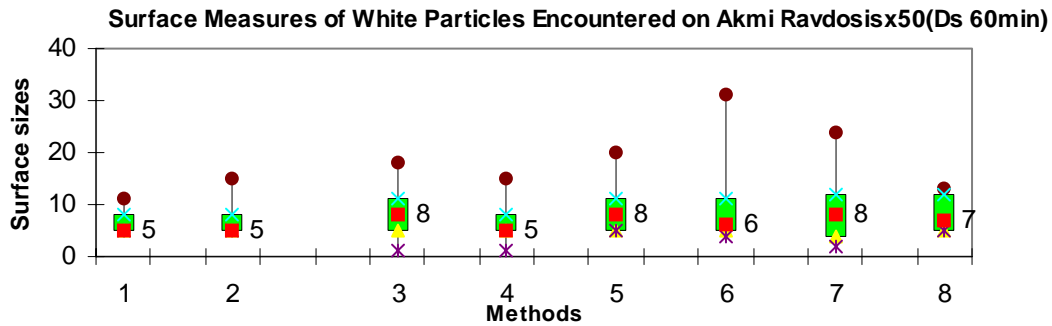
Figure 3.56
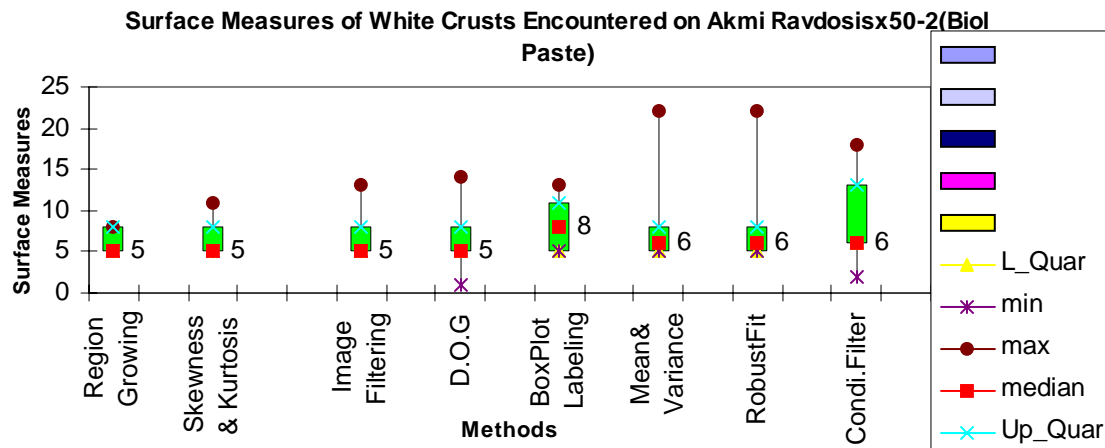
Figure 3.57

By observing diagrams 3.55-3.57 it becomes evident that the Conditional Thickening algorithm detects surfaces which are spread in higher values than the white particles detected by the other algorithms. The case of the diagram 3.55, evidences that the median white particle's size, as was

defined by the Conditional Thickening Algorithm, is equal to 11 the Lower-Quartile=5, Upper-Quartile =18 while algorithm determined the greater surface values is the Mean-Variance Algorithm. The same variables were determined to be equal 8, 5, 13, for the median, lower-quartile, and upper-quartile, respectively.

In the following section the diagrams concerning the distribution of white particles surface sizes encountered at the cannelure located on unsheltered areas are presented. The first diagram depicts the distribution for a surface before the application of any chemical cleaning, while the next diagram displays how the distribution is affected after the intervention with the anionic resin (Ds 30min).
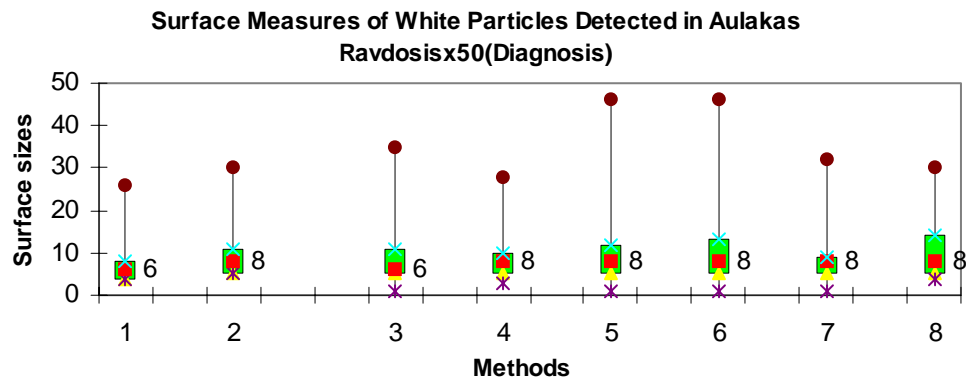
Figure 3.58
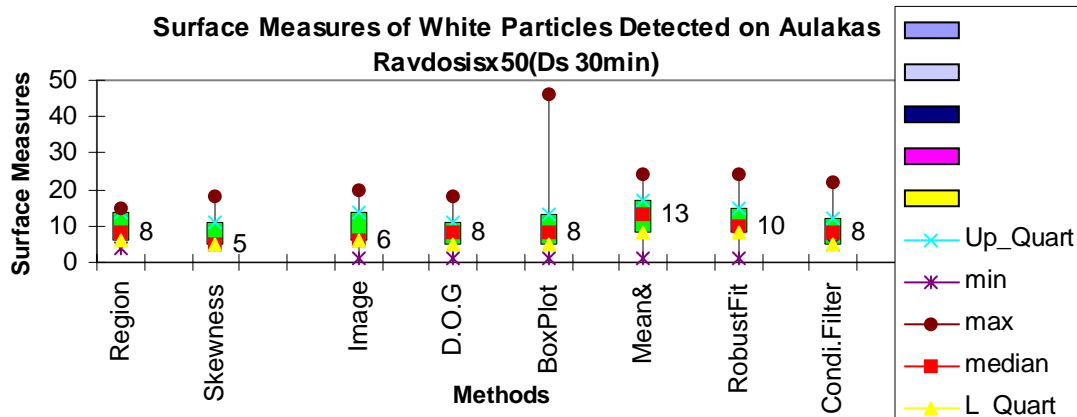
Figure 3.59

By comparing the diagram 3.58 with the diagram 3.59 it can be observed that the white particles detected on the cleaned surface demonstrate sizes, which are spread at lower values. This can be explained by taking into consideration the statistical data displayed at diagram 3.33.

111

It can be seen there that each algorithm applied to the surface, treated with the anionic resin showed that, the number of the remaining white particles is about 10. Thus, for statistical reasons it is expectable to observe a distribution of white spots surface sizes ranging at greater values.

3.8   Observations on the Thickness of the Spots

Another aspect studied in this work was the determination of the thickness of the detected spots. The approach used to calculate the thickness of the spots was rather qualitative. More specifically, the examined parameter is the color intensity at the areas defined as white or black particles .At first the process followed in order to compute these intensities is described. Afterwards, areas defined as black\white particles according to the detection and segmentation process were labeled using the labeling algorithm discussed in the previous chapter. The next step was to find the intensity's value for each of the labels (areas determined as black/white particles). Finally some statistical data were excluded in order to have a broader view. The calculated statistical data are defined below:

Mean Intensity of Black Spots*: It returns the mean intensity value of pixels that constitute the Black particles.*

Dev (Black Spots):* Dev (Black Spots) returns the standard deviation of the intensity values, which were determined for the black spots.*

Lower-Quartile (Black)*: The value returned by this variable is greater than the 25 % of the color intensity values which were computed and correspond to color intensity values encountered on black spots.*

Upper-Quartile (Black) *: The value returned by this variable is greater than the 75 % of the color intensity values which were computed and correspond to color intensity values on black spots.*
The same definitions are valid for the case of White crusts. In the tables below the statistical results obtained by this process are reported.

*Table 4 reports the results obtained for estimation of the thickness of black and white particles originating from the cannelure located on sheltered areas. (As it was discussed earlier in this chapter, we denote this untreated surface with the name '**Aulakas-Ravdosis x50 (Ke images))**

Table 4

	Region Growing	Image Filtering	Skewness And Kurtosi	Mean -Variance Threshold	BoxPlot Thresholding	RobustFit Thresholding	Difference Of Gaussians	Conditional Thickening
Num of black Spots	*1103*	*856*	*1026*	*843*	*700*	*800*	*924*	*744*
Num of white Spots	*1303*	*777*	*1219*	*1244*	*1165*	*1065*	*623*	*705*
Mean Intensity Of black spots	*55,560*	*48,603*	*63,793*	*55,601*	*53,235*	*53,255*	*58,063*	*57,89*
Dev (Black Spots)	*0,1134*	*0,165*	*0,192*	*0,214*	*0,254*	*0,249*	*0,241*	*0,223*
Mean Intens, Of white spots	*129,37*	*135,866*	*111,258*	*113,78*	*115,145*	*113,567*	*135,886*	*123,78*
Dev (White Spots)	*0,202*	*0,279*	*0,233*	*0,225*	*0,255*	*0,277*	*0,237*	*0,233*
Lo-Quart (Black)	*48*	*44*	*54*	*50*	*49*	*45*	*51*	*49*
Up_Quart (Black)	*63*	*52*	*72*	*61*	*64*	*67*	*70*	*73*
Lo_Quar (White	*118*	*121*	*102*	*103*	*110*	*99*	*125*	*109*
Up_Quar r (White Spots)	*141*	*152*	*130*	*129*	*148*	*137*	*146*	*147*

By observing the data presented in the table above, it can be argued that the distribution of intensity values obtained by different algorithms demonstrate similarities. More specifically, it can be seen that Gaussian detector and Conditional Thickening Algorithm have similar distributions of gray value intensities. The 3 labeling algorithms also exhibit a similarity in the distribution of gray values intensities.

113

The same surface after the chemical intervention with the anionic resin is studied.

Table 5

	Region Growing	Image Filtering	Skewness And Kurtosi	Mean - Variance Threshold	BoxPlot Thresholding	RobustFit Thresholding	Difference Of Gaussians	Conditional Thickening
Num of black Spots	*127*	*10*	*4*	*54*	*14*	*135*	*36*	*62*
Num of white Spots	*72*	*8*	*88*	*91*	*35*	*14*	*16*	*13*
Mean Intensity Of black spots	*60,705*	*68*	*69,355*	*69,195*	*65,212*	*72,527*	*68,272*	*75,74*
Dev (Black Spots)	*0,879*	*0,688*	*1,082*	*0,459*	*1,075*	*0,835*	*0,416*	*0,305*
Mean Intensity Of white spots	*102,089*	*108,318*	*90,27*	*100,006*	*99,724*	*93,826*	*103,126*	*103,633*
Dev (White Spots)	*0,841*	*2,775*	*0,830*	*0,511*	*1,041*	*2,832*	*1,699*	*1,293*
Lo-Quart (Black Spots)	*48*	*59*	*66*	*59*	*57*	*59*	*60*	*67*
Up-Quart (Black Spots)	*71*	*75*	*74*	*76*	*78*	*82*	*79*	*84*
Lo-Quart (White Spots)	*93*	*100*	*83*	*89*	*91*	*85*	*97*	*95*
Up-Quart (White Spots)	*109*	*121*	*111*	*105*	*117*	*104*	*114*	*120*

The similarities observed in the data depicted in table 4, are not so obvious on the data presented on this table. This is reasonable because after the surface cleaning (by the anionic resin), there are less decay areas detected on the stone surface. Thus, the mean gray pixel value is computed by processing less in number black/white particles. By comparing the data reported to table 4 with those of data presented in table 5 it can be argued that the distribution of gray values is spread on higher values in the image representing the cleaned surface.

Table 6 demonstrates the thickness of black and white spots (detected at the same cannelure) after the chemical intervention with the Biological Paste.

Table 6

	Region Growing	Image Filtering	Skewness And Kurtosi	Mean - Variance Threshold	BoxPlot Thresholding	RobustFit Thresholding	Difference Of Gaussians	Conditional Thickening
Num of black Spots	*40*	*26*	*38*	*24*	*17*	*23*	*5*	*23*
Num of white Spots	*56*	*18*	*19*	*68*	*42*	*26*	*44*	*48*
Mean Intensity Of black spots	*77,166*	*79,157*	*83,612*	*83,811*	*83,413*	*83,641*	*85,846*	*68,2*
Dev (Black Spots)	*0,612*	*0,621*	*0,803*	*0,498*	*0,755*	*1,654*	*2,990*	*1,70*
Mean Intensity Of white spots	*152,068*	*173,388*	*173,890*	*138,203*	*143,85*	*158,897*	*145,57*	*149,341*
Dev (White Spots)	*1,875*	*3,026*	*3,337*	*1,293*	*2,178*	*5,423*	*3,596*	*2,147*
Lo-Quart (Black)	*70*	*73*	*70*	*75*	*77*	*74*	*78*	*61*
Up-Quart (Black)	*88*	*89*	*98*	*101*	*91*	*104*	*106*	*77*
Lo-Quart (White)	*139*	*167*	*165*	*129*	*126*	*154*	*136*	*135*
Up-Quart (White Spots)	*160*	*178*	*181*	*153*	*151*	*168*	*161*	*154*

By observing the data reported in table 6 it can be stated that all the algorithms determined the distribution of gray values with little deviations. Thus, it is obvious that the mean intensity of gray values corresponding to black particles was determined to be around 80. As it can be seen the distribution of gray values in the surface cleaned by the Biological Paste is spread to higher values than the distribution of gray values of the image representing the stone surface before the chemical cleaning or the surface treated by the anionic resin (table 5).

*Finally, **table 7** shows how the data are affected after the chemical intervention with the wet micro blasting*

Table 7

	Region Growing	Image Filtering	Skewness And Kurtosi	Mean - Variance Threshold	BoxPlot Thresholding	RobustFit Thresholding	Difference Of Gaussians	Conditional Thickening
Num of black Spots	*23*	*42*	*10*	*54*	*20*	*48*	*23*	*3*
Num of white Spots	*27*	*24*	*43*	*11*	*9*	*4*	*6*	*9*
Mean Intensity Of black spots	*93,916*	*66,495*	*93,91*	*91,911*	*91,010*	*90,023*	*87,266*	*73,211*
Dev (Black Spots)	*0,525*	*0,560*	*0,534*	*0,787*	*1,045*	*1,136*	*1,679*	*1,212*
Mean Intensity Of white spots	*140,822*	*171*	*148,824*	*168,086*	*174*	*186*	*171,833*	*173,94*
Dev (White Spots)	*1,128*	*1,378*	*1,287*	*2,63*	*2,796*	*1,001*	*1,514*	*1,33*
Lo_Quart (Black Spots)	*87*	*58*	*88*	*75*	*78*	*80*	*76*	*62*
Up_Quart (Black Spots)	*105*	*77*	*110*	*109*	*111*	118	*103*	*96*
Lo_Quart (White Spots)	*128*	*161*	*133*	*158*	*153*	175	*162*	*165*
Up_Quart (White Spots)	*152*	*178*	*164*	*177*	*188*	190	*178*	*183*

The data presented in table 7 shows that the distribution of gray values representing black particles is spread to higher values than the distributions of gray values above studied. This observation is related to the efficient removal of black crusts from the stone surface, where the wet micro blasting is used. Thus, it can be argued that the black particles, encountered on images representing stone surfaces, cleaned by the wet micro blasting, are thinner in thickness.

In the following sequence of tables, data concerning the color intensity values of regions detected as black or white particles on the arris located on sheltered areas are reported. This specimen is also defined by the name akmi ravdosisx50. At first the untreated surface was studied.

Table 8

	Region Growing	Image Filtering	Skewness And Kurtosi	Mean - Variance Threshold	BoxPlot Thresholding	RobustFit Thresholding	Difference Of Gaussians	Conditional Thickening
Num of black Spots	*620*	*571*	*637*	*532*	*574*	*503*	*798*	*498*
Num of white Spots	*237*	*322*	*261*	*324*	*256*	*223*	*291*	*232*
Mean Intensity Of black spots	*90,67*	*88,226*	*104,44*	*92,583*	*93,289*	*86,643*	*100,71*	*95,978*
Dev (Black Spots)	*0,159*	*0,162*	*0,213*	*0,192*	*0,182*	*0,227*	*0,315*	*0,1916*
Mean Intensity Of white spots	*166,1*	*163,20*	*119,81*	*160,13*	*160,14*	*165,63*	*160,14*	*162,34*
Dev (White Spots)	*0,376*	*0,231*	*0,272*	*0,236*	*0,280*	*0,433*	*0,364*	*0,370*
Lo-Quar (Black)	*82*	*80*	*94*	*83*	*84*	*77*	*88*	*85*
Up-Quart (Black)	*100*	*98*	*116*	*103*	*104*	*99*	*114*	*107*
Lo-Quar (White	*154*	*155*	*110*	*152*	*151*	*156*	*151*	*154*
Up_Quar (White Spots)	*174*	*171*	*159*	*168*	*168*	*175*	*170*	*171*

By reading the data presented in the table above, it can be observed that the distribution of gray values representing the black particles are spread to higher values in table 8(arris located on sheltered areas) than in table 4(cannelure located on sheltered areas). It should also be highlighted that Box Plot and Mean-Variance labeling Algorithms demonstrate similar distributions of gray values.

117

Table 9 shows the data obtained from the study of the arris surface after the chemical cleaning with the Biological Paste (Biol. Paste).

Table 9

	Region Growing	Image Filtering	Skewness And Kurtosi	Mean -Variance Threshold	BoxPlot Thresholding	RobustFit Thresholding	Difference Of Gaussians	Conditional Thickening
Num of black Crusts	*20*	*33*	*35*	*34*	*34*	*26*	*27*	*19*
Num of white Crusts	*15*	*18*	*15*	*20*	*16*	*20*	*40*	*30*
Mean Intensity Of black crusts	*103,9*	*103,57*	*110,36*	*107,73*	*110,19*	*110,9*	*112,41*	*101,12*
Dev (Black Crusts)	*0,674*	*0,521*	*0,893*	*0,496*	*0,484*	*0,324*	*2,230*	*1,167`*
Mean Intensity Of white crusts	*151,2*	*152,88*	*136,76*	*148,42*	*141,80*	*148,42*	*134,63*	*144,42*
Dev (White Crusts)	*1,157*	*1,1*	*0,918*	*1,025*	*1,169*	*1,025*	*1,219*	*1,117*
Lo_Quart (Black)	*98*	*98*	*105*	*102*	*105*	*108*	*100*	*96*
Up_Quart (Black)	*110*	*109*	*116*	*114*	*116*	*114*	*114*	*110*
Lo_Quart (White)	*159*	*150*	*130*	*143*	*145*	*143*	*124*	*134*
Up_Quart (White Crusts)	*166*	*159*	*144*	*154*	*154*	*154*	*145*	*153*

In table 9 it can be observed that the distribution of gray values representing black particles are spread to higher values than in table 8. The opposite observation is valid for the distribution of gray values representing the white particles. This feature reflects the fact that the application of the chemical cleaning methods eliminated the thickness of the white\black particles that continue to be present on stone surfaces.

Table 10 shows the data obtained from the study of the arris surface after the chemical cleaning with the anionic resin (Ds 60 min).

Table 10

	Region Growing	Image Filtering	Skewness And Kurtosi	Mean -Variance Threshold	BoxPlot Thresholding	RobustFit Thresholding	Difference Of Gaussians	Conditional Thickening
Num of black Spots	*51*	*20*	*43*	*38*	*29*	*26*	*58*	*10*
Num of white Spots	*17*	*26*	*51*	*32*	*33*	*31*	*26*	*11*
Mean Intensity Of black spots	*96,63*	*95,71*	*108,35*	*101,37*	*98,716*	*97,182*	*105,11*	*105,148*
Dev (Black Spots)	*0,657*	*1,574*	*0,855*	*0,818*	*1,129*	*1,19*	*1,426*	*2,135*
Mean Intensity Of white spots	*163,14*	*159,39*	*134,08*	*154,18*	*152,67*	*154,18*	*154,68*	*156*
Dev (White Spots)	*1,104*	*0,854*	*0,641*	*0,502*	*1,23*	*0,803*	*1,214*	*1,007*
Lo_Quart (Black)	*88*	*89*	*98*	*90*	*88*	*93*	*101*	*82*
Up_Quart(Black)	*101*	*99*	*113*	*111*	*100*	*109*	*113*	*119*
Lo_Quart (White)	*159*	*155*	*126*	*149*	*147*	*149*	*149*	*149*
Up_Quart (White Spots)	*166*	*163*	*144*	*160*	*159*	*160*	*161*	*162*

By observing the data presented on the above table it can be argued that the distribution of gray values is spread to higher values in comparison with the table 8 but they are spread in lower values if they are compared to the distribution depicted in image 9. Furthermore, it is clear that different algorithms determined similar distributions of gray values, representing the black spots. This observation is valid in the Gaussian detector and the Conditional Thickening Algorithm

Table 11 *demonstrates the data obtained by processing the specimen concerning the case of the*
cannelure located on unsheltered areas (before the chemical cleaning).

Table 11

	Region Growing	Image Filtering	Skewness And Kurtosi	Mean - Variance Threshold	BoxPlot Thresholding	RobustFit Thresholding	Difference Of Gaussians	Conditional Thickening
Num of black Spots	280	294	264	256	263	223	334	225
Num of white Spots	34	85	48	51	61	49	72	56
Mean Intensity Of black spots	95,72	95,593	102,81	97,098	93,924	96,885	103,39	96,31
Dev (Black Spots)	0,216	0,211	0,273	0,233	0,334	0,255	0,280	0,284
Mean Intensity Of white spots	143,7	144,37	140,16	144,21	143,6	143,77	144,37	146,5
Dev (White Spots)	0,823	0,446	0,486	0,391	0,446	0,819	0,377	0,574
Lo_Quar (Black)	91	91	97	92	88	91	95	90
Up_Quar(Black)	107	102	114	115	102	105	114	104
Lo_Quar (White	137	137	133	137	136	135	137	158
Up_Quart(White Spots)	154	153	148	152	151	153	151	153

By comparing the distribution of gray values, representing black spots as it is obtained by the
data on tables 4 and 11, it can be argued that in table 11 the distribution of gray values is spread
to higher values. There are also some similarities in the distributions of gray values determined
by the algorithms studied at this work. More Specifically, it can be seen that the labeling
algorithms determined a similar distribution of gray values while a similarity is also valid for the
Gaussian detector and the Conditional Thickening Algorithm.

Finally, in table 12, the case of the cannelure located on unsheltered areas after the cleaning with Ds-30min is studied.

Table 12

	Region Growing	Image Filtering	Skewness And Kurtosi	Mean -Variance Threshold	BoxPlot Thresholding	RobustFit Thresholding	Difference Of Gaussians	Conditional Thickening
Num of black Spots	*79*	*38*	*60*	*46*	*22*	*39*	*35*	*14*
Num of white Spots	*8*	*15*	*10*	*19*	*18*	*20*	*14*	*11*
Mean Intens. Of black spots	*99,90*	*93,029*	*91,23*	*96,53*	*93,31*	*95,722*	*99,431*	*98,326*
Dev (Black Spots)	*0,545*	*0,934*	*0,623*	*0,708*	*1,36*	*0,868*	*1,413*	*1,774*
Mean Inten. Of white spots	*165,7*	*157,62*	*172,44*	*152,23*	*153,81*	*153,58*	*156,74*	*156,28*
Dev (White Spots)	*1,099*	*0,965*	*1,12*	*0,893*	*0,939*	*0,836*	*1,465*	*1,01*
Lo_Quart (Black)	*80*	*88*	*85*	*91*	*78*	*82*	*88*	*87*
Up_Quart (Black)	*104*	*103*	*97*	*106*	*95*	*102*	*109*	*107*
Lo_Quart (White)	*159*	*149*	*161*	*140*	*143*	*144*	*147*	*147*
Up_Quart (White Spots)	*174*	*165*	*174*	*162*	*162*	*162*	*169*	*164*

As for the data presented in the above table, it can also be seen that the distribution of gray values representing black spots are spread to higher values than the distribution of gray values depicted in the table 11. This fact is reasonable, as the data in the current table represent the deterioration state on the cannelure located at unsheltered areas after the treatment with the anionic resin.

*The results revealed that the color intensity values, of black particles, spread to lower values in the case of table **4**. For convenience the mean Intensity gray values of the regions defined as black spots for the three studied untreated surfaces are reported below. More Specifically, the case of the canellure located on sheltered areas (denoted as Aulakas-ravdosisx50 (Diagnosis) (Ke_Images)), the arris located at the same area (denoted as Akmi-ravdosisx50 (Diagnosis) (Ke_Images)), as well as the cannelure located on unsheltered areas (denoted as Aulakas ravdosisx50 (Diagnosis) (Ks_Images)) are reported.*

Table 13

Aulakas ravdosisx50 (Diagnosis) (Ke_Images)							
Mean Intensity Of black spots	55,560	48,603	63,793	55,601	53,235	53,255	58,063	57,89

Akmi ravdosisx50 (Diagnosis) (Ke_Images)							
Mean Intensity Of black spots	90,67	88,226	104,44	92,583	93,289	86,643	100,71	95,978

Aulakas ravdosisx50 (Diagnosis) (Ks_Images)							
Mean Intensity Of black spots	95,72	95,593	102,81	97,098	93,924	96,885	103,39	96,31

By observing the results of table 13 it can be deduced that the mean gray value of the pixels that constitute black crusts, is lower in the case of the cannelure located on sheltered areas (Aulakas ravdosisx50 (Diagnosis) (Ke_Images)) and higher in the case of the cannelure located on unsheltered areas (Aulakas ravdosisx50 (Diagnosis) (Ks_Images)). This result is quite expectable, because the deterioration diagnosis on Ke-surfaces and more specifically on cannelures evidenced the presence of high amounts of argilo-silicate deposits. Further comparison concerning the color intensity before and after the cleaning methods application could be dangerous because the specimens examined before and after the chemical cleaning methods are not the same. Consequently, the samples under consideration may demonstrate differences in surface texture or in the distribution of minerals. We can see though that the distribution of gray values corresponding to decay areas is spread in lower values in the case of untreated surfaces. An

exception is observed for the case of the cleaning with the anionic resin, where the distribution of gray values representing black particles ranges at similar values. An example demonstrating this feature is reported in table 14.

Table 14

Aulakas ravdosisx50 (Ke_Images)								
Mean Intensity Of black spots(Diagnosis)	55,560	48,603	63,793	55,601	53,235	53,255	58,063	57,89
Mean Intensity Of black spots(Biol Paste)	77,166	79,157	83,612	83,811	83,413	83,641	85,846	68,2
Mean Intensity Of black spots(wet micro blasting)	93,916	66,495	93,91	91,911	91,010	90,023	87,266	73,211
Mean Intensity Of black spots (Ds 60min)	60,705	68	69,355	69,195	65,212	72,527	68,272	75,74
Akmi ravdosisx50 (Diagnosis) (Ke_Images)								
Mean Intensity Of black spots(Diagnosis)	90,67	88,226	104,44	92,583	93,289	86,643	100,71	95,978
Mean Intensity Of black crusts(Biol. Paste)	103,9	103,57	110,36	107,73	110,19	110,9	112,41	101,12
Mean Intensity Of black spots (Ds 60min)	96,63	95,71	108,35	101,37	98,716	97,182	105,11	105,148
Aulakas ravdosisx50 (Ks_Images)								
Mean Intensity Of black spots(Diagnosis)	95,72	95,593	102,81	97,098	93,924	96,885	103,39	96,31
Mean Intens. Of black spots(Ds 30min)	99,90	93,029	91,23	96,53	93,31	95,722	99,431	98,326

The relation between the crust thickness and the low intensity of color on black spots, which approved by the study of the FOM images permit us to extend our study to images obtained by a digital camera. At this point it should be stated that the deterioration patterns on the images taken by the digital camera are depicted as areas exhibiting color alteration, but information concerning the texture of the studied surface cannot be extracted. As it was mentioned in the introduction of this chapter, the algorithms, which are implemented in this survey, were structured as modifications on algorithms, which were previously used in detecting cancerous tissues on medical images. The areas on a medical image that were determined to be cancerous

demonstrated a different range in color. Thus, it is obvious that the deterioration effects, which are visible by the digital camera monitoring system, exhibit some common characteristics with the medical images.

In the following sections are presented some results obtained by applying the algorithms that we implemented here on images taken by a digital Camera.

3.9   Processing of Images Obtained by a digital Camera.

The images demonstrated below were taken in order to check the efficiency of the algorithms, developed in this work, in detecting decay areas in digital camera images. More specifically, the specimen displayed in the following image depicts a stone surface after the cleaning by a laser system. By a macroscopic observation of the stone surface we can observe the presence of black strains on the surface. These strains are the vestiges of deterioration after the cleaning.

In the following figure the specimen under consideration is displayed as is monitored by the digital camera. At the bottom of the picture the signs of deterioration are obvious. In order to study the corrosion effects we chose to split this image into three parts and study the black particles on each of them.

| (a) | (b) | (c) |
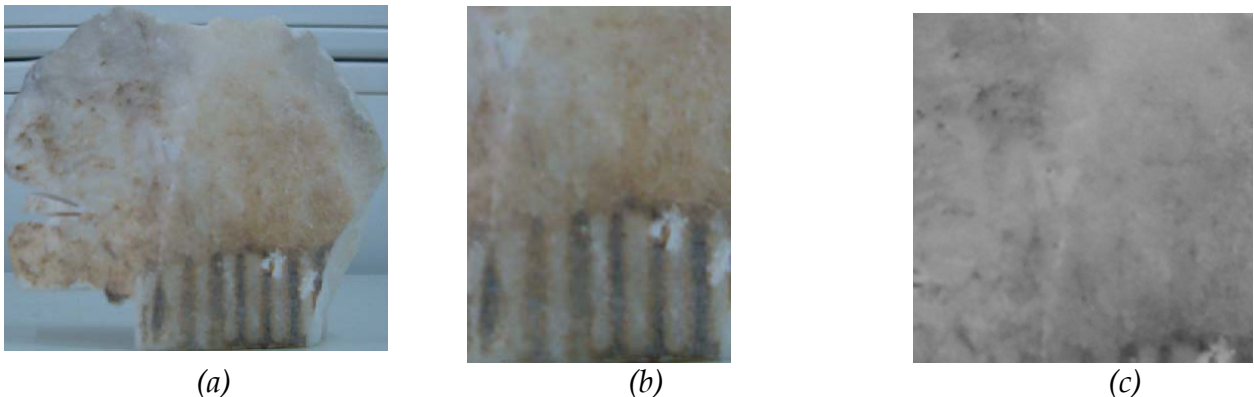
Figure 3.60

Figure 3.60(a) depicts the image of the whole stone under consideration while images (b) and (c) illustrate two sub regions of the stone.

 Further to the processing of the above images we have applied the algorithms to two other images, which are shown in the following figures. In the following sections the results derived after the application of some specific algorithms are reported. Except for the images depicting

locations where problematic regions prevail, it is also demonstrated some statistical data extracted by the processing.
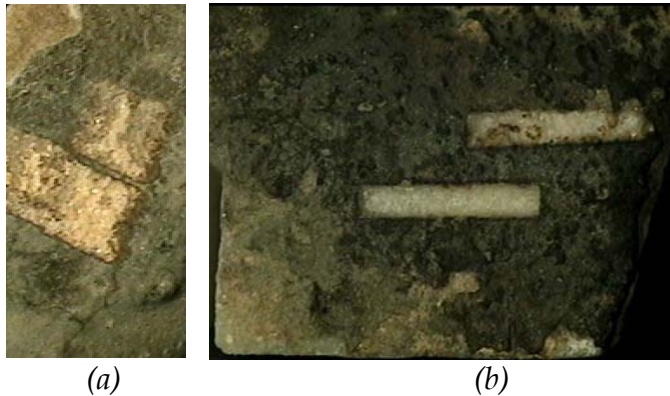

(a)   (b)

Figure 3.61

Figure 3.61 illustrates stone surfaces with deterioration effects. On these surfaces we can observe streaks, which have been cleaned.

At this point the images obtained after the process of detecting black and white particles are shown. Images 3.61(a) and (b) display results, which are associated with the detected particles after the application of Skewness and Kurtosis Algorithm. According to the author's opinion it manages to isolate more accurately the problematic regions. A feature of the images 3.61(a) and (b) is that the surface depicted contains cavities and heterogeneous background, thus some of the algorithms demonstrate a high false positive rate. Image 3.60 illustrates a more homogeneous surface; because of the better focus, corroded images where more reliably detected.

Images 3.60 display the results illustrating the black and white particles detected by the algorithms: Labeling Algorithm (Box plot Thresholding), Gaussian Detector (D.O.G), Conditional Thickening, Region Growing, Skewness and Kurtosis.

3.9.1 Labeling Algorithm (Box plot Thresholding)

(a)   (b)   (c)
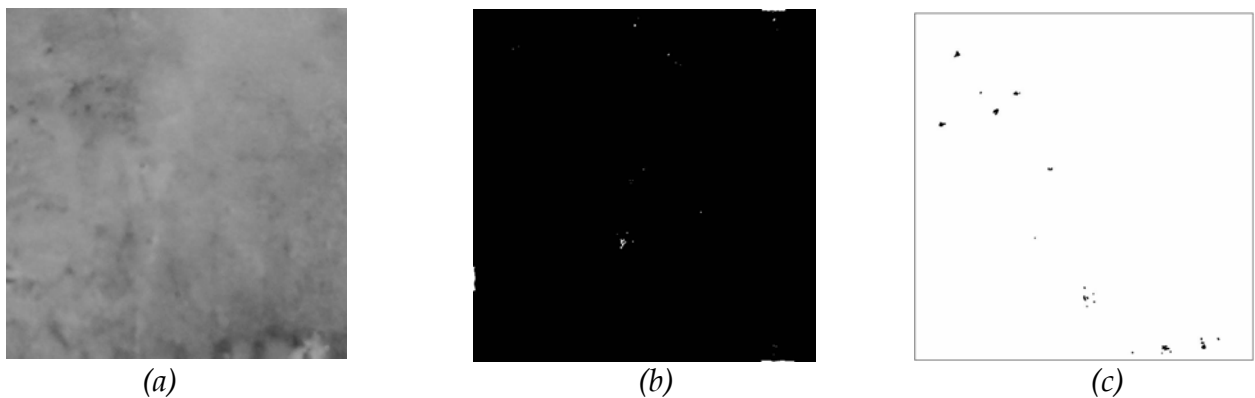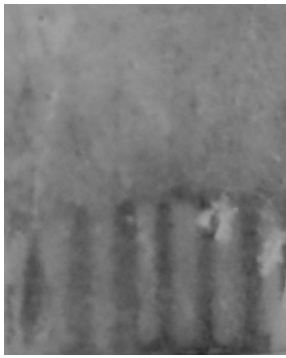
Figure 3.62

(a)   (b)   (c)

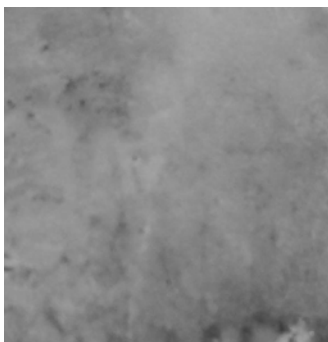**figure**   **3.63**

Figure 3.62 (b) demonstrates the white particles and 3.62(c) displays the black particles detected on the image 3.62(c) while figure 3.63(b) and (c) depicts the white and black particles detected on image 3.63(a).

By superimposing the problematic regions detected by the algorithm on the original image it can be seen that the black and white particles are defined with a good accuracy. By observing the image 3.63(c) it is obvious that the regions determined as black crusts seem like black strains. It could be explained by the fact that the focus is larger. Furthermore we should state at this point that the algorithm studied in the current sub section was used to reduce the false positives as it takes into consideration the background features of each sub region of the surface.

3.9.2 Region Growing Algorithm

In the following images we can see the black and white particles detected on the surfaces under consideration, after the application of the current algorithm.
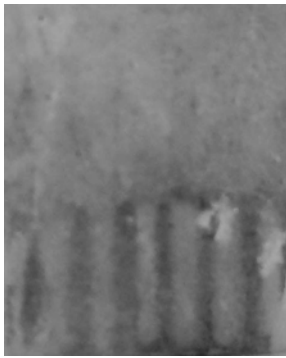

(a)   (b)   (c)

Figure 3.64

126
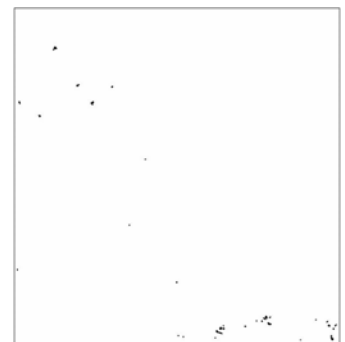
(a) (B) (c)

Figure 3.65

In the image 3.64(b) and (c) we can see the white and black particles, respectively that we detected at the scheme 3.64(a). The same holds for the sequence of images 3.65, where we can see the black and white particles detected on image 3.65(a). In the image 3.65(b) we can observe that very few white spots are present.

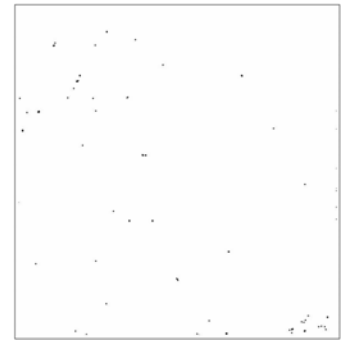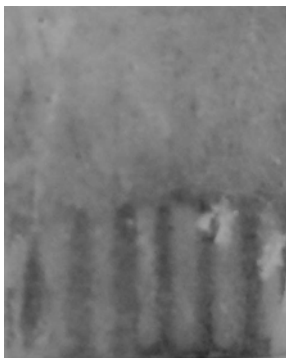*In the following sub section we are displaying the results obtained after the application of the Skewness and Kurtosis algorithms on the images that we study.*

3.9.3 Skewess and Kurtosis
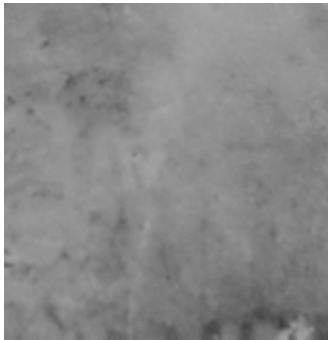
(a) (b) (c)

Figure 3.66

(a) (b) (c)

Figure 3.67

(a)	*(b)*	*(c)*

Figure 3.68

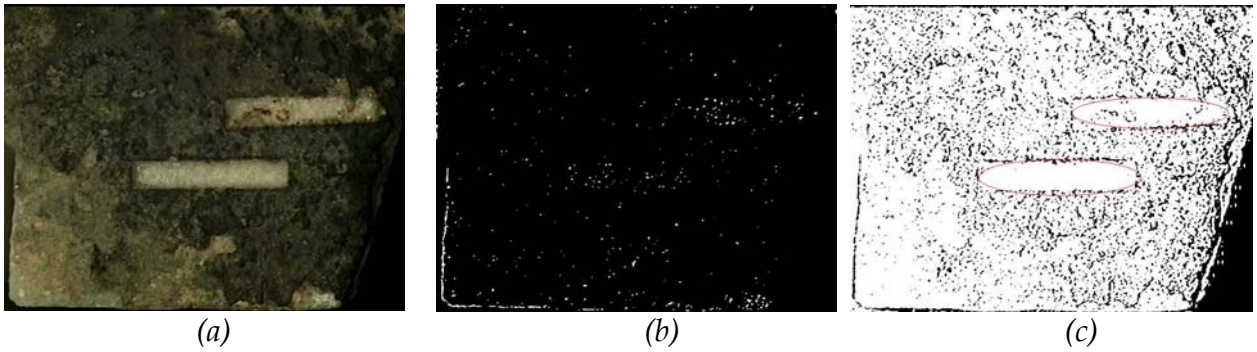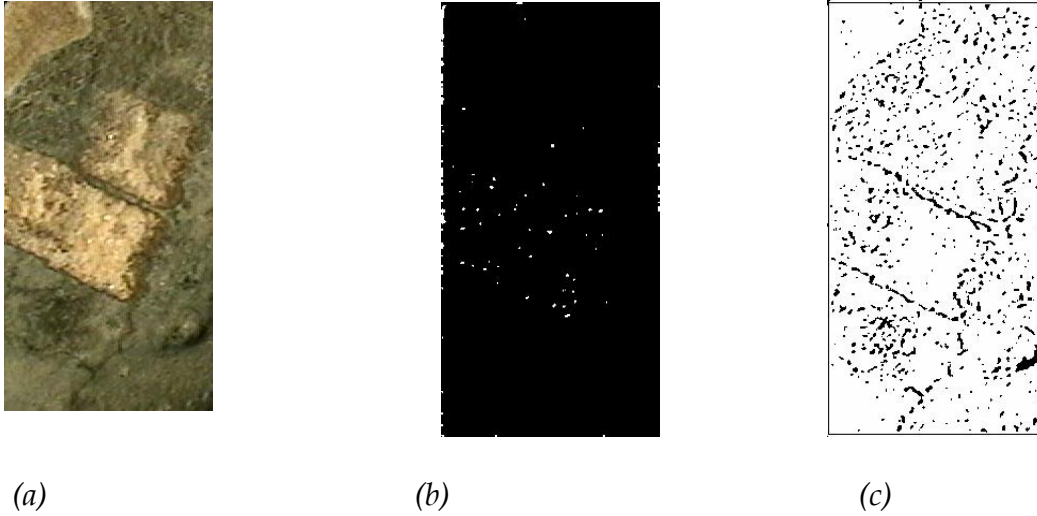|		
(a)	*(b)*	*(c)*
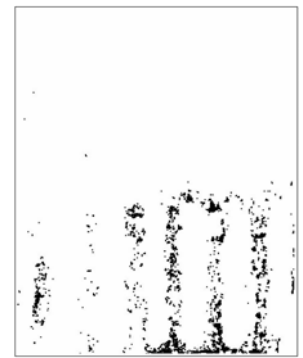
Figure 3.69

In the figures above we can see how the Skewness and Kurtosis Algorithm detect white or black particles on the surfaces that we studied. In the images 3.68(b),(c) as well as in the images 3.69(b),(c) we can see that the Algorithm does not determine problematic regions on the streaks which are already cleaned. In the image 3.68(c) the cleaned regions are encircled with red color.

In the sub section below we can see how the Gaussian Detector defined the black and white particles in the studied images.
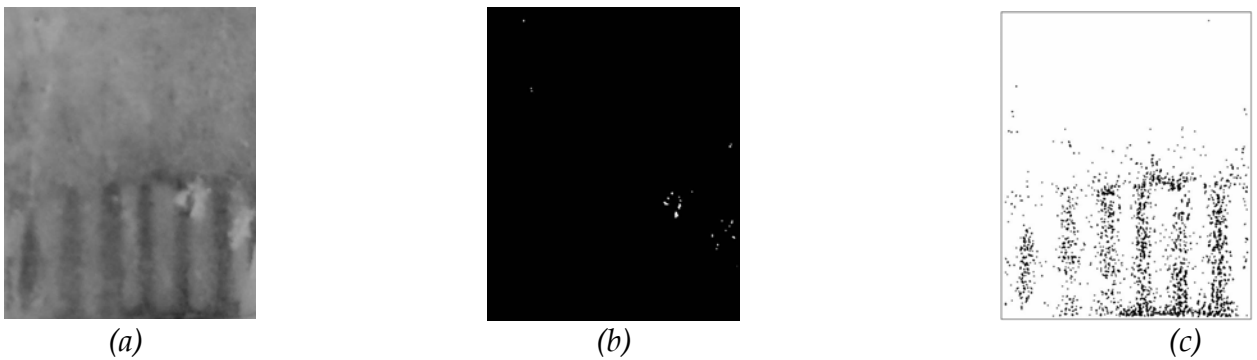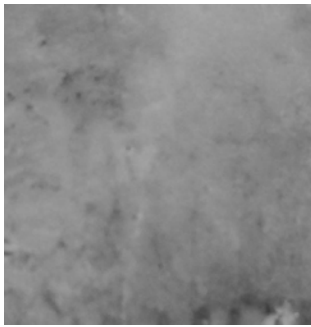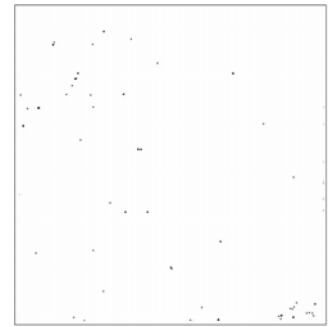
3.9.4 Gaussian Detector (D.O.G)

(a)	*(b)*	*(c)*

Figure 3.70

(a)	*(b)*	*(c)*

Figure 3.71

Figures 3.70(b), 3.71(b) depict the white particles which are present on the image 3.70(a) and 3.71(a), while images 3.70(c), 3.71(c) show the black crusts detected on the surface.

If someone observes the image in greater detail he could see that the regions determined as black crusts by the Gaussian detector are smaller in size than those detected by the other algorithms but they are more in number. This fact can be explained very easily if we take into consideration that the Gaussian detector usually splits a region, defined as an entity by the other algorithms, into two or more sub regions.

At last the results depicting the white and dark regions as the Conditional Thickening Algorithm detected them are presented.
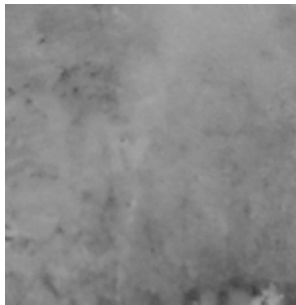
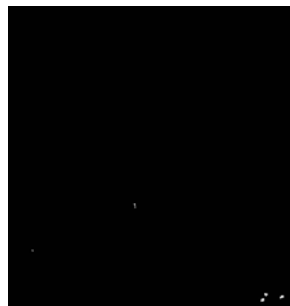### 3.9.5 Conditional Thickening Algorithm

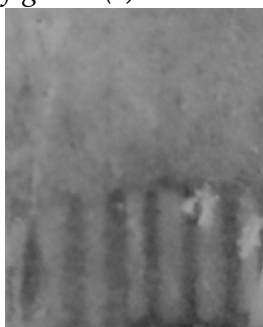|		
fig 3.72(a)	*fig 3.72(b)*	*fig 3.72(c)*

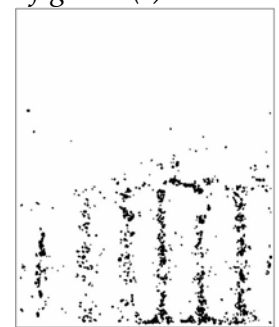|		
(a)	*(b)*	*(c)*

Figure 3.73

In the images 3.72(b), (c) we can observe the white and black particles respectively detected on the image 3.72(a). Similarly, images 3.73(b) and (c) are depicting the white and black regions that were defined by the Conditional Thickening Algorithm on the image 3.73(a).

As it was reported when we studied FOM images, the Conditional Thickening Algorithm detected black regions, which are greater in size and preserved the shape of the spots.

4 CONCLUSIONS AND FURTHER WORK

This thesis examines the issue of detecting deterioration patterns on historical stone monuments. The deterioration patterns, which were detected and studied, were classified into two broad categories defined by the terms "black particles" and "white particles". This discrimination was performed according to the chemical composition of the deterioration patterns. The images examined depicted the degradation state observed on areas of the monument where different deteriorative factors prevailed. The results obtained by this study were quite reasonable and in accordance with the diagnosis of the erosion as this was estimated by the chemists. Except for the detection and classification of the decay areas encountered on stone surfaces, an attempt was made to estimate the efficiency of various chemical cleaning methods in the removal of degraded areas.

The algorithms, which were developed in this thesis, managed to detect the degraded areas on stone surfaces with various accuracy and sensitivity. Furthermore the results related to the efficiency of the chemical cleaning methods are in accordance with those stated by the chemists. For instance we mention the case of the chemical cleaning of stone surfaces by using the anionic resin. This method was defined to be less suitable for the removal of black crusts (mainly consisted of: metal oxides, quartz, organic constituents). Such a result was also derived by chemists that estimated the deterioration state of the monument after the application of the specific chemical cleaning method. An aspect of high importance for the current thesis was to study the sizes of black/white particles that cover the stone surfaces before the chemical treatment and after it. The distribution of the sizes of the deterioration patterns was studied separately for each deterioration pattern (black/white particles) and the results obtained indicate the features of the erosion detected on the studied surfaces. The number of present deterioration patterns on a stone surface as well as the percentage of the surface covered by black or white crusts was considered to be a measure indicating the erosion state of the stonework. The results extracted after the application of the algorithms reveal that these measures of deterioration are in accordance with the assessment of the degradation state as it was estimated by the chemical analyses.

*Various algorithms were implemented with the aim of detecting deterioration patterns on stone surfaces. All these algorithms managed to detect the degradation effects with a very good accuracy, but each one is appropriate for a different feature. It was evidenced that the **Labeling Algorithms**, which were implemented in this work, had the lower false positive and false negative rates while they managed to detect very efficiently the locations on an image where the black/white particles prevail. On the other hand the **Conditional Thickening Algorithm** was efficient in detecting with a better accuracy the shape of the areas, which were determined as deterioration patterns. Other algorithms developed in this work such as the **Skew ness and kurtosis algorithm** exhibit an important feature that is the ability to detect degraded areas in inhomogeneous background. Thus, we do not derive a specific algorithm that guarantees the best performance. All the algorithms implemented in this work contribute in the estimation of the problem by approaching better a specific feature.*

Further investigations could be focused towards determining the exact degraded areas of a stonework that are removed after the chemical treatment with a specific method. This objective requires the monitoring of a stone surface prior to any chemical treatment and after the chemical cleaning is conducted. This process would reveal the type of pollutant that each of the chemical treatment methods manages to remove, as well as the way in which the extent and thickness of the degraded areas are eliminated. An important aspect is also to extract some other features concerning the shape of the deterioration patterns. This type of information would be valuable in performing pattern recognition in the deterioration particles. For instance the gypsum particles are defined by the chemists that to be encountered as needle-shaped crystals. In order to extract information related to the shape of the decay areas, the shape of the deterioration patterns should be studied after the segmentation process. The development of methods, which compute the thickness of the black crusts detected on stone surfaces, is very important, as it would contribute in the determination of the extent of the erosion phenomena. A further approach could also be the determination of the color alteration of the stone's surface after the application of chemical cleaning methods. The alteration in the lustre of the stonework after the chemical treatment is also an important issue, which in combination with the color alteration can be used in order to determine the appropriateness of specific methods in removing the pollutant without affecting the stone. As it was evidenced, the algorithms implemented in the current thesis manage to

detect decay areas on images obtained by a digital camera overcoming the need for microscopy. Further investigations could be focused towards extracting information by this image that is related to the thickness of decay areas as well as to study the extent (in size) of the degraded areas.

References

[1] The effects of ozone and NOx on the deterioration of Calcareous stone (S.W Massey)

[2] Effect of airborne particle on $SO2$ - calcite reaction (Hasan Boke[a,b], E. Hale Goktuk[a], Emine N. Caner-Saltik[b], Sahindre Demirci[a])

[3] Innovative techniques for the characterization of encrustation on Pentelic Marble from the Parthenon (P. Maravelaki-Kalaitzaki)

[4] Possible alteration of monuments caused by particles emited into the atmosphere carrying strong primary acidity. (P. Primerano[a], S. Di.Pasquale[a],L. Mavilia[b],F . Coriglaino)

[5] Influence of atmospheric pollutants on the biodeterioration of stone (E . Zanardini[a] , P . Abbruscato, N. Ghedini[b,c], M. Realini[d] , C. Sorlini[a])

[6] Biodeterioration of Stones (Rakesh Kumar ,Anuradha V. Kumar)

[7] Building Stone and related weathering in the architecture of the ancient city of Naples (Maurizio de Gennaro[a*],Domenico Calcatera[b] , Piergiulio Cappelleti[a] , Allesio Langella[c] , Vincenzo Morra[a])

[8] Weathering of Soapstone at Norwegian Monuments (Dr. Per Storemyr)

[9] Deterioration of stone materials in the Angkor Monuments Cambodia (E . Uchida , Y.Ogawa, N. Maeda [a] , T . Nakawaga [b])

[10] V.Lebrun, C.Toussaint, E. Pirard

"On the use of image analysis for quantitative monitoring of stone alteration"

[11] Sowmya Mahadevan, David Casasent,

"Detection of triple junction parameters in microscope images"

[12] Murat Deriven, M.Koray Balci, Ugur.M. Leloglu

"Feature extraction method for marble tile classification"

[13] Goldeberg D.E,

"Genetic Algorithms in search, Optimization and Machine Learning"

[14]   David L.D 1991, "Handbook of Genetic Algorithms", Van Nostrand Reihold

[15]   Michalewicz Z, "Genetic Algorithms + Data Structures", Evolution Programs, 3rd Ed. Springer Verlag.

[16]   Bhanu and Lee S.1994 "Genetic Learning for adaptive Image Segmentation", Kluwer academic Press.

[17]   Yoshimura M. and Oe S., 1999 "Evolutionary segmentation of texture image using Genetic Algorithms towards Automatic Decision of Optimum Number of Segmentation Areas"

[18]   Bhadakar S. M., Zhang Y. and Potter W.D 1994,
"An edge Detection technique using Genetic Algorithm based optimization"

 [19]   Andrey P. 1999, "Selectionist relaxation: Genetic Algorithms applied to image Segmentation "

[20]   Kokla Vassiliki, Psarrou Alexandra, Konstantinou Vassilis "Image Processing a helpful tool in the art Conservation"

[21]   Michail Pappas, Ioanis Pitas "Old painting digital color restoration"

[22]   Carmen Serrano, Javier Piaz-Trujillo, Begona Acha and Rangaraj M.Rangayyan "Use of 2D linear prediction error to detect micro-calcifications in mammograms"

[23]   L.Shen, R.M Rangayyan, J.E Leo Dessautels   "Detection and Classification of Mammographic calcifications "

[24]   G.R Kuduvalli, R.M Rangayyan "An Algorithm for direct Computation of 2-D linear prediction coefficients".

[25]   M.F Salfity, G.H Kaufuman, P.Grannito "A Computer-Aided Diagnosis for Automated Detection and classification of clustered microcalcifications in mammograms"

[26]   Dengler J., Behrens, S., Desaga, J.F, "Segmentation of Micro-calcifications in Mammograms"

[27]   M.Nafi Guran, Yasemin Yardimci, A.Enis Cetin, Rashid "Automated Detection of Microcalcifications in Mammograms"